다중신호 천문학 (1)

김정리
이화여자대학교 물리학과

2024 수치상대론 및 중력파 여름학교

강의개요

다중신호천문학1: 다중신호 및 중력파 천문학을 이해하는데 필요한 천문학/천체물리학 기본 개념

다중신호천문학2: 다중신호천문학 연구와 기본 개념 활용 사례

**“exceptional advancements in our understanding of fundamental physics,
the dynamics of dense matter, and the cosmic history of compact objects.”**

quoted from abstract of Capote et al. (2024)

Constants and Units

(to two significant digits)

Gravitational constant	G	=	6.7×10^{-8} erg cm g^{-2}
Speed of light	c	=	3.0×10^{10} cm s^{-1}
Solar mass	$M_\odot$	=	2.0×10^{33} g
Solar luminosity	$L_\odot$	=	3.8×10^{33} erg s^{-1}
Solar radius	$r_\odot$	=	7.0×10^{10} cm
Astronomical unit	1 AU	=	1.5×10^{13} cm
Parsec	1 pc	=	3.1×10^{18} cm $= 3.3$ l.y.
Year	1 yr	=	3.15×10^{7} s

21세기는 중력파로 우주를 관측할 수 있는 시대!

초기 우주

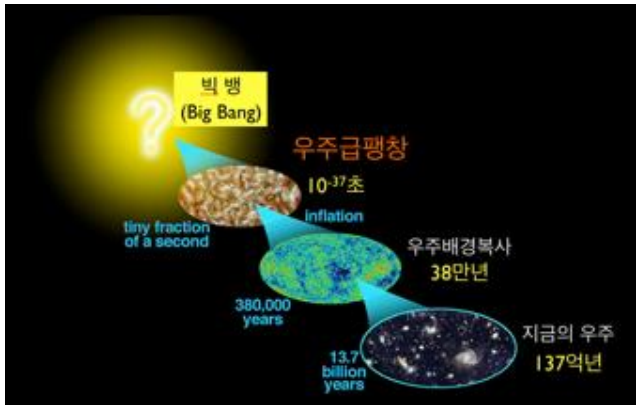

블랙홀, 중성자별 "쌍성" (binaries)

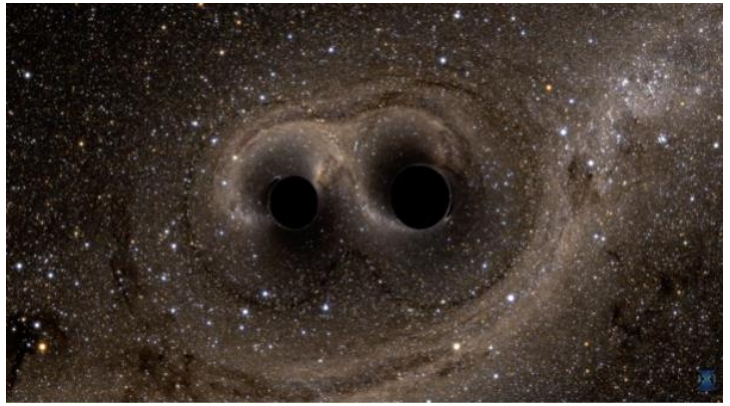

우리 은하내 초신성

GW frequency: 10^{-16} Hz (early Universe) ~ 10,000 Hz (supernovae)

Multi-Messenger Astronomy (MMA) 다중신호 천문학

가능한 모든 장비를 활용, 관측으로부터 추출 가능한 모든 정보를 유기적으로 분석하여 하나의 천체(현상)를 보다 심층적, 종합적으로 이해한다

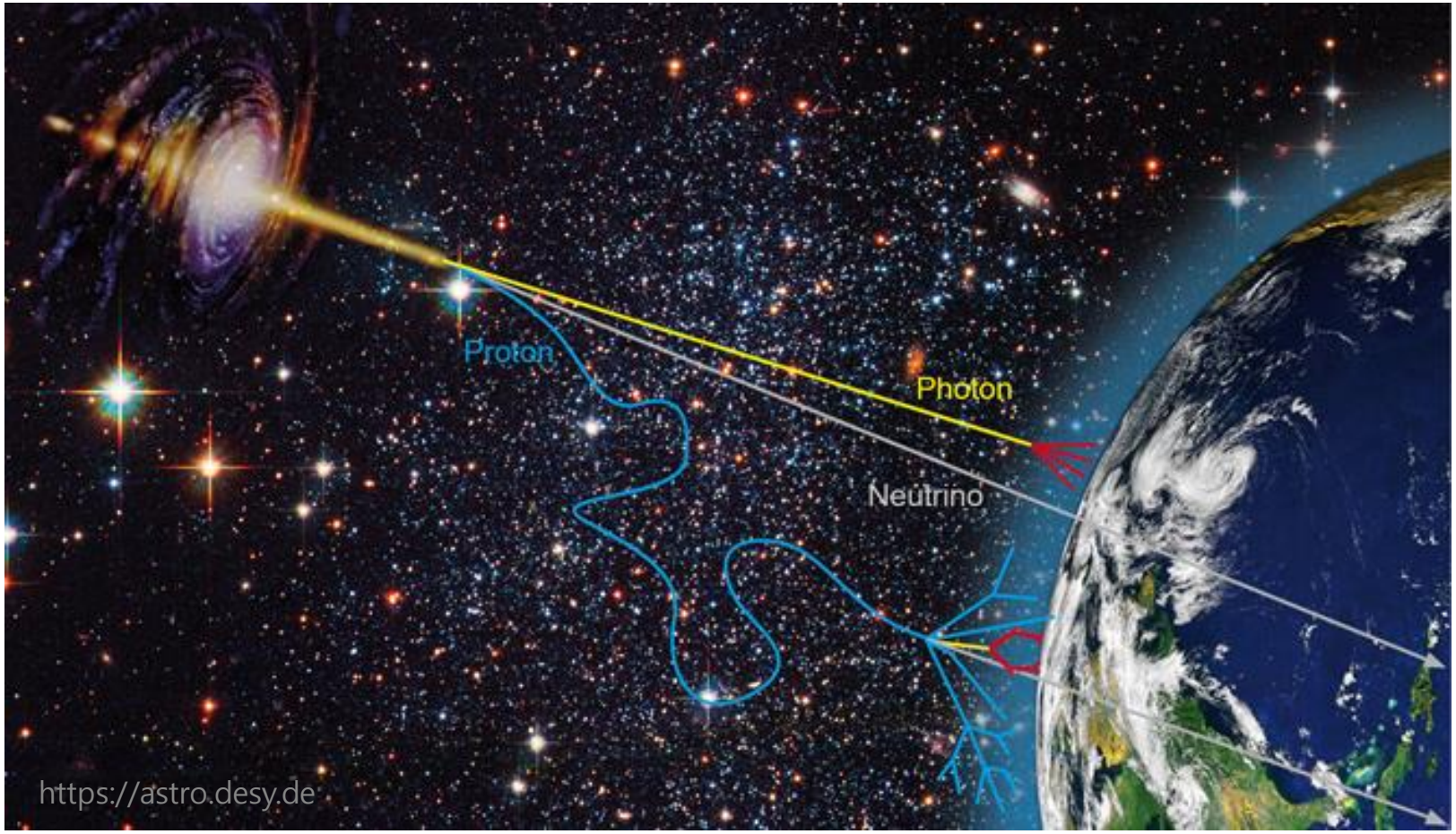

“중력파원(源)” gravitational-wave sources

중력파원의 종류

구분 기준이 다양하다

이 강의에서는 10-2000 Hz 대역의 중력파원의 종류를 주로 알아본다

- 신호 (분석) 기준 ← 관측자의 시각. 관측 천문학
- 천문학적 (근원)기준 ← 관측/이론 천문학
- 파형 (모델) 기준 ← 이론 천문학/천체물리학/중력이론

중력파 관측 ➔ 모수 추정을 통한 천체 물리량 측정

- **[밀집쌍성병합]에서 방출되는 중력파에 담겨있는 정보**

  질량, 거리 ➔ 중력파원의 종류, 생성, 진화

  스핀, 궤도 모양 ➔ 생성 과정에서 일어나는 상호작용

  천구상의 위치 + 거리 ➔생성 환경, 우주론

감마선으로 본 우주 "돌발천체"
("transients" = one-time strong emission of lights 섬광?)

10-2000 Hz 대역에서는 중력파 신호(현상)이
주로 "돌발천체" 로 관측된다

관련 용어

- 밀집성 compact object

  백색왜성, 중성자별, 블랙홀

  White dwarf (WD), Neutron star (NS) and **Black hole (BH)**

  ➔ 무거운 별의 마지막 진화 단계, 고중력고밀도천체

  "상대론적" 천체 (특수상대성이론이 아닌 일반상대성이론을 적용해야 운동방정식을 정확히 기술할 수 있다)

- 밀집쌍성 = compact binaries

중력파 = 우주를 보는 새로운 창

밀집쌍성이 관측가능한 중력파원인 이유

가속하는 질량

"상대론적" 시스템

"천체(현상)" **밀집성**

중력파의 세기 "진폭"
시공간 곡률의 변형률 (strain) h(t) $\frac{2G}{c^4}\frac{1}{r}\frac{\partial^2 Q}{\partial t^2}$ 변형률 h(t) → 작은

$$Q^T{}_{ij} = \int \rho(\mathbf{x}) \left[r_i r_j - \frac{1}{3} r^2 \delta_{ij} \right] d^3 r$$

$Q^T{}_{ij}$: 질량 사중극자 모멘트

r : 근원까지의 거리

Ann. Phys. (Berlin) **529**, No. 1–2, 1600209 (2017) / DOI 10.1002/andp.201600209

annalen der physik

The basic physics of the binary black hole merger GW150914

*LIGO Scientific and VIRGO Collaborations**,**

우주 중력파 신호의 세기(진폭)은 매우 약하다 ➔ 초정밀 관측 기기 필요

$f_{gw} = 2\, f_{orb}$ distance chirp mass

$$h_0 = 1.5 \times 10^{-21} \left(\frac{f_{\rm gw}}{10^{-3}\ {\rm Hz}}\right)^{2/3} \left(\frac{1\ {\rm kpc}}{r}\right) \left(\frac{\mathcal{M}}{M_\odot}\right)^{5/3}$$

characteristic binary mass = chirp mass (M_c)

Mc = 1.2 M_{sun}, m1=m2=1.4 M_{sun}.

At f_{gw}=100 Hz, r=100 Mpc, h_0=10^{-23}

binary inspiral

$$M_c = \frac{(m_1 m_2)^{3/5}}{(m_1 + m_2)^{1/5}}$$

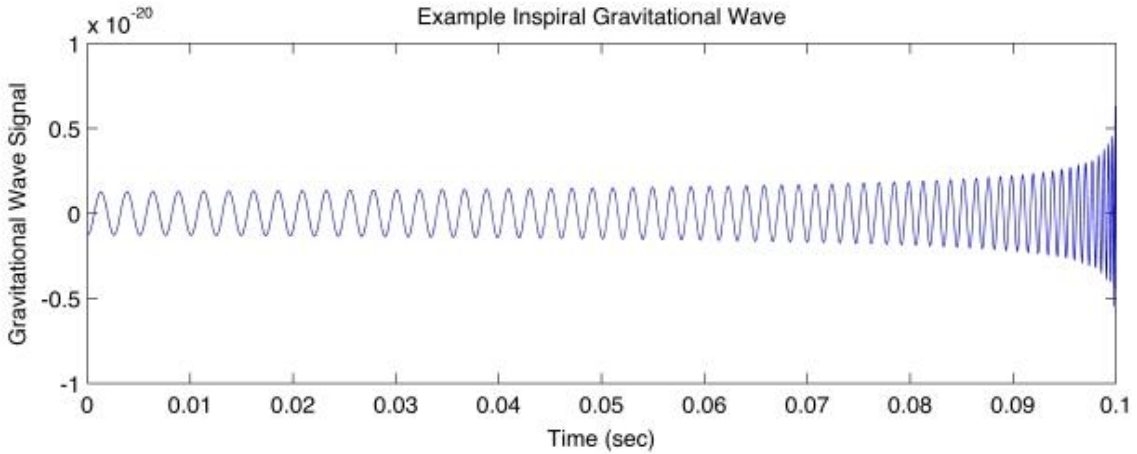

"chirp"

An example signal from an inspiral gravitational wave source [Image: A. Stuver/LIGO]

블랙홀 Black Holes (BHs)

BBH = binary black holes

블랙홀 쌍성

빛관측 불가능
강한 중력파원 천체

$$r_{\mathrm{Schwarz}}(m) = \frac{2Gm}{c^2} = 2.95\left(\frac{m}{\mathrm{M}_\odot}\right)\mathrm{km}$$

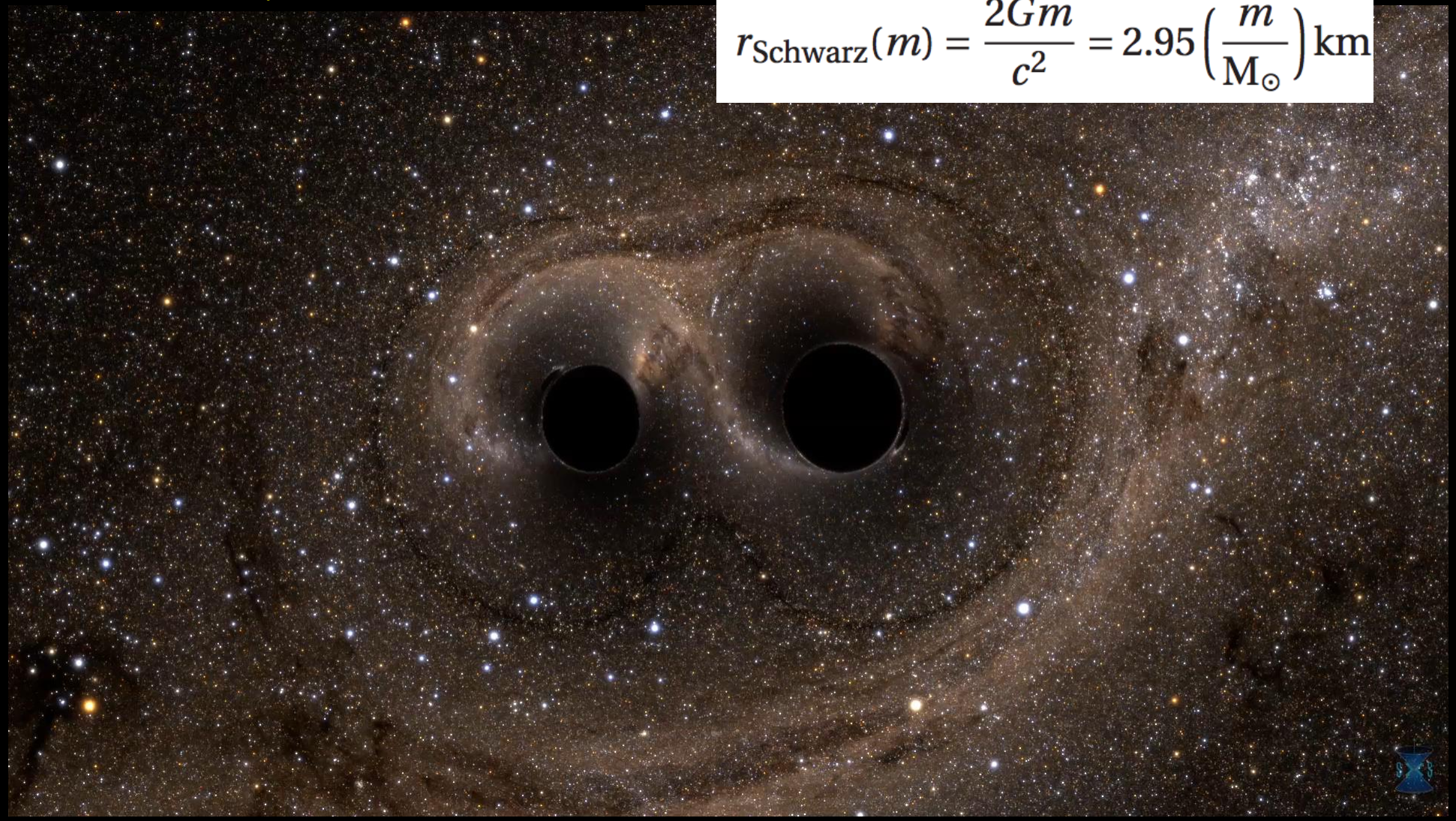

중성자별의 특별한 종류 "펄서" ➔ 전파 펄서는 "우주 등대"라고도 불린다

펄서 = 중성자별의 한 종류. 빠르게 자전하며 강한 표면 자기장을 띄고 있다.

펄서의 자전 주기: 밀리초 ~ 10초 , 우리 은하에서 3000여개의 전파 펄서 발견

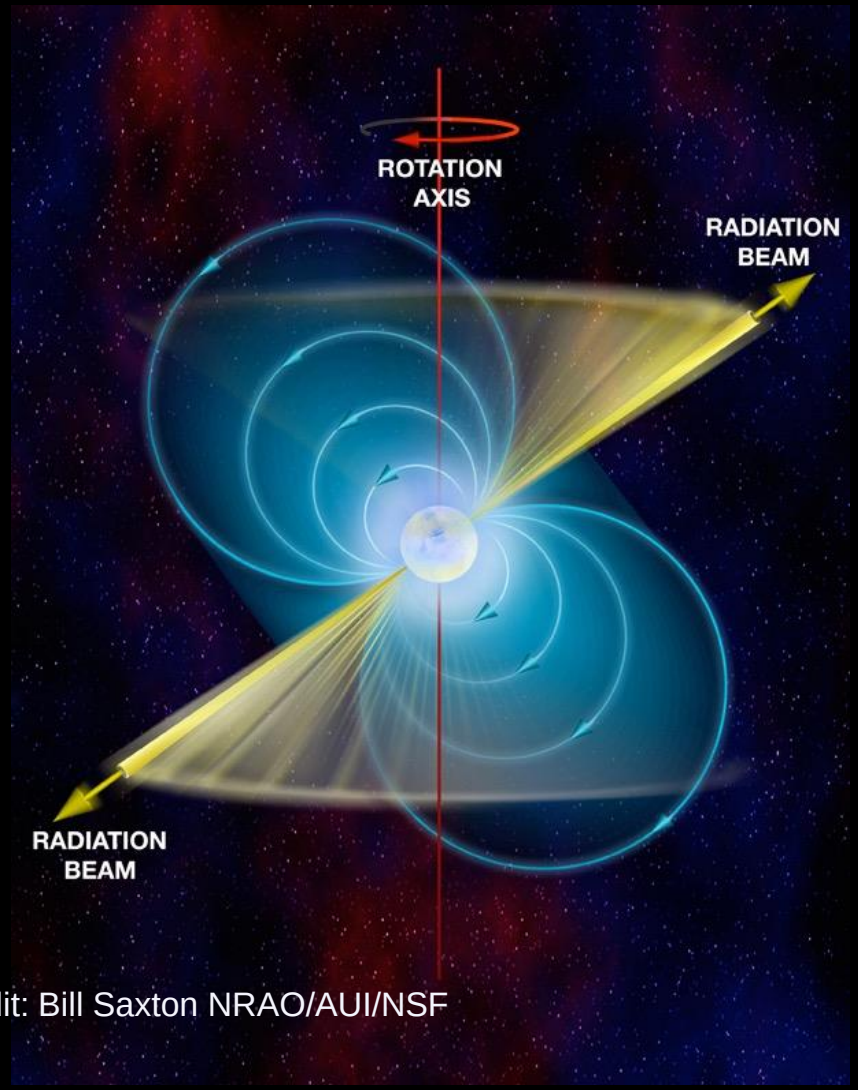

Credit: Bill Saxton NRAO/AUI/NSF

X-ray image
of a Crab pulsar
(NASA)

International GW Detector Network

2015-now : 20-2000 Hz, Earth-based km-scale laser interferometers (3-4km)

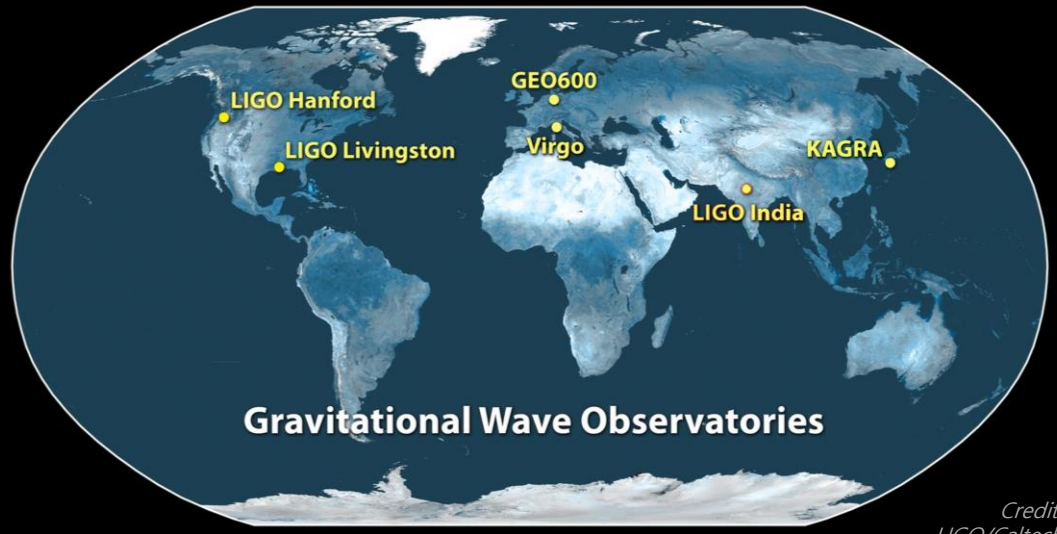

Credit: LIGO/Caltech


LIGO


Virgo


KAGRA


LIGO-India

2nd generation detectors

International GW Detector Network

2015-now : 20-2000 Hz, Earth-based km-scale laser interferometers (3-4km)

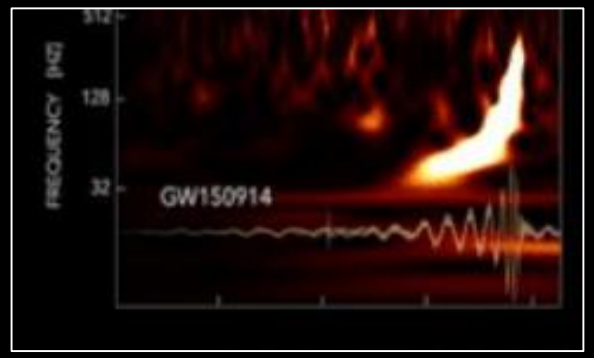

BBH: < 0.5 sec
20-600 Hz
inspiral-merge-ringdown

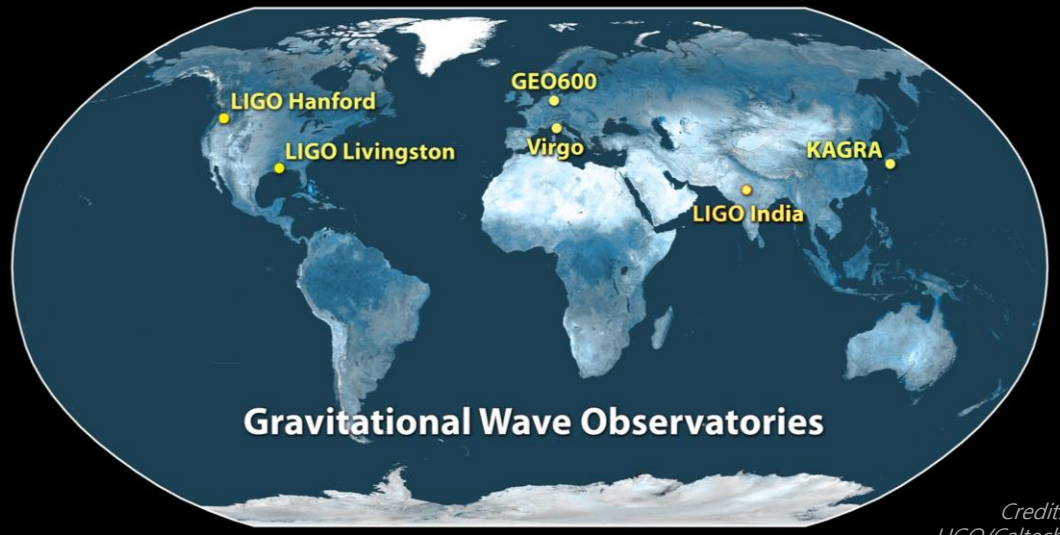

Credit: LIGO/Caltech

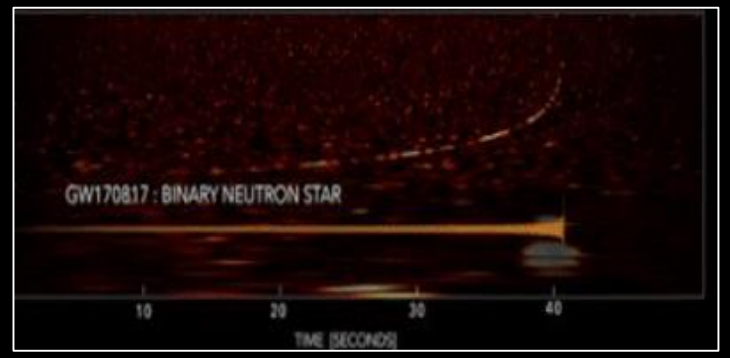

NSNS: ~ 100 s
20-2000 Hz
inspirals only

O4a: 2023.05.24 ~ 2024.01.16 (7.5 months)

O4b: 2024.04.10 ~ 2025.6.9 (15 months, longest span!)

https://observing.docs.ligo.org/plan/

Gravitational Wave (GW) astronomy & astrophysics as of today

- various GW sources are expected, compact binary coalescences (CBCs) are detected/observed/cataloged
- diverse types of signals in a time-frequency space are classified, searched, analyzed
- Since GW150914, matched-filtering in 20-600 Hz is proved to be the most successful search scheme for stellar-mass binary black holes (BBHs)
- good sensitivity toward 2 kHz is important for NS binaries

At present, the 'observable' GW universe is a 'transient' universe

Questions and goals:

- other GWs with diff origins, signal types
- upgrades of existing detectors
- 3rd generation detectors
- beyond the LVK band observations (PTA,LISA,deci-Hz, ...)

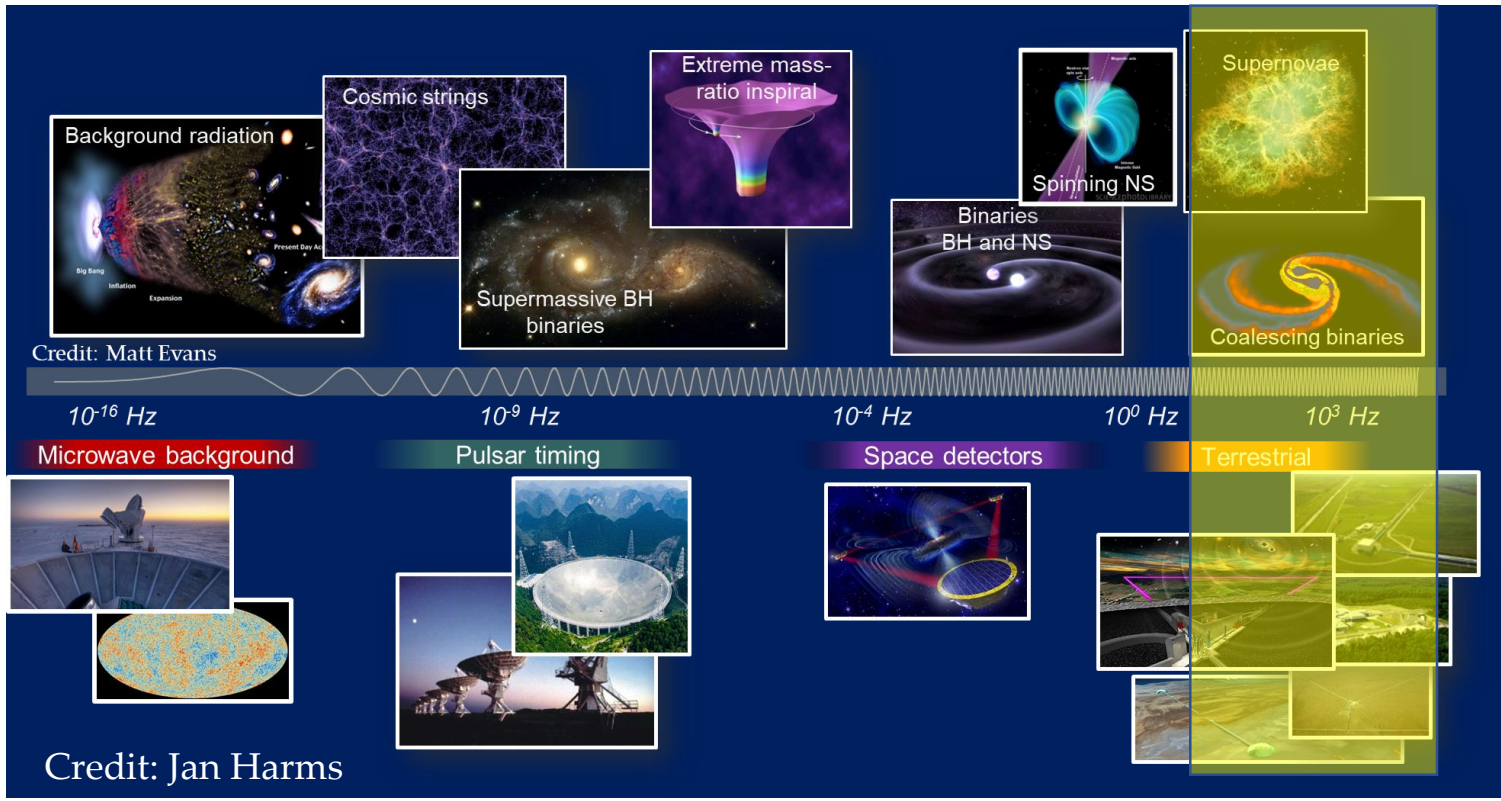

뉴턴 중력과 쌍성 운동

쌍성의 궤도운동이 시간과 공간을 변화시키지 않음

$$P^2 = \frac{4\pi^2}{G}\left(\frac{a^3}{m_1 + m_2}\right)$$

if $e = 0$

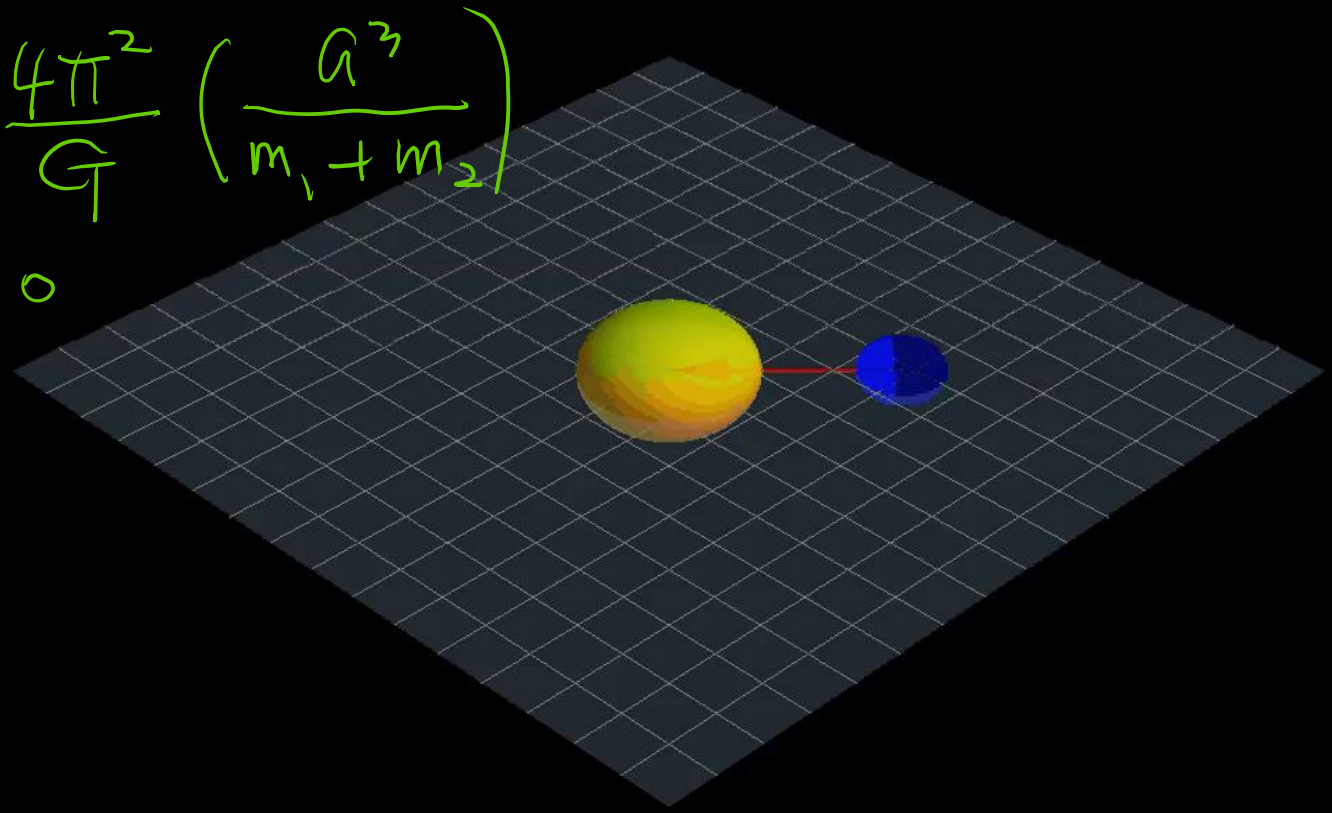

Credit: Carl Rodriguez

아인슈타인 중력과 쌍성 운동

쌍성의 궤도운동이 시간과 공간을 변화시킨다 “시공간에 발생한 잔물결”

➔ 섭동이 쌍성으로부터 빛의 속력으로 “퍼져 " 나간다

➔ 중력파

➔ 쌍성의 에너지와 각운동량이 감소한다

➔ 궤도 크기가 감소하면서 두 천체가 가까워진다

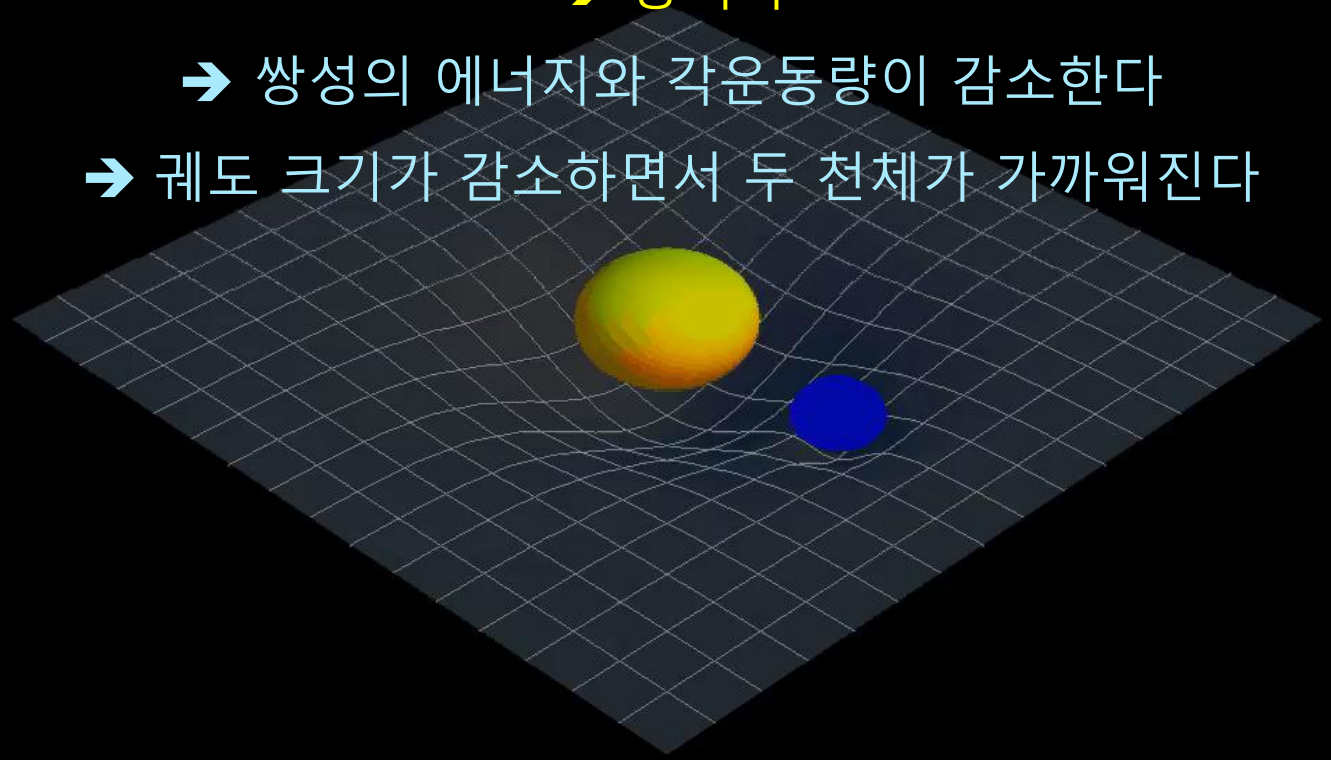

Credit: Carl Rodriguez

아인슈타인 중력과 쌍성 운동

나선접근궤도 단계에서 방출되는 중력파

$$\tilde{h}(f) = \mathcal{A}e^{i\Psi}$$

진폭, 위상을 알면
중력파를 기술할 수 있다

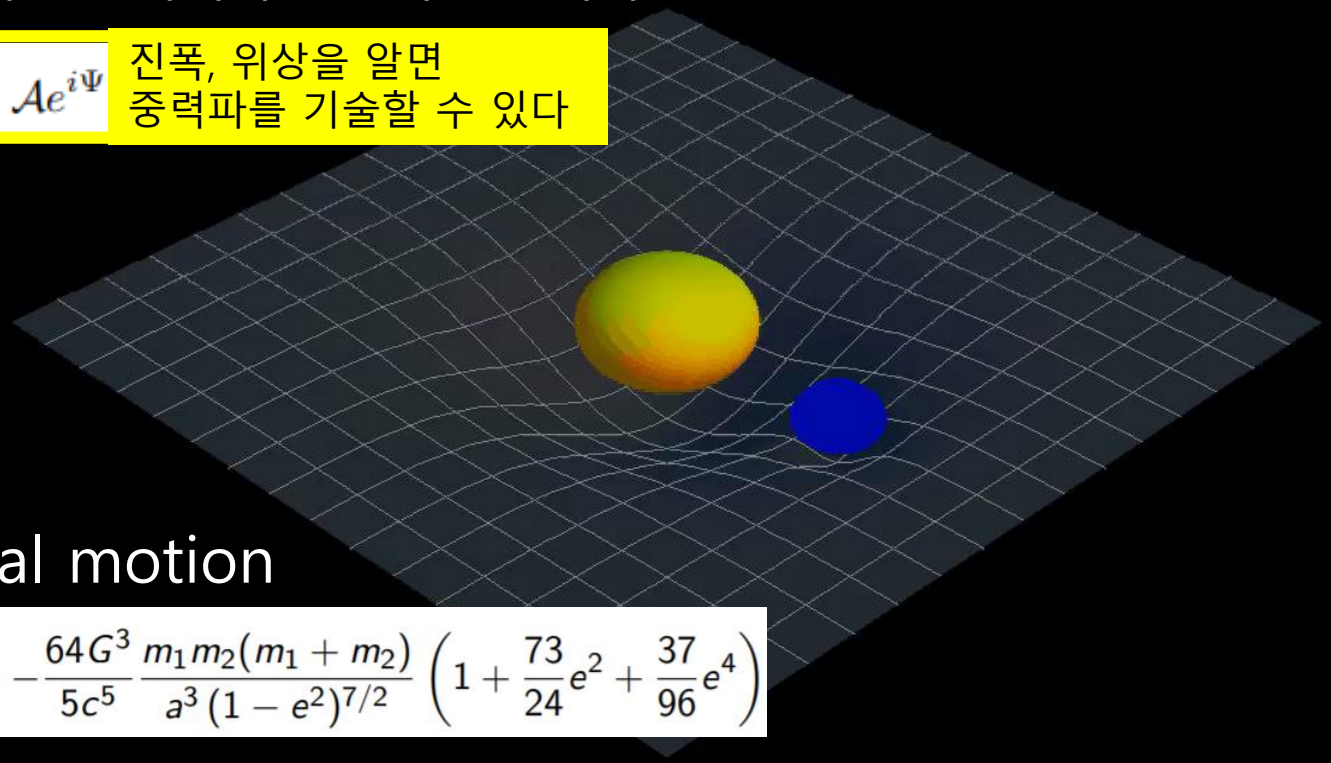

inspiral motion

$$\left\langle \frac{da}{dt} \right\rangle = -\frac{64G^3}{5c^5} \frac{m_1 m_2 (m_1 + m_2)}{a^3 (1 - e^2)^{7/2}} \left(1 + \frac{73}{24}e^2 + \frac{37}{96}e^4\right)$$

circularization

$$\left\langle \frac{de}{dt} \right\rangle = -\frac{304}{15} e \frac{G^3 m_1 m_2 (m_1 + m_2)}{c^5 a^4 (1 - e^2)^{5/2}} \left(1 + \frac{121}{304}e^2\right)$$

Credit: Carl Rodriguez

밀집 쌍성 병합 compact binary coalescences (CBCs)

1975년 전파 관측➔ 중성자별-펄서 쌍성 (1993년 노벨물리학상)

2015년 최초 중력파 관측 ➔ 블랙홀-블랙홀 쌍성 (2017년 노벨물리학상)

검출기: km급 레이저 간섭계 (지구)

주파수 대역: 10-2000 Hz

신호 길이: 0.1초 ~ 1분

신호 모양: 처프 신호 (chirp, 시간이 지남에 따라 주파수가 커지는 신호)

구성 천체: 백색왜성, 중성자별, 별질량 블랙홀 < 300 Msun

공전주기: 케플러 제3법칙 ➔ 공전주파수의 2배 = 중력파 주파수

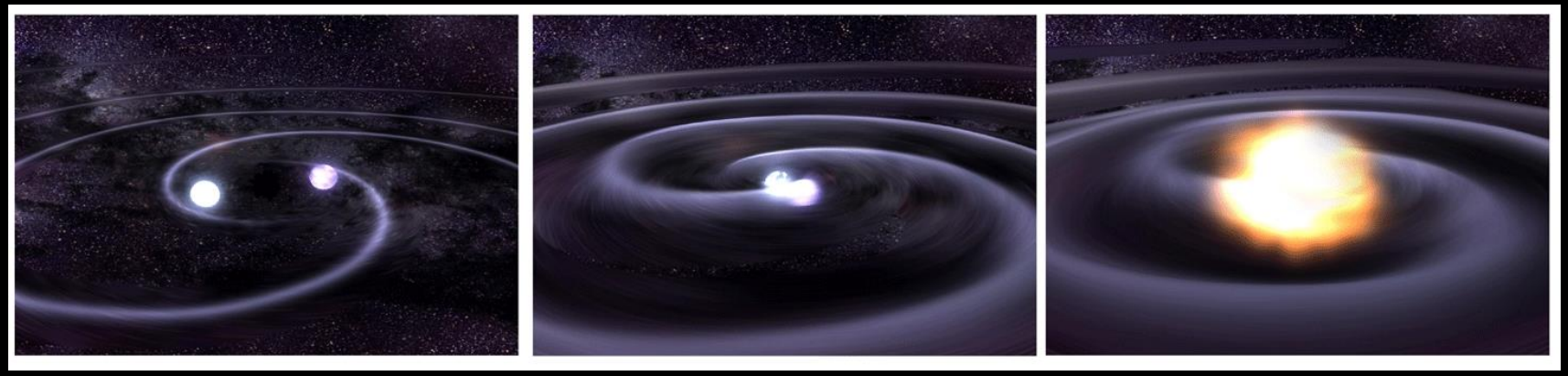

Compact binary coalescences (CBCs) samples

4 catalog papers : GWTC 1, 2, 2.5, 3 "CBC transients only"

Mostly BBHs, SNRs are dominated by inspiral phases

TABLE III.
from GWTC-1

11 events
including
1 NS-NS inspiral

Event	$m_1/M_\odot$	$m_2/M_\odot$	$\mathcal{M}/M_\odot$	$\chi_{\rm eff}$	$M_f/M_\odot$	a_f	$E_{\rm rad}/(M_\odot c^2)$	$\ell_{\rm peak}/({\rm erg\,s^{-1}})$	$d_L/{\rm Mpc}$	z	$\Delta\Omega/{\rm deg}^2$
GW150914	$35.6^{+4.7}_{-3.1}$	$30.6^{+3.0}_{-4.4}$	$28.6^{+1.7}_{-1.5}$	$-0.01^{+0.12}_{-0.13}$	$63.1^{+3.4}_{-3.0}$	$0.69^{+0.05}_{-0.04}$	$3.1^{+0.4}_{-0.4}$	$3.6^{+0.4}_{-0.4}\times10^{56}$	440^{+150}_{-170}	$0.09^{+0.03}_{-0.03}$	182
GW151012	$23.2^{+14.9}_{-5.5}$	$13.6^{+4.1}_{-4.8}$	$15.2^{+2.1}_{-1.2}$	$0.05^{+0.31}_{-0.20}$	$35.6^{+10.8}_{-3.8}$	$0.67^{+0.13}_{-0.11}$	$1.6^{+0.6}_{-0.5}$	$3.2^{+0.8}_{-1.7}\times10^{56}$	1080^{+550}_{-490}	$0.21^{+0.09}_{-0.09}$	1523
GW151226	$13.7^{+8.8}_{-3.2}$	$7.7^{+2.2}_{-2.5}$	$8.9^{+0.3}_{-0.3}$	$0.18^{+0.20}_{-0.12}$	$20.5^{+6.4}_{-1.5}$	$0.74^{+0.07}_{-0.05}$	$1.0^{+0.1}_{-0.2}$	$3.4^{+0.7}_{-1.7}\times10^{56}$	450^{+180}_{-190}	$0.09^{+0.04}_{-0.04}$	1033
GW170104	$30.8^{+7.3}_{-5.6}$	$20.0^{+4.9}_{-4.6}$	$21.4^{+2.2}_{-1.8}$	$-0.04^{+0.17}_{-0.21}$	$48.9^{+5.1}_{-4.0}$	$0.66^{+0.08}_{-0.11}$	$2.2^{+0.5}_{-0.5}$	$3.3^{+0.6}_{-1.0}\times10^{56}$	990^{+440}_{-430}	$0.20^{+0.08}_{-0.08}$	921
GW170608	$11.0^{+5.5}_{-1.7}$	$7.6^{+1.4}_{-2.2}$	$7.9^{+0.2}_{-0.2}$	$0.03^{+0.19}_{-0.07}$	$17.8^{+3.4}_{-0.7}$	$0.69^{+0.04}_{-0.04}$	$0.9^{+0.0}_{-0.1}$	$3.5^{+0.4}_{-1.3}\times10^{56}$	320^{+120}_{-110}	$0.07^{+0.02}_{-0.02}$	392
GW170729	$50.2^{+16.2}_{-10.2}$	$34.0^{+9.1}_{-10.1}$	$35.4^{+6.5}_{-4.8}$	$0.37^{+0.21}_{-0.25}$	$79.5^{+14.7}_{-10.2}$	$0.81^{+0.07}_{-0.13}$	$4.8^{+1.7}_{-1.7}$	$4.2^{+0.9}_{-1.5}\times10^{56}$	2840^{+1400}_{-1360}	$0.49^{+0.19}_{-0.21}$	1041
GW170809	$35.0^{+8.3}_{-5.9}$	$23.8^{+5.1}_{-5.2}$	$24.9^{+2.1}_{-1.7}$	$0.08^{+0.17}_{-0.17}$	$56.3^{+5.2}_{-3.8}$	$0.70^{+0.08}_{-0.09}$	$2.7^{+0.6}_{-0.6}$	$3.5^{+0.6}_{-0.9}\times10^{56}$	1030^{+320}_{-390}	$0.20^{+0.05}_{-0.07}$	308
GW170814	$30.6^{+5.6}_{-3.0}$	$25.2^{+2.8}_{-4.0}$	$24.1^{+1.4}_{-1.1}$	$0.07^{+0.12}_{-0.12}$	$53.2^{+3.2}_{-2.4}$	$0.72^{+0.07}_{-0.05}$	$2.7^{+0.4}_{-0.3}$	$3.7^{+0.4}_{-0.5}\times10^{56}$	600^{+150}_{-220}	$0.12^{+0.03}_{-0.04}$	87
GW170817	$1.46^{+0.12}_{-0.10}$	$1.27^{+0.09}_{-0.09}$	$1.186^{+0.001}_{-0.001}$	$0.00^{+0.02}_{-0.01}$	≤ 2.8	≤ 0.89	≥ 0.04	$\geq 0.1\times10^{56}$	40^{+7}_{-15}	$0.01^{+0.00}_{-0.00}$	16
GW170818	$35.4^{+7.5}_{-4.7}$	$26.7^{+4.3}_{-5.2}$	$26.5^{+2.1}_{-1.7}$	$-0.09^{+0.18}_{-0.21}$	$59.4^{+4.9}_{-3.8}$	$0.67^{+0.07}_{-0.08}$	$2.7^{+0.5}_{-0.5}$	$3.4^{+0.5}_{-0.7}\times10^{56}$	1060^{+420}_{-380}	$0.21^{+0.07}_{-0.07}$	39
GW170823	$39.5^{+11.2}_{-6.7}$	$29.0^{+6.7}_{-7.8}$	$29.2^{+4.6}_{-3.6}$	$0.09^{+0.22}_{-0.26}$	$65.4^{+10.1}_{-7.4}$	$0.72^{+0.09}_{-0.12}$	$3.3^{+1.0}_{-0.9}$	$3.6^{+0.7}_{-1.1}\times10^{56}$	1940^{+970}_{-900}	$0.35^{+0.15}_{-0.15}$	1666

Binary black holes (BH-BH binaries)

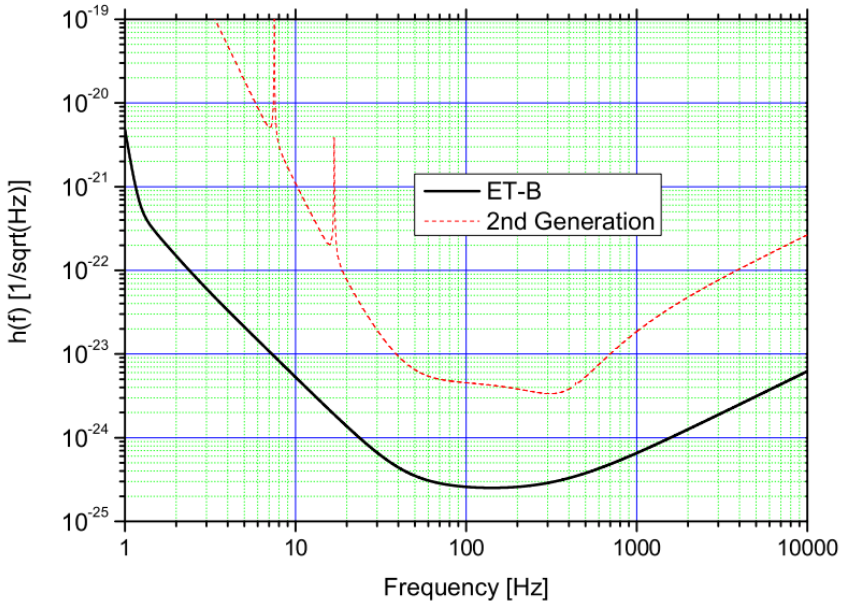

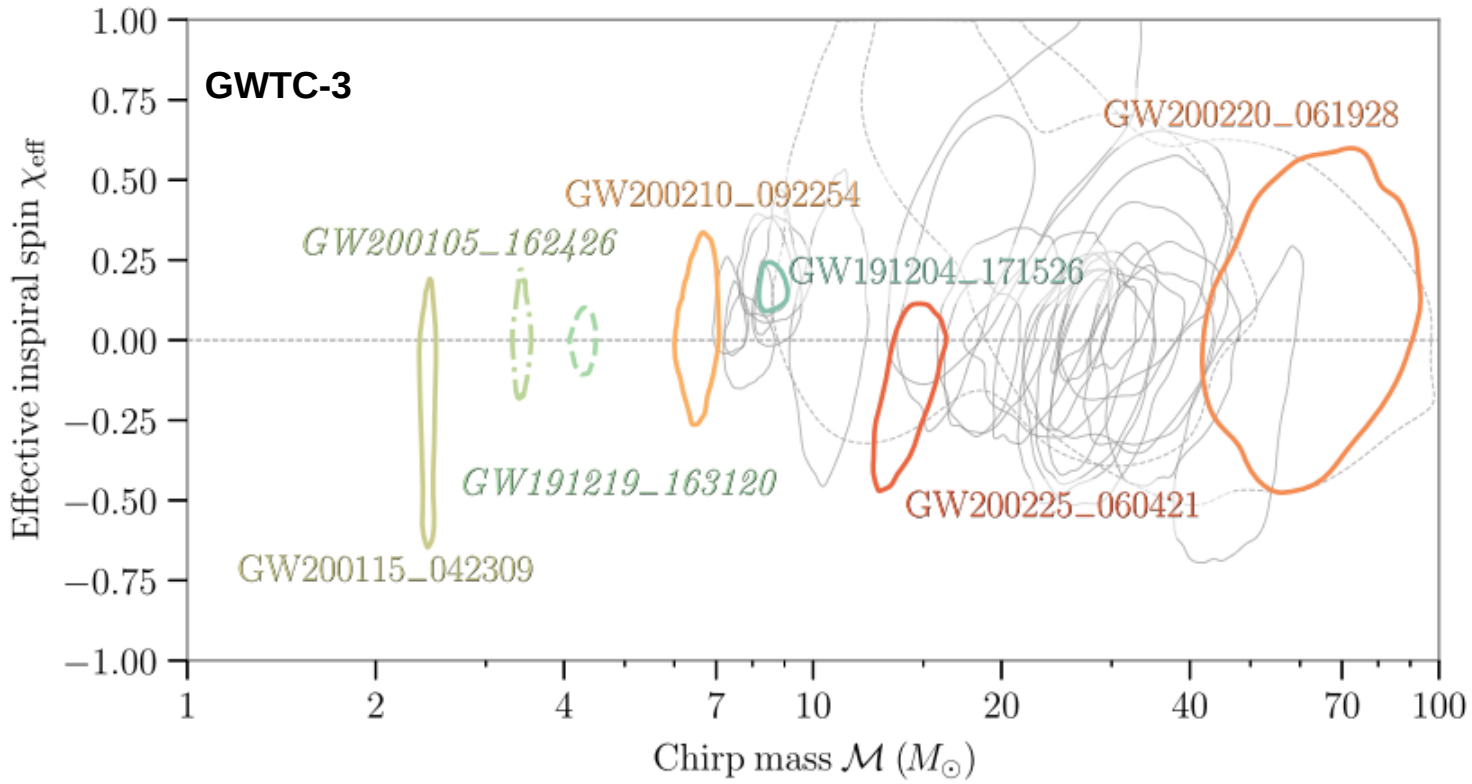

Eccentricity and masses of dynamically-formed BBHs

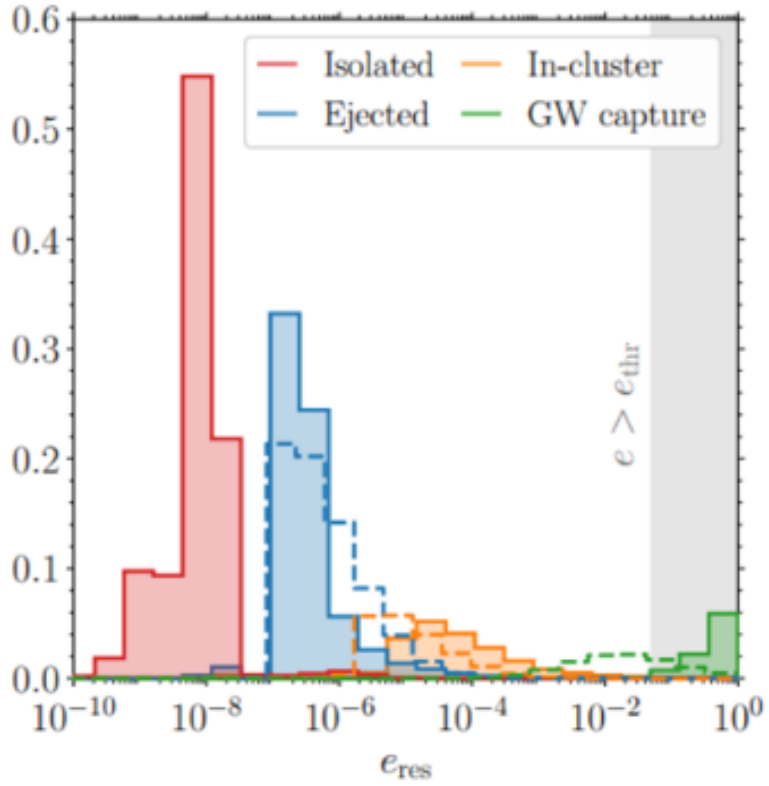

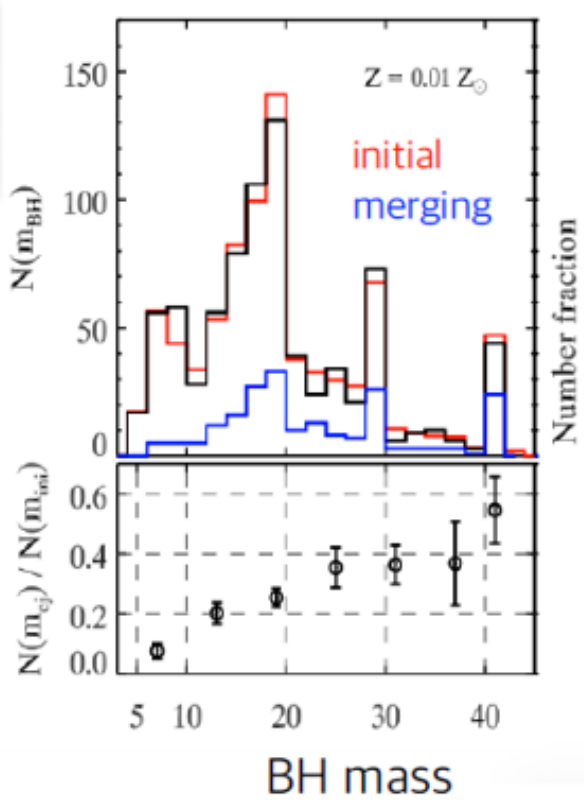

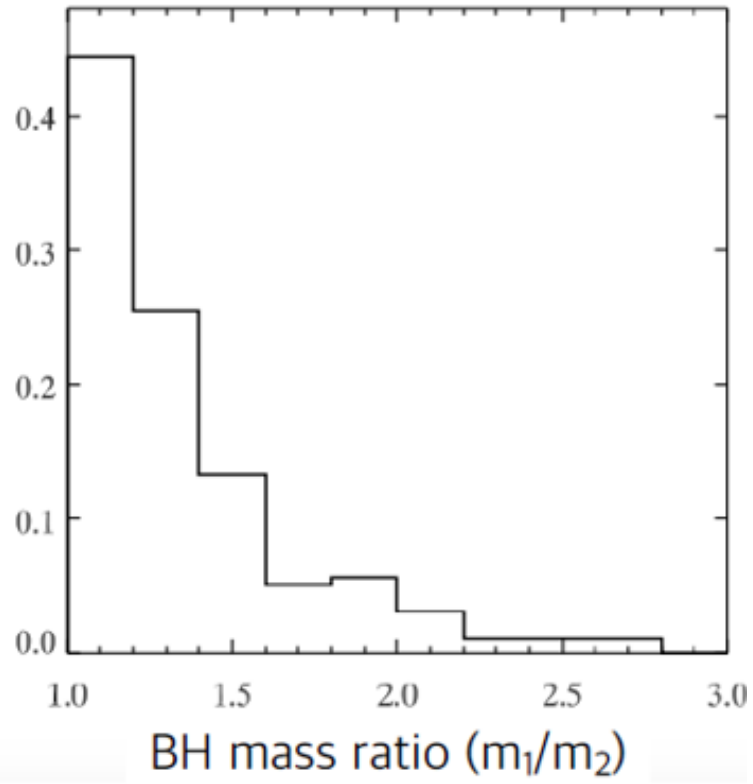

Fumagalli et al (2024)

dynamic pop : Rapster + CMC “Monte Carlo”

isolated (disk) pop : StarTrack

(eccentricity is defined at 10 Hz, e_thr = 0.05

Bae, CK, et al. (2014), Park, CK, et al. (2017)

N-body, 30% of BBHs are ejected,
30% of ejected BBHs are merging ones

StarTrack BH distribution ➔ equal-mass CBCs are majority among the ejected binaries

NS-BH binaries from O3 : GW200105, GW200115

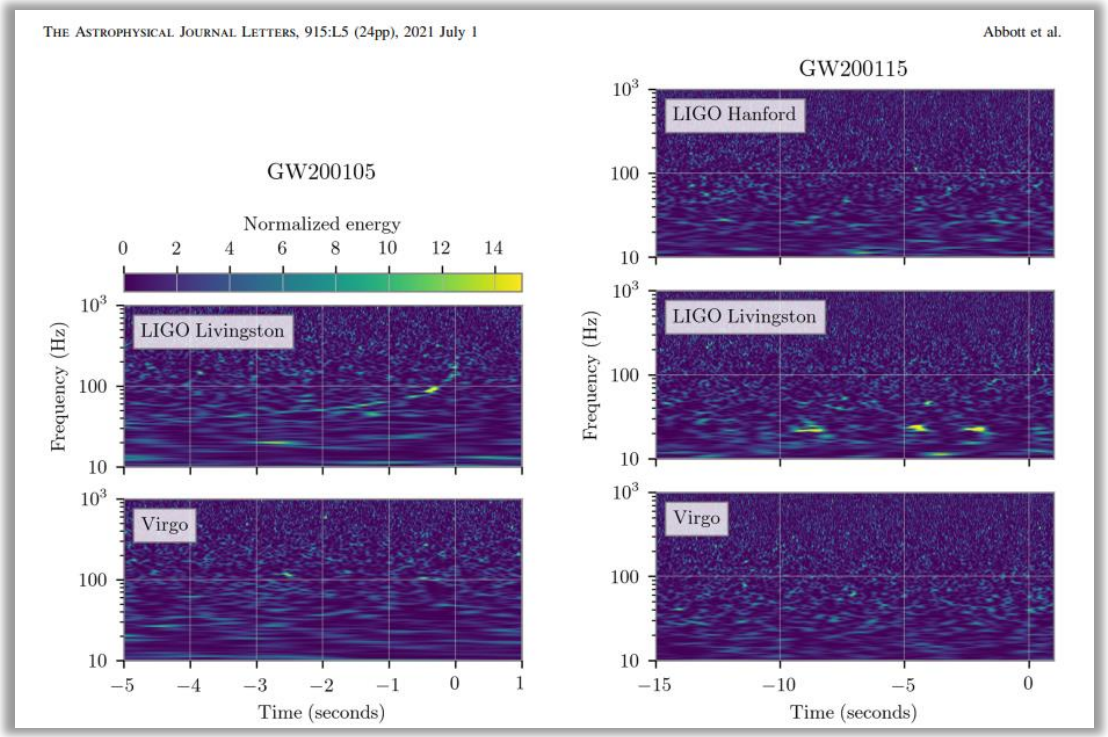

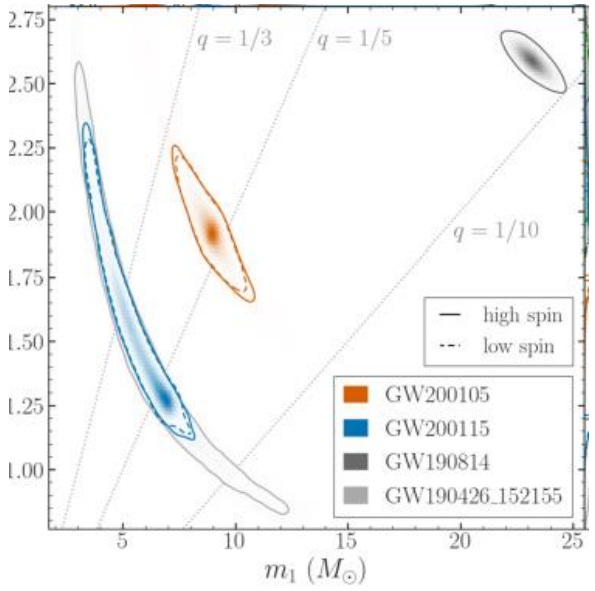

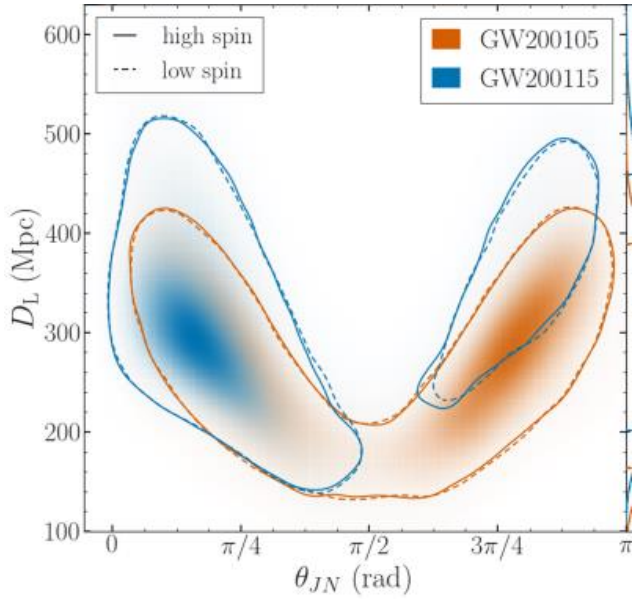

Abbott et al. (2020)
https://iopscience.iop.org/article/10.3847/2041-8213/ac082e/pdf

questions on populations

heaviest NS vs lightest BH : precise mass measurements

inverted evolution : NSBH like PSR J1906+0746?

NS-BH binaries from O3 : GW200105, GW200115

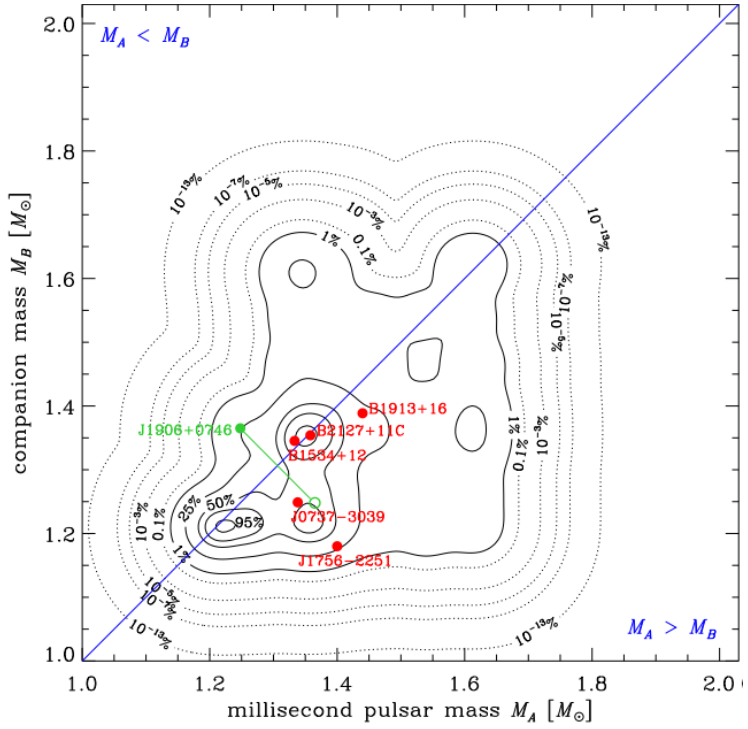

Pejcha et al. (2012)
pulsar vs companion masses

$Z = Z_\odot$

Y_e core

no fallback

$\mathcal{M}_{max} = 100\ M_\odot$

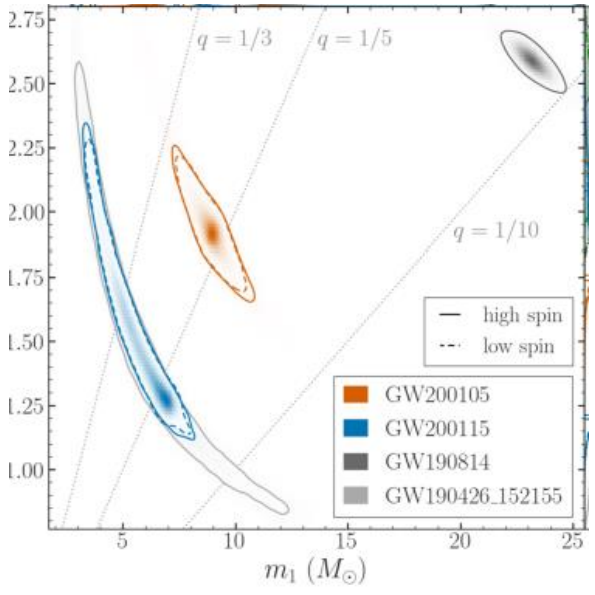

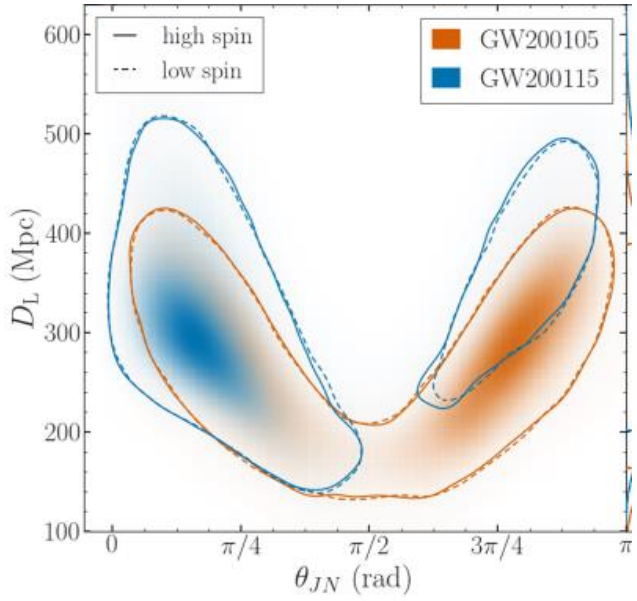

Abbott et al. (2020)
https://iopscience.iop.org/article/10.3847/2041-8213/ac082e/pdf

questions

mass and spin: precise mass/spin measurements

inverted mass-transfer : a NSBH like PSR J1906+0746?

+ **EM counterparts, rates, test of GR . . .**

NS-NS binaries: localization, masses, NS EOS

GW170817/GR170817A (NS-NS) : clear chirp from inspiral motion of the two NSs. Best localization was possible due to its proximity (40 Mpc) + GW polarization wrt response function of L1,H1,V1 detectors
➔ radio to gamma-ray follow-ups, host galaxy (NGC4993), NS-NS merger/short GRB/kilonova scenario

Not so lucky for GW190425 (200 Mpc) for other NS-NS candidates

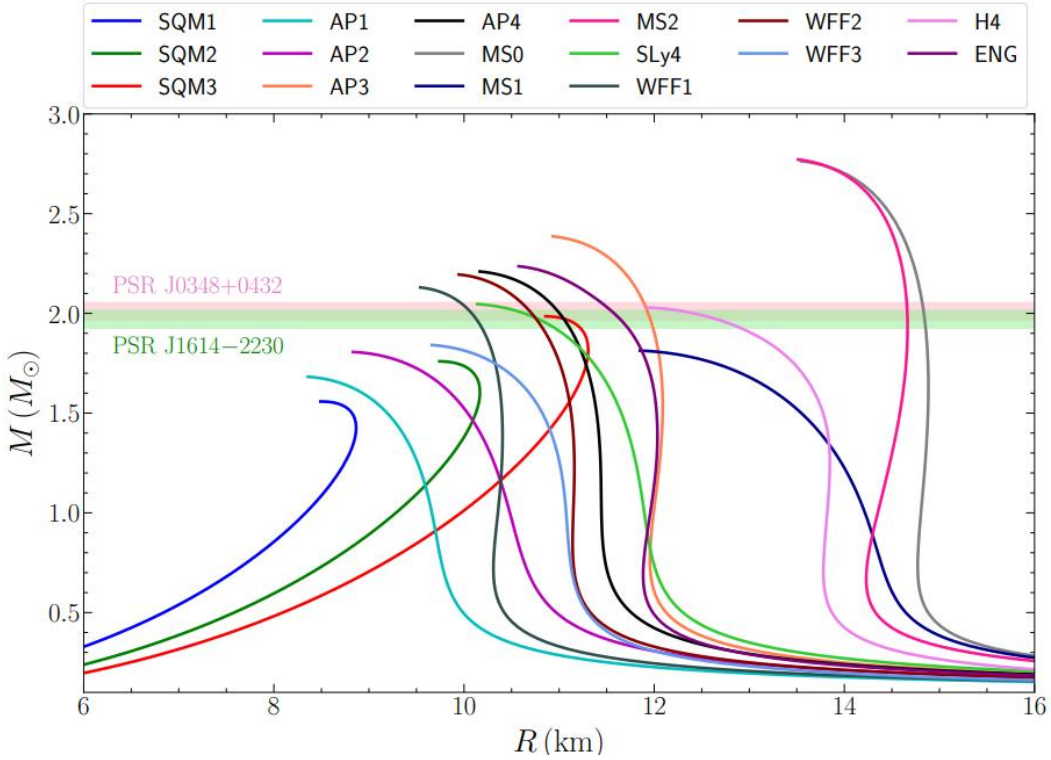

Hu et al. (2023) https://arxiv.org/pdf/2303.17185

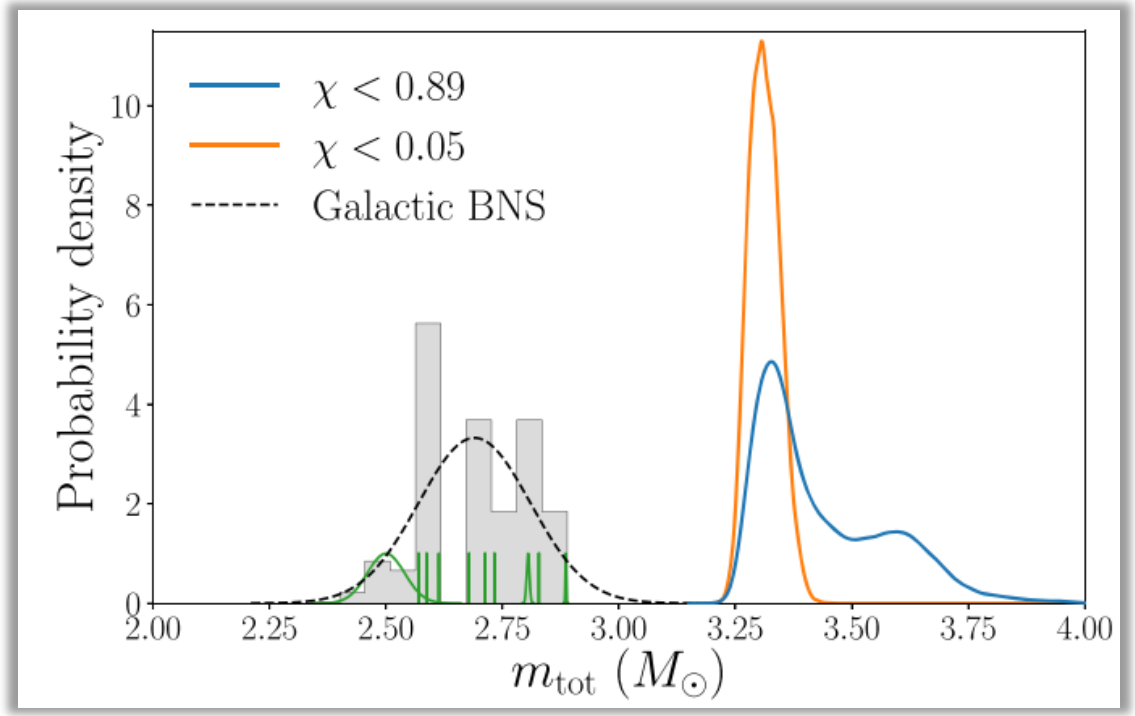

Abbott et al. (2020) https://arxiv.org/pdf/2001.01761

Multi-Messenger Astronomy (MMA) prospects for NS-NS binaries

- 3-detector observation for better localization [Y]
- Good sensitivity toward 600+ Hz to measure tidal deformability parameters from inspiral signals [N]
- Accessibility in 3-6 kHz band for observing the merger phase & remnant [N]

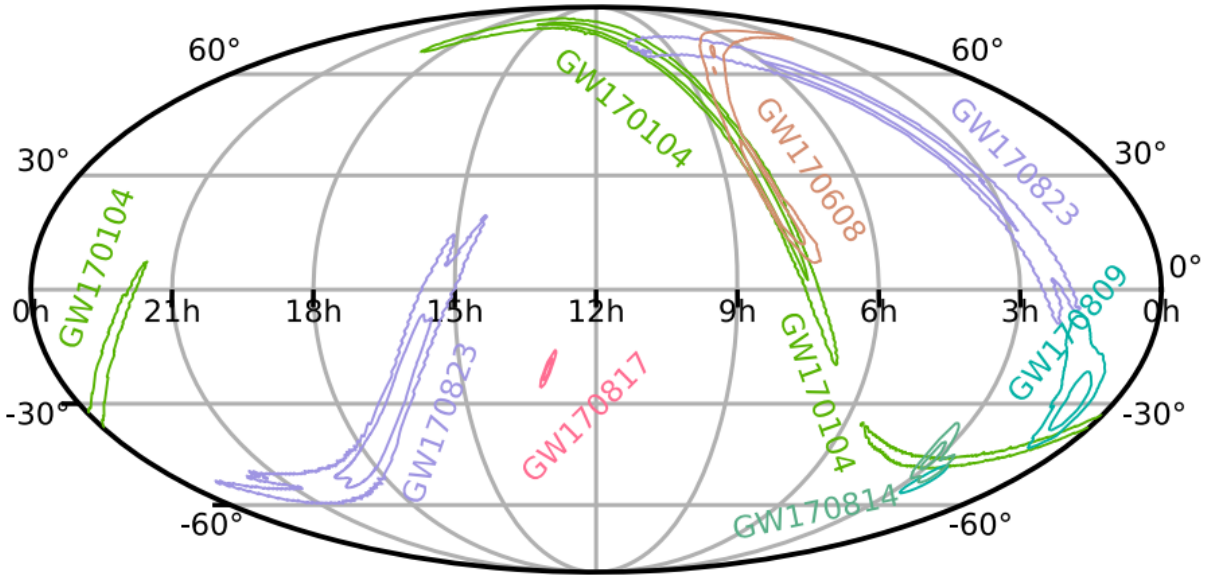

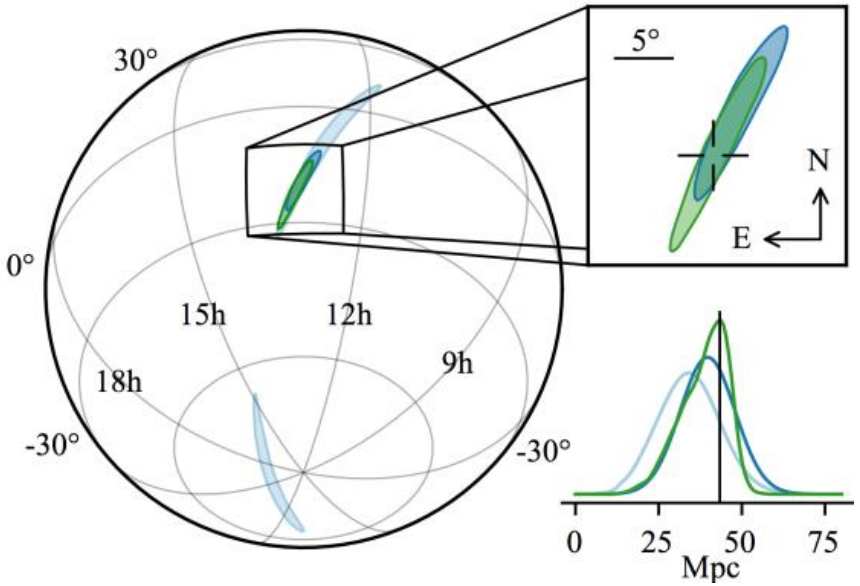

Fig3. from Abbott et al (2017) ApJL

무거운 별의 진화와 중력파원

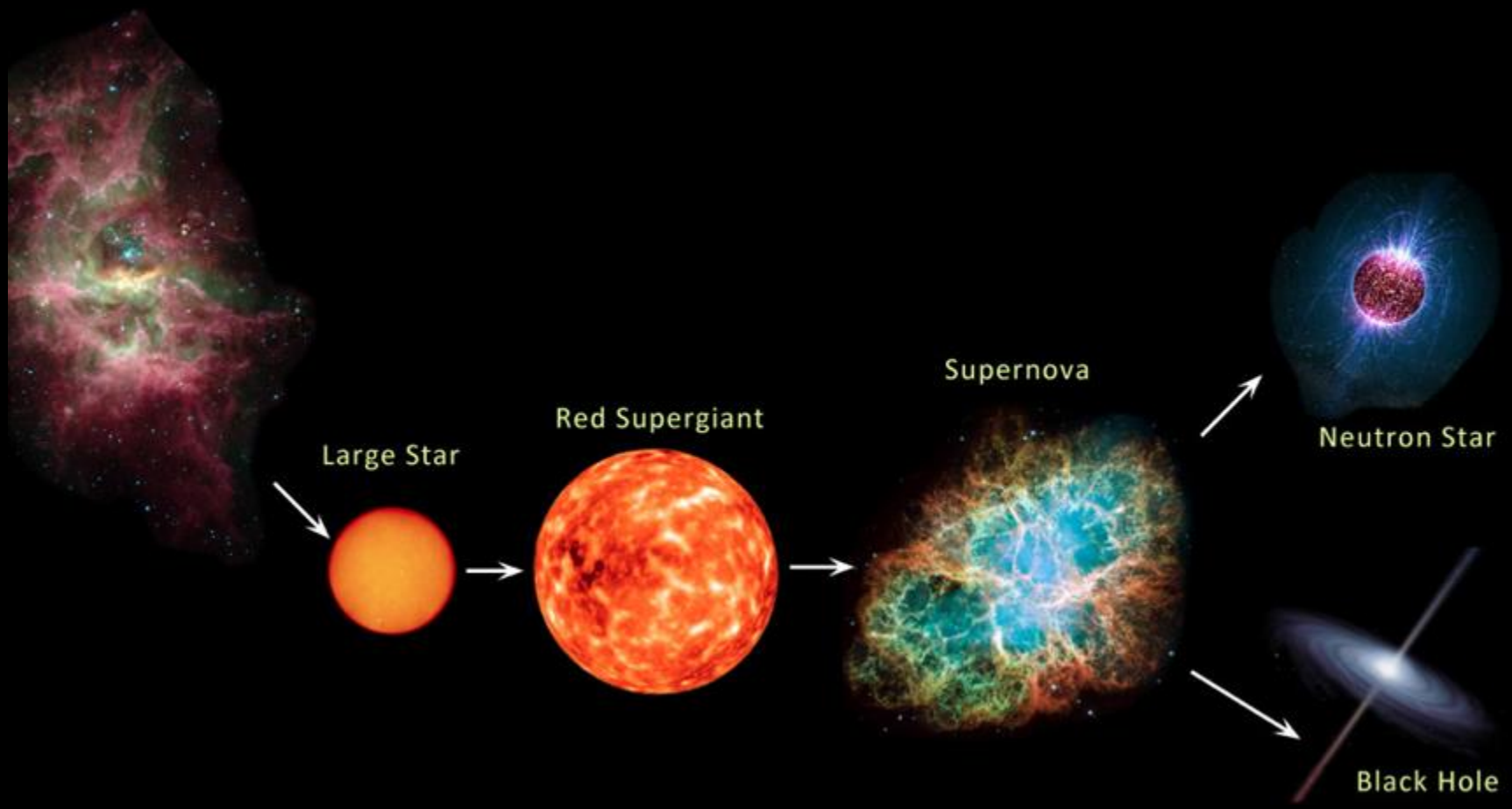

http://essayweb.net/astronomy/images/Stellar_Evolution_large.jpg

isolated binaries formed and resided in a galactic disk

Credit: ESA/Gaia

Evolution of a binary

"standard" binary evolution in a galactic disk

- initial conditions (mass ratio, separation, metallicity)
- common envelope
- supernovae
- mass/angular momentum transfer

and many more!

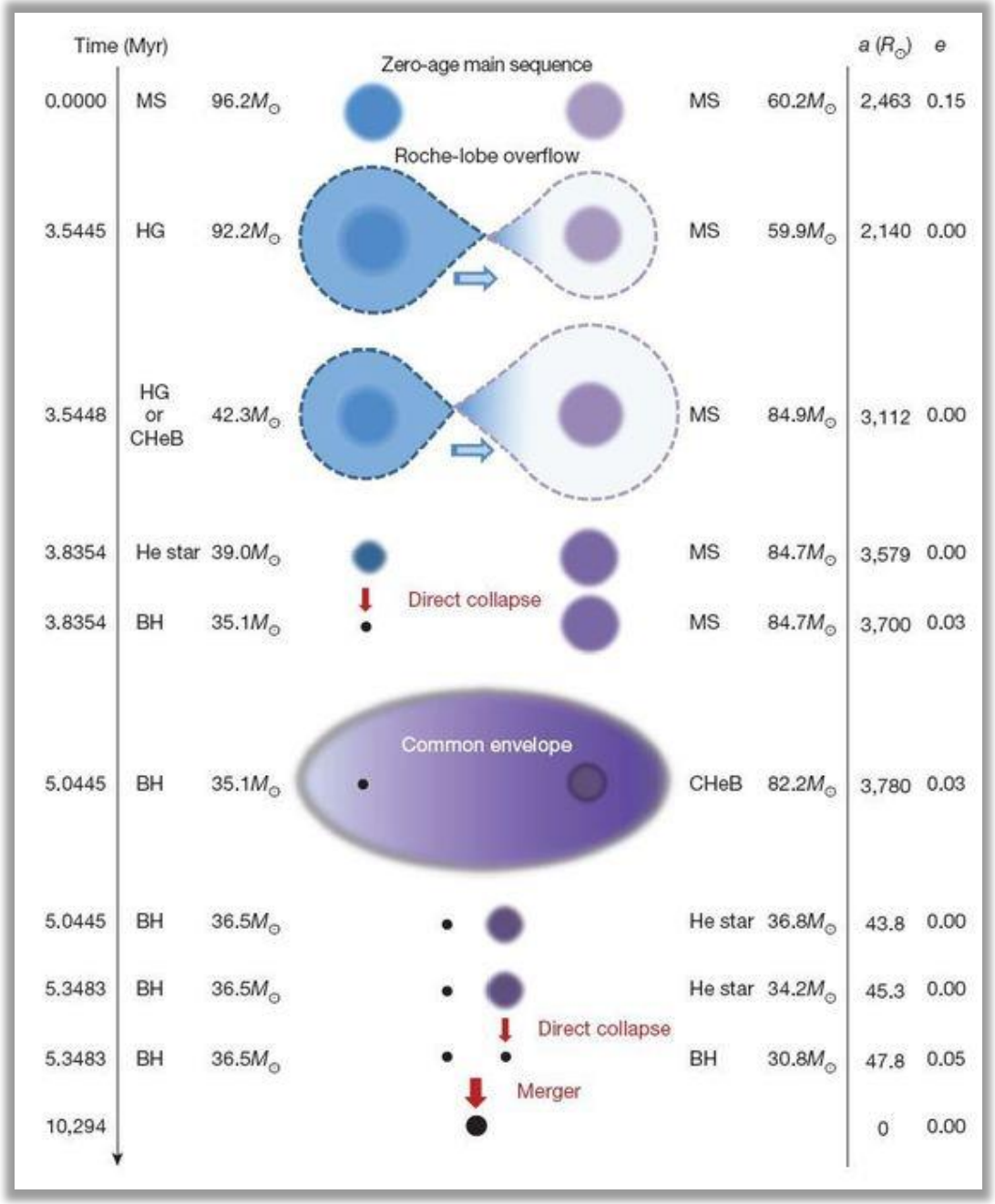

https://www.nature.com/articles/nature18322

Some binaries can be formed in dense stellar environments !
stellar dynamics are important

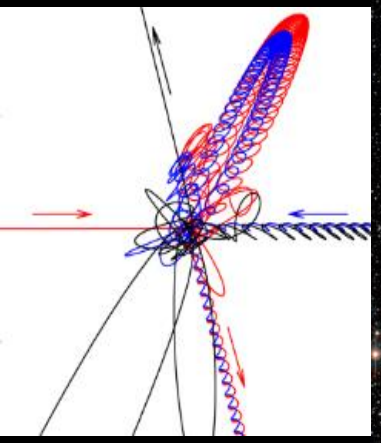

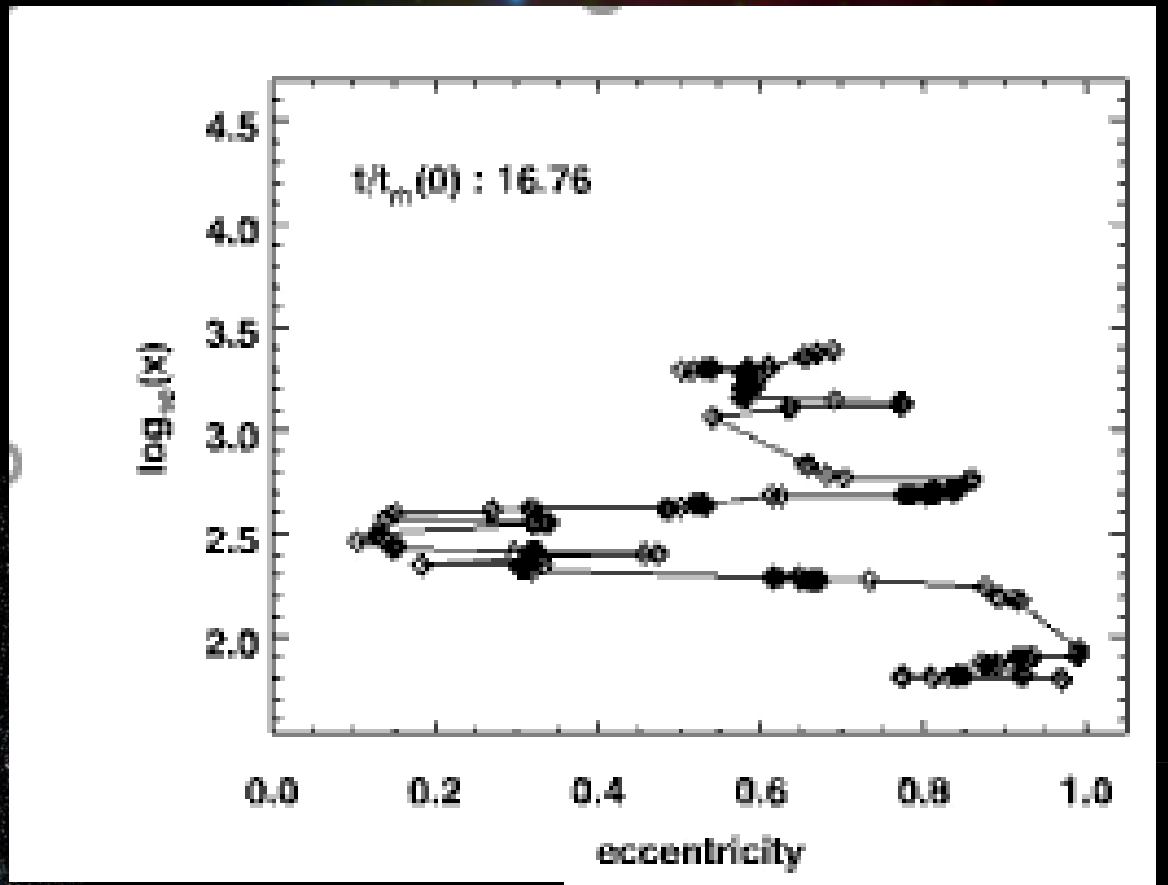

animation by Dawoo Park

NOTE: Residual eccentricity as a systematic uncertainty on the formation channels of binary black holes

Fumagalli et al. (2024)

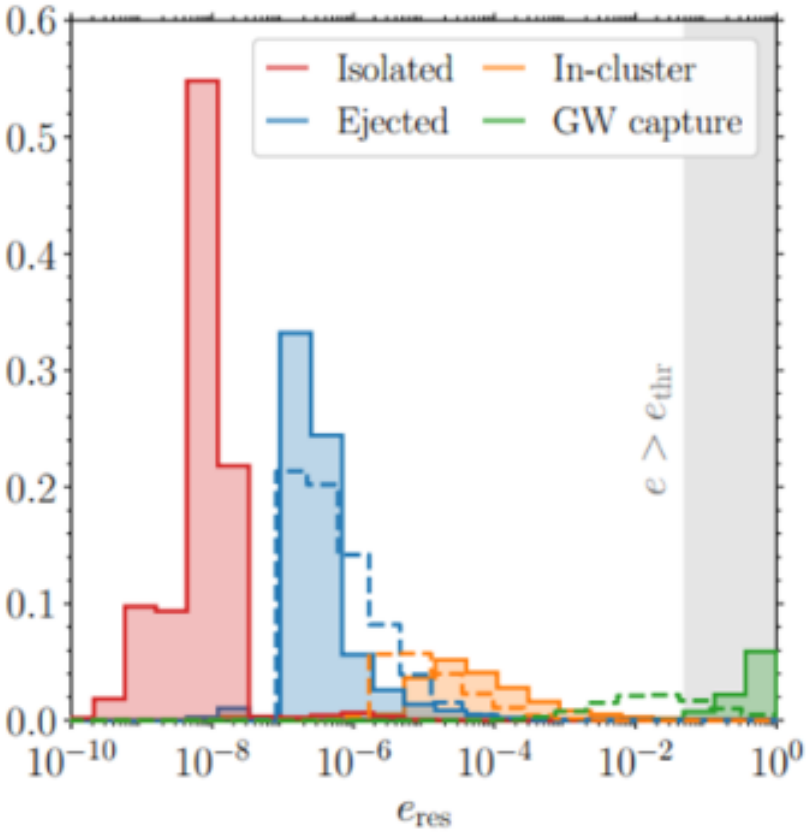

f(e) distribution from astrophysical simulations
dynamic pop: Rapster and CMC “Monte Carlo”
isolated pop: StarTrack

(eccentricity is defined at 10 Hz)

	GW150914			GW151226			BNS		
e_0 (10 Hz)	$\Delta T(0.9)$	$\Delta T(0.99)$	$\Delta T(0.999)$	$\Delta T(0.9)$	$\Delta T(0.99)$	$\Delta T(0.999)$	$\Delta T(0.9)$	$\Delta T(0.99)$	$\Delta T(0.999)$
10^{-1}	0.0525 d	0.293 d	1.08 d	0.356 d	1.99 d	7.31 d	12.5 d	69.9 d	257 d
10^{-2}	18 d	0.282 yr	1.04 yr	0.343 yr	1.91 yr	7.04 yr	12.1 yr	67.3 yr	248 yr
10^{-3}	17.0 yr	94.9 yr	349 yr	115 yr	643 yr	2370 yr	4050 yr	22 600 yr	83 200 yr
10^{-4}	5710 yr	31 900 yr	117 000 yr	38 700 yr	216 000 yr	795 000 yr	1.36 Myr	7.60 Myr	28.0 Myr
10^{-5}	1.92 Myr	10.7 Myr	39.4 Myr	13.0 Myr	72.6 Myr	267 Myr	0.457 Gyr	2.55 Gyr	9.39 Gyr

Favata, CK, et al. (2021)

binary motion and GWs

let's consider binaries consisting of compact objects

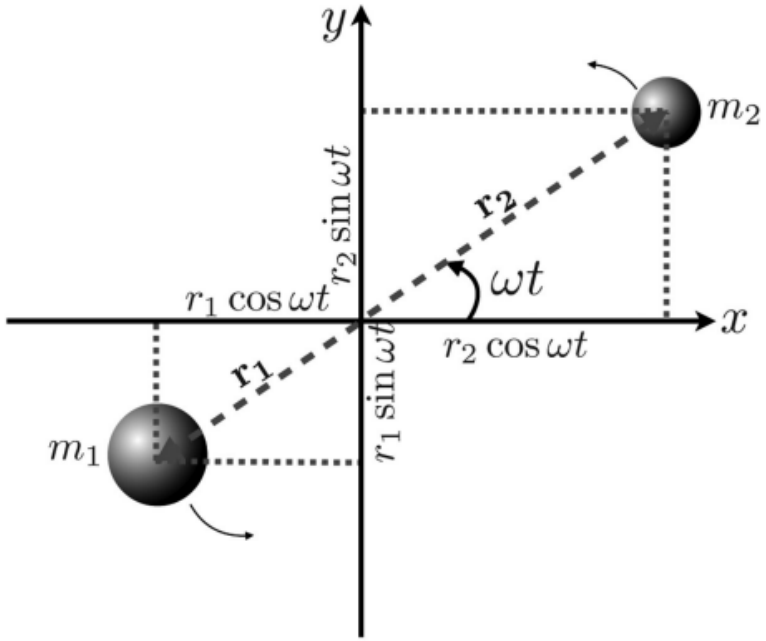

Figure A1 A two-body system, m_1 and m_2 orbiting in the xy-plane around their C.O.M.

중력파원의 질량에는
많은 정보가 담겨있다

$$\tilde{h}(f) = \mathcal{A}e^{i\Psi}$$

GW h(f)
➔ amplitude, phase

- 개별질량(m1, m2), 질량비(q=m2/m1, m2 < m1)

- 처프 질량 chirp mass ➔ 중력파 진폭을 좌우

$$\mathcal{M}_c = (m_1 m_2)^{3/5}/(m_1 + m_2)^{1/5}$$

$$h_0 = \frac{2\mathcal{M}^{5/3}(\pi f_{\rm gw})^{2/3}}{d_L}$$

- 대칭 질량비 symmetric mass ratio ➔ 중력파 위상을 좌우

$$\eta = m_1 m_2/(m_1 + m_2)^2$$

정확한 파형 모델 ➔ 측정 정밀도 개선

GW emission modeling

based on https://link.springer.com/article/10.12942/lrr-2009-2

6.5.3.2 Evolution equation for the orbital phase. Starting from these expressions, one requires that gravitational radiation comes at the expense of the binding energy of the system (see, e.g., [134]):

flux energy loss "luminosity"

$$\mathcal{F} = -\frac{dE}{dt}, \tag{115}$$

the *energy balance* equation. This can then be used to compute the (adiabatic) evolution of the various quantities as a function of time. For instance, the rate of change of the orbital velocity $\omega(t) = v^3/M$ (M being the total mass) can be computed using:

$$\frac{d\omega(t)}{dt} = \frac{d\omega}{dv}\frac{dv}{dE}\frac{dE}{dt} = \frac{3v^2}{M}\frac{\mathcal{F}(v)}{E'(v)}, \quad \frac{dv}{dt} = \frac{dv}{dE}\frac{dE}{dt} = \frac{-\mathcal{F}(v)}{E'(v)}, \tag{116}$$

where $E'(v) = dE/dv$. Supplemented with a differential equation for t,

$$dt = \frac{dt}{dE}\frac{dE}{dv} = -\frac{E'(v)}{\mathcal{F}}, \tag{117}$$

→ integrate dt from ini to coal

one can solve for the evolution of the system's orbital velocity. Similarly, the evolution of the orbital phase $\varphi(t)$ can be computed using

time to merge

$$\frac{d\varphi(t)}{dt} = \frac{v^3}{M}, \quad \frac{dv}{dt} = \frac{-\mathcal{F}(v)}{E'(v)}. \tag{118}$$

orbital evolution and GW emission timescale

based on
https://arxiv.org/pdf/2204.04449.pdf

$$t_c = \frac{5D_0c^5}{256\eta(GM)^3}$$

point-mass, no spin, circular orbit

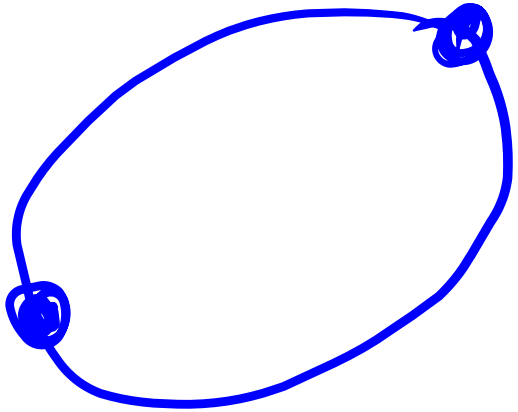

(size
spin
e) affect dynamics timescale

h(t)

데이터로부터 "시스템"을 추정(이해)할 수 있다

$$f_{\mathrm{GW}}^{-8/3}(t) = \frac{(8\pi)^{8/3}}{5}\left(\frac{G\mathcal{M}}{c^3}\right)^{5/3}(t_c - t)$$

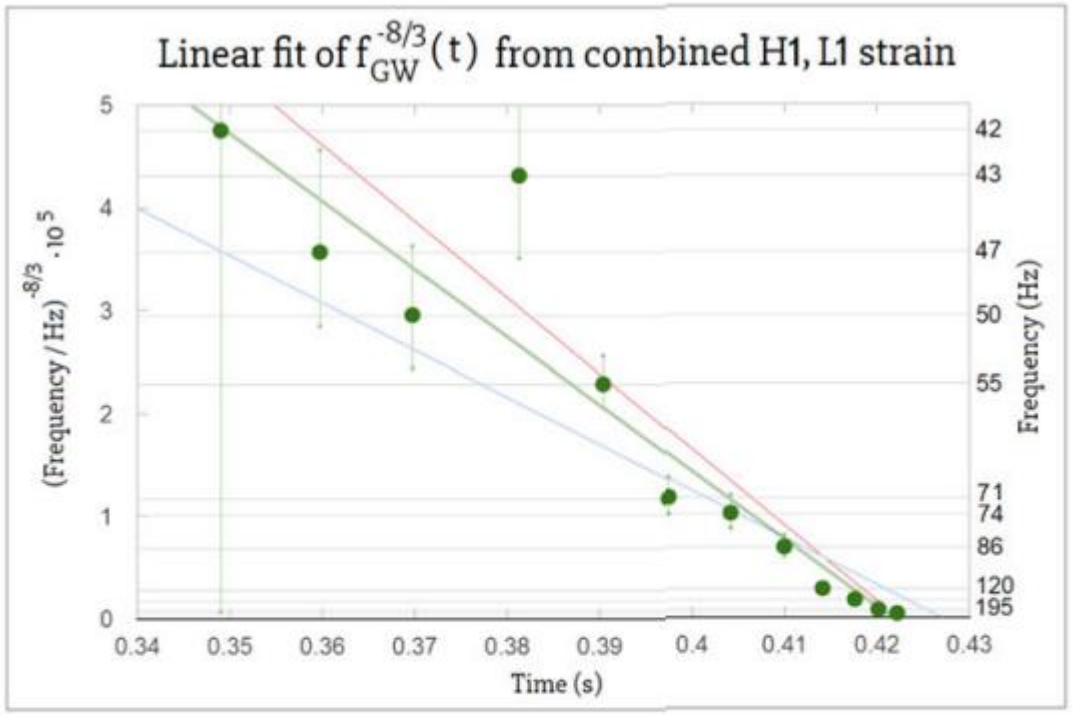

Figure 3 A linear fit (green) of $f_{\mathrm{GW}}^{-8/3}(t)$. While this interpolation used the combined strain data from H1 and L1 (in fact, the sum of L1 with time shifted and sign-flipped H1, as explained). A similar fit can be done using either H1 or L1 strain independently. The

쌍성의 질량, 질량비에 따라 중력파 파형이 달라진다

Chirp mass:

$$\mathcal{M} = \frac{(m_1 m_2)^{3/5}}{(m_1 + m_2)^{1/5}} = \frac{c^3}{G}\left[\frac{5}{96}\pi^{-8/3} f^{-11/3}\dot{f}\right]^{3/5}$$

Mass ratio:

$$q = \frac{m_2}{m_1}$$

$(m_2 < m_1)$

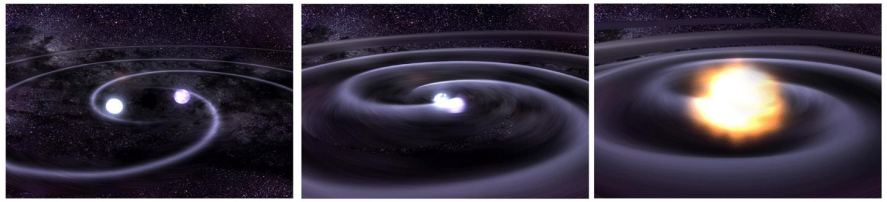

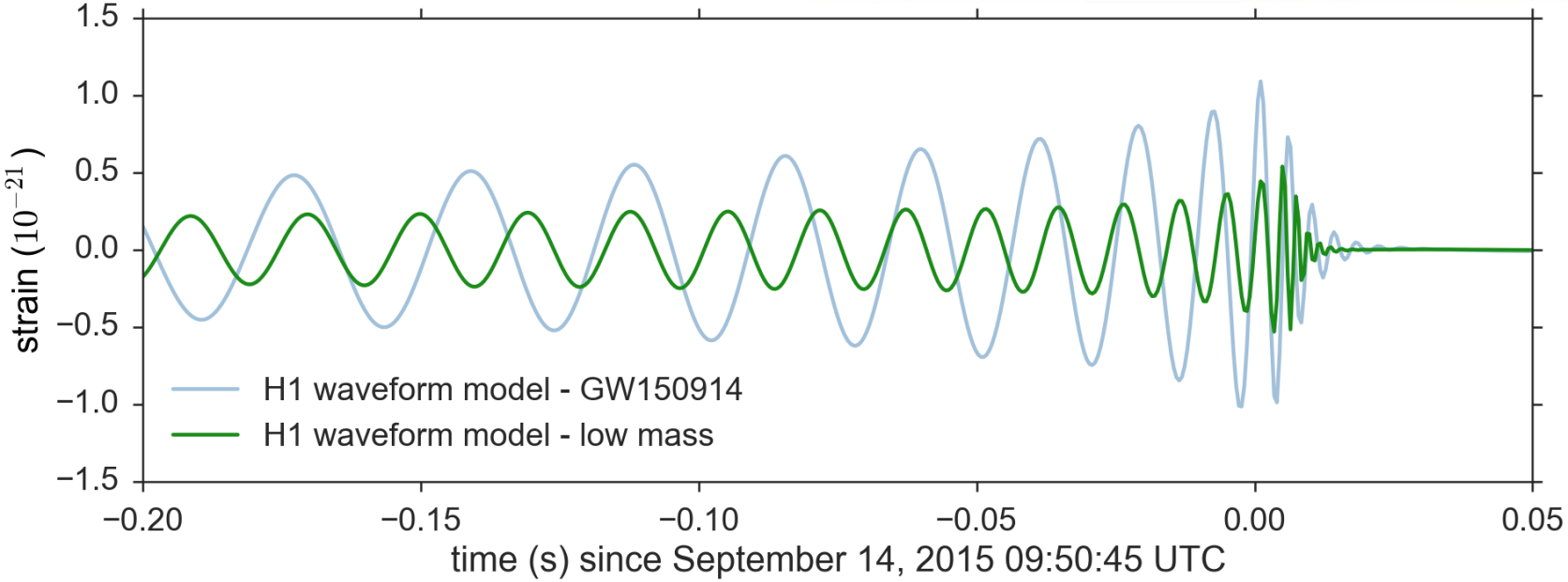

original slide credit: Vivien Raymond

쌍성의 스핀 크기, 각도에 따라 중력파 파형이 달라진다

(s1, s2, L1) ➔ 총 각운동량

스핀-각운동량이 나란하지 않으면 ➔ 세차운동

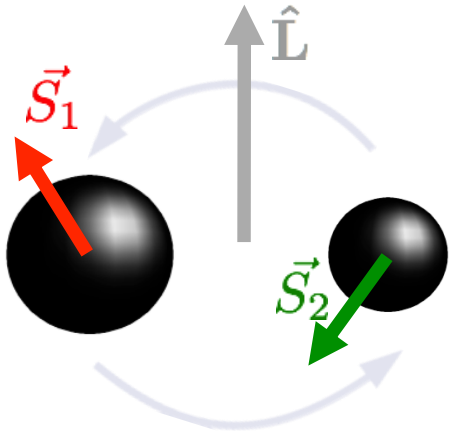

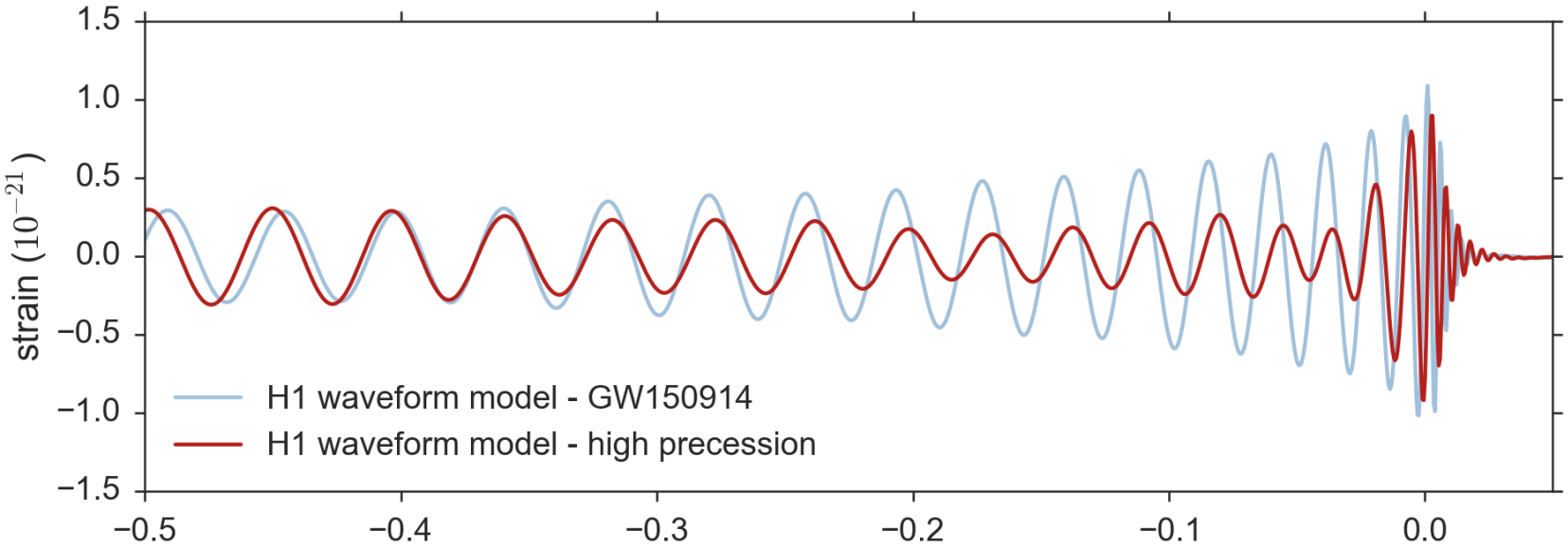

original slide credit: Vivien Raymond

spin directions and eta : GW200105 (BH-NS)

Consider the BH spin only: a1z

Compare two examples:
a1z = +0.5 (up) or **a1z=** -0.5 (down)
Spin directions does not change SNR

When a black hole's spin is **down** (anti-aligned with its orbital angular momentum), the equal-mass posterior can be completely ruled-out.

a poster @ LVK Meeting March 2023 (**G2300256-v2**)

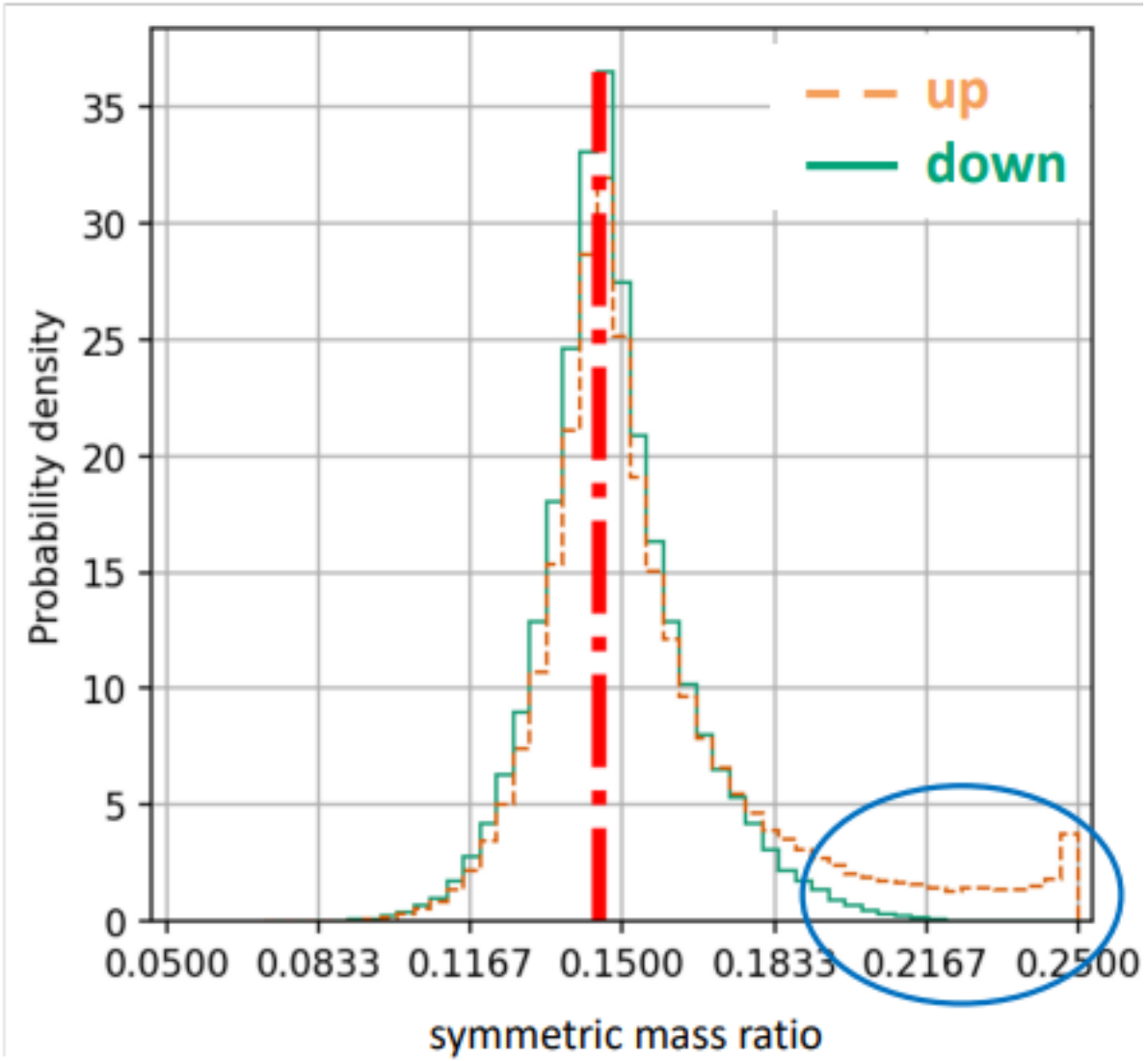

강한 세차운동을 하면서 병합하는 밀집쌍성에서 방출되는 중력파 신호

➔ 단순한 처프 신호에 비해 **복잡하다** + "burst-like"하여 잡음과 혼동되기 쉽다

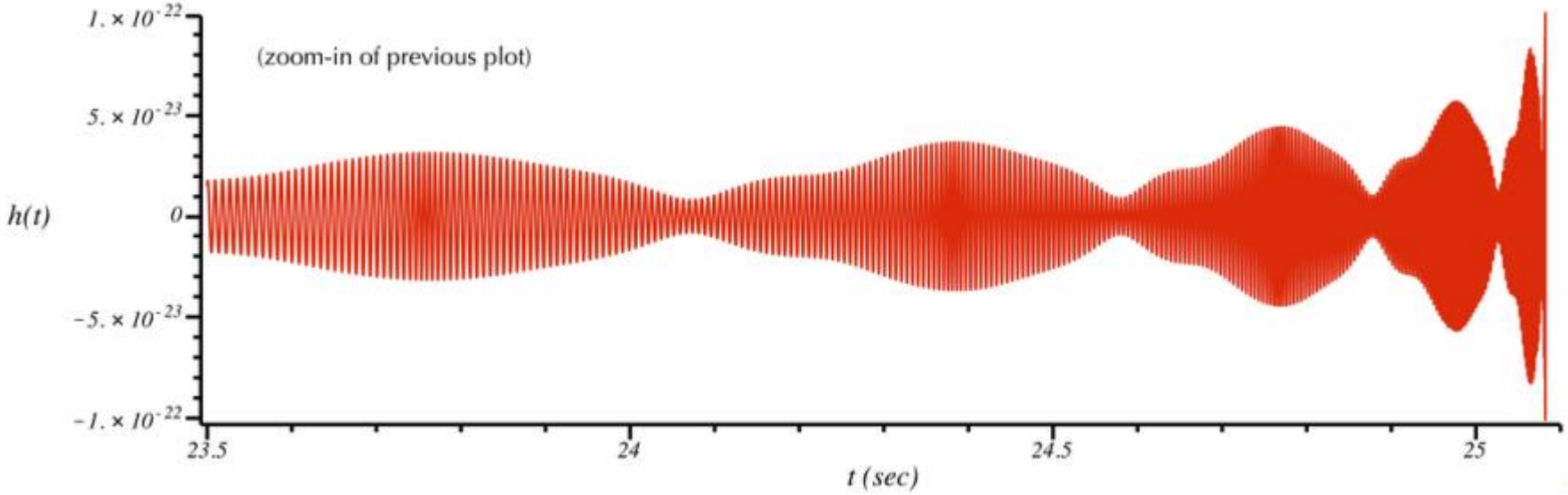

Precessing binary black hole inspiral waveform, m1 = 0.5, m2 = 5 solar masses;
spin1 = 0, spin2 = 0.99 (Kerr dimensionless spin parameter);
spin2 initially misaligned from initial orbital angular momentum by 60 degrees;
detector direction 140 degrees away from initial orbital angular momentum;
initial frequency is 2 f_orb = 40 Hz; ending frequency is 2 f_orb = 4282 Hz.

from Neil Cornish's presentation (2006)
https://indico.cern.ch/event/626266/contributions/2807647/attachments/1593043/2522572/SF6.pdf

쌍성의 궤도모양(이심율)에 따라 중력파 파형이 달라진다

➔ 중력파 신호 분석으로 궤도모양을 재구성할 수 있다

➔ **저주파수 대역 감도 개선** 필요한 이유

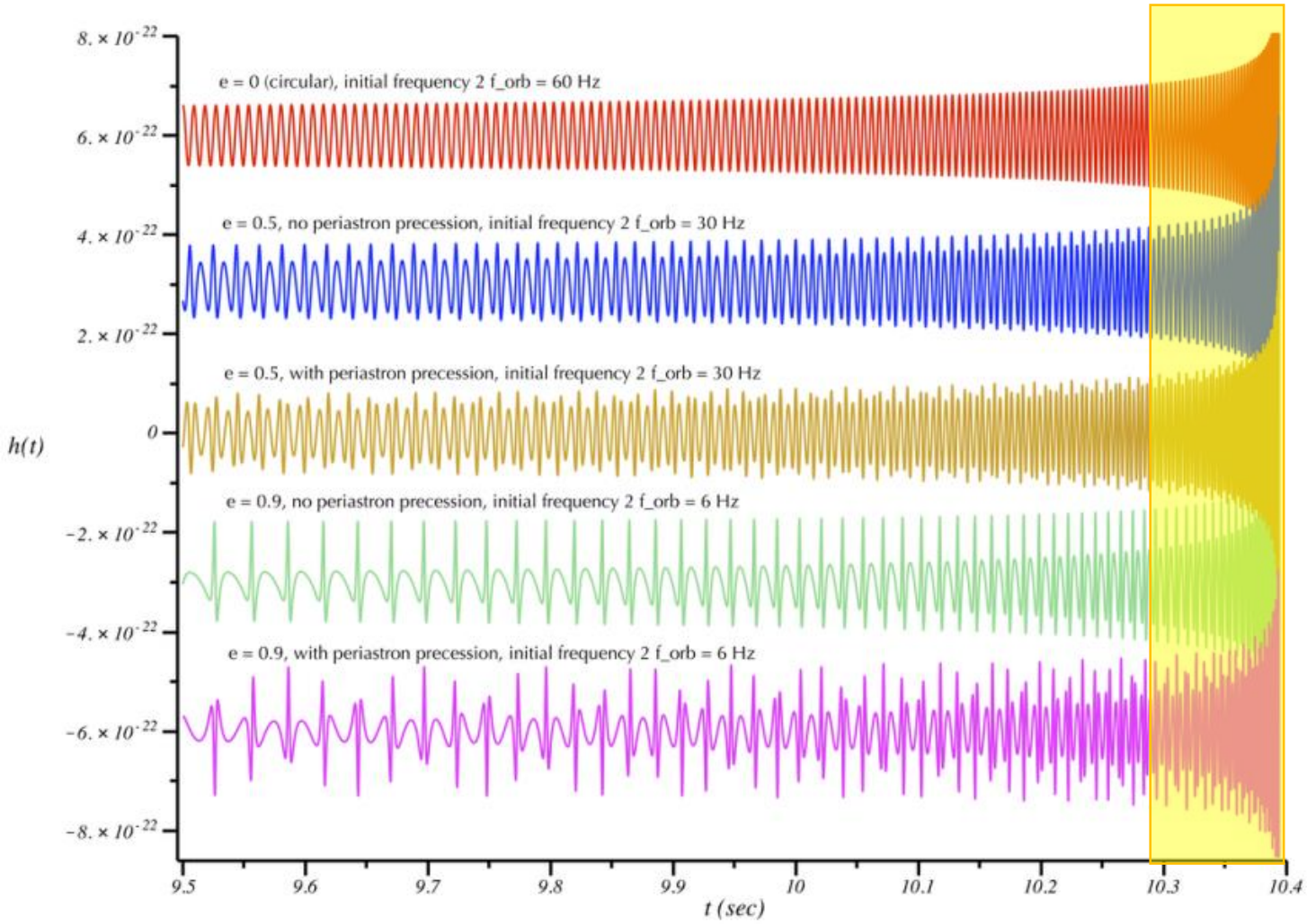

원궤도 "처프신호"

e=0.5

e=0.9 "burst 신호"

How many parameters are required to describe the GW waveform

CBC = compact binary coalescence = collision of two compact objects

These are direct observables available by GW observations

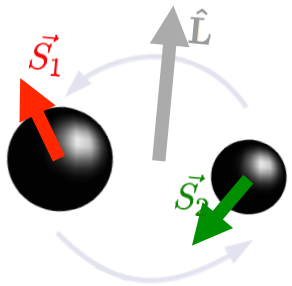

② **two masses (m1, m2) or (eta, chirpmass) etc...**

① d_L **(luminosity) distance**

① ψ **polarization (of gravitational radiation) "angle wrt LOS")**

① ϕ_0 phase

① i inclination (angle of an orbit w.r.t. the line of sight)
eccentricity

① t_c coalescence time

② **two parameters to determine the location in sky (RA, dec)
"latitude, azimuth angle in the Galactic coordinates)**

+ ⑥ for $\vec{S}_1, \vec{S}_2$ + ① for e ⇒ 9 ~ 16 params

step1: varying (m1,m2) to find the “phase”
step2: varying d to find the “amplitude”

in fact, step 1,2 are done at the same time (m1,m2,d)
==> 9~16 parameters to fully characterize a binary

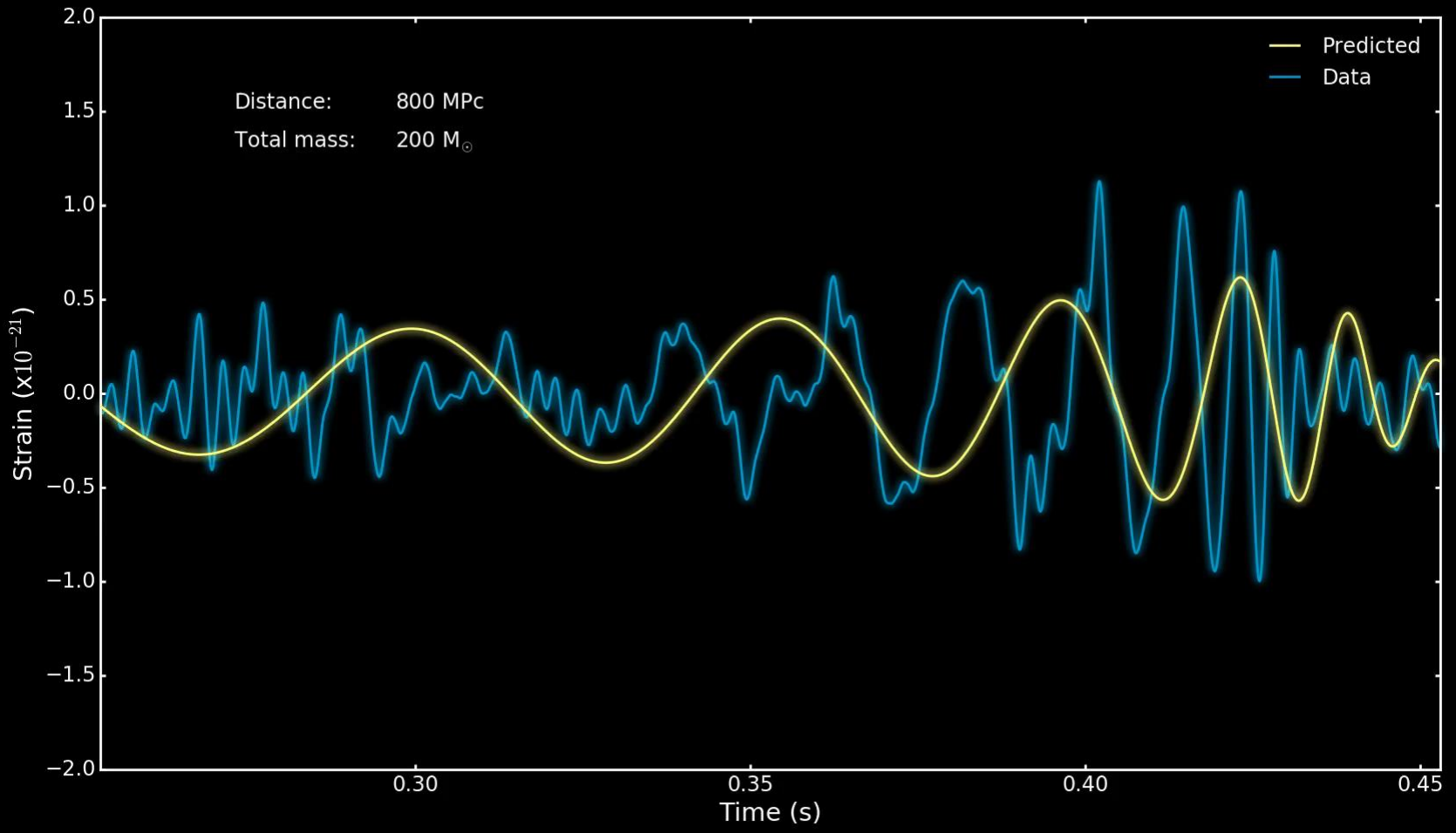

physical parameters in terms of probability density functions

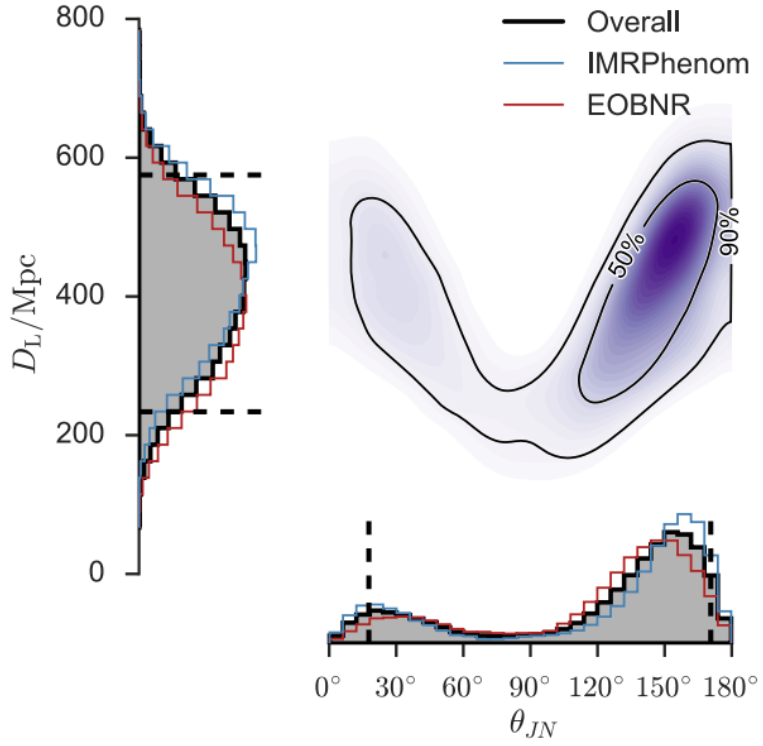

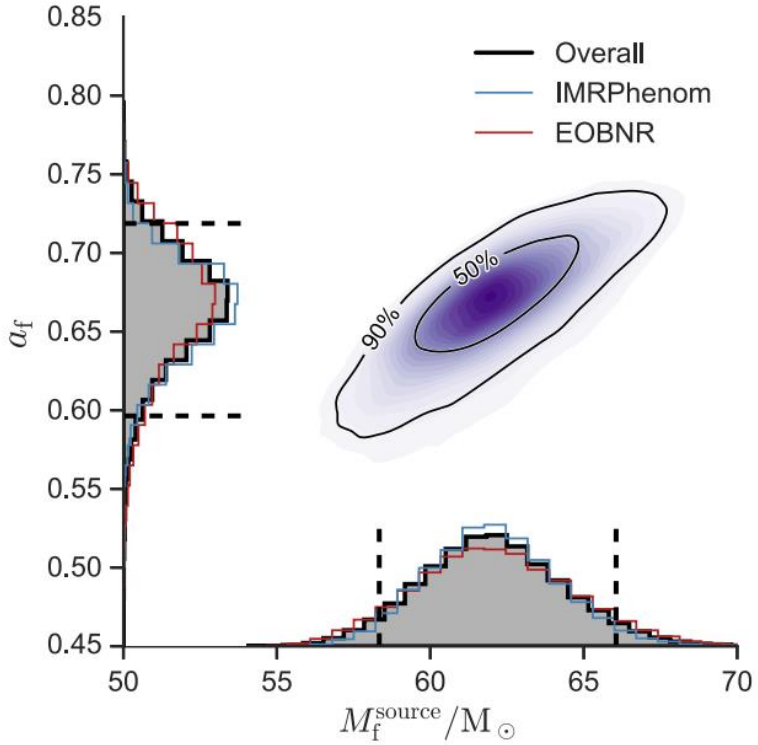

from
https://journals.aps.org/prl/pdf/10.1103/PhysRevLett.116.241102

다중신호 천문학 (2)

김정리
이화여자대학교 물리학과

2024 수치상대론 및 중력파 여름학교

GWTC-2: Compact Binary Coalescences Observed by LIGO and Virgo During the First Half of the Third Observing Run

chirp mass $\mathcal{M} = \frac{(m_1 m_2)^{3/5}}{(m_1 + m_2)^{1/5}}$

effective spin $\chi_{\rm eff} = \frac{(m_1 \vec{\chi}_1 + m_2 \vec{\chi}_2) \cdot \hat{L}_{\rm N}}{m_1 + m_2}$

Event	M ($M_\odot$)	$\mathcal{M}$ ($M_\odot$)	m_1 ($M_\odot$)	m_2 ($M_\odot$)	$\chi_{\rm eff}$	$D_{\rm L}$ (Gpc)	z	$M_{\rm f}$ ($M_\odot$)	$\chi_{\rm f}$	$\Delta\Omega$ (deg^2)	SNR
GW190408_181802	$42.9^{+4.1}_{-2.9}$	$18.3^{+1.8}_{-1.2}$	$24.5^{+5.1}_{-3.4}$	$18.3^{+3.2}_{-3.5}$	$-0.03^{+0.13}_{-0.19}$	$1.58^{+0.40}_{-0.59}$	$0.30^{+0.06}_{-0.10}$	$41.0^{+3.8}_{-2.7}$	$0.67^{+0.06}_{-0.07}$	140	$15.3^{+0.2}_{-0.3}$
GW190412	$38.4^{+3.8}_{-3.7}$	$13.3^{+0.4}_{-0.3}$	$30.0^{+4.7}_{-5.1}$	$8.3^{+1.6}_{-0.9}$	$0.25^{+0.08}_{-0.11}$	$0.74^{+0.14}_{-0.17}$	$0.15^{+0.03}_{-0.03}$	$37.3^{+3.9}_{-3.9}$	$0.67^{+0.05}_{-0.06}$	21	$18.9^{+0.2}_{-0.3}$
GW190413_052954	$56.9^{+13.1}_{-8.9}$	$24.0^{+5.4}_{-3.7}$	$33.4^{+12.4}_{-7.4}$	$23.4^{+6.7}_{-6.3}$	$0.01^{+0.29}_{-0.33}$	$4.10^{+2.41}_{-1.89}$	$0.66^{+0.30}_{-0.27}$	$54.3^{+12.4}_{-8.4}$	$0.69^{+0.12}_{-0.13}$	1400	$8.9^{+0.4}_{-0.8}$
GW190413_134308	$76.1^{+15.9}_{-10.6}$	$31.9^{+7.3}_{-4.6}$	$45.4^{+13.6}_{-9.6}$	$30.9^{+10.2}_{-9.6}$	$-0.01^{+0.24}_{-0.28}$	$5.15^{+2.44}_{-2.34}$	$0.80^{+0.30}_{-0.31}$	$72.8^{+15.2}_{-10.3}$	$0.69^{+0.10}_{-0.12}$	520	$10.0^{+0.4}_{-0.5}$
GW190421_213856	$71.8^{+12.5}_{-8.6}$	$30.7^{+5.5}_{-3.9}$	$40.6^{+10.4}_{-6.6}$	$31.4^{+7.5}_{-8.2}$	$-0.05^{+0.23}_{-0.26}$	$3.15^{+1.37}_{-1.42}$	$0.53^{+0.18}_{-0.21}$	$68.6^{+11.7}_{-8.1}$	$0.68^{+0.10}_{-0.11}$	1000	$10.7^{+0.2}_{-0.4}$
GW190424_180648	$70.7^{+13.4}_{-9.8}$	$30.3^{+5.7}_{-4.2}$	$39.5^{+10.9}_{-6.9}$	$31.0^{+7.4}_{-7.3}$	$0.15^{+0.22}_{-0.22}$	$2.55^{+1.56}_{-1.33}$	$0.45^{+0.22}_{-0.21}$	$67.1^{+12.5}_{-9.2}$	$0.75^{+0.08}_{-0.09}$	26000	$10.4^{+0.2}_{-0.4}$
GW190425	$3.4^{+0.3}_{-0.1}$	$1.44^{+0.02}_{-0.02}$	$2.0^{+0.6}_{-0.3}$	$1.4^{+0.3}_{-0.3}$	$0.06^{+0.11}_{-0.05}$	$0.16^{+0.07}_{-0.07}$	$0.03^{+0.01}_{-0.02}$	–	–	9900	$12.4^{+0.3}_{-0.4}$
GW190426_152155	$7.2^{+3.5}_{-1.5}$	$2.41^{+0.08}_{-0.08}$	$5.7^{+4.0}_{-2.3}$	$1.5^{+0.8}_{-0.5}$	$-0.03^{+0.33}_{-0.30}$	$0.38^{+0.19}_{-0.16}$	$0.08^{+0.04}_{-0.03}$	–	–	1400	$8.7^{+0.5}_{-0.6}$
GW190503_185404	$71.3^{+9.3}_{-8.0}$	$30.1^{+4.2}_{-4.0}$	$42.9^{+9.2}_{-7.8}$	$28.5^{+7.5}_{-7.9}$	$-0.02^{+0.20}_{-0.26}$	$1.52^{+0.71}_{-0.66}$	$0.29^{+0.11}_{-0.11}$	$68.2^{+8.7}_{-7.5}$	$0.67^{+0.09}_{-0.12}$	94	$12.4^{+0.2}_{-0.3}$
GW190512_180714	$35.6^{+3.9}_{-3.4}$	$14.5^{+1.3}_{-1.0}$	$23.0^{+5.4}_{-5.7}$	$12.5^{+3.5}_{-2.5}$	$0.03^{+0.13}_{-0.13}$	$1.49^{+0.53}_{-0.59}$	$0.28^{+0.09}_{-0.10}$	$34.2^{+3.9}_{-3.4}$	$0.65^{+0.07}_{-0.07}$	230	$12.2^{+0.2}_{-0.4}$
GW190513_205428	$53.6^{+8.6}_{-5.9}$	$21.5^{+3.6}_{-1.9}$	$35.3^{+9.6}_{-9.0}$	$18.1^{+7.3}_{-4.2}$	$0.12^{+0.29}_{-0.18}$	$2.16^{+0.94}_{-0.80}$	$0.39^{+0.14}_{-0.13}$	$51.3^{+8.1}_{-5.8}$	$0.69^{+0.14}_{-0.12}$	490	$12.9^{+0.3}_{-0.4}$
GW190514_065416	$64.2^{+16.6}_{-9.6}$	$27.4^{+6.9}_{-4.3}$	$36.9^{+13.4}_{-7.3}$	$27.5^{+8.2}_{-7.7}$	$-0.16^{+0.28}_{-0.32}$	$4.93^{+2.76}_{-2.41}$	$0.77^{+0.34}_{-0.33}$	$61.6^{+16.0}_{-9.2}$	$0.64^{+0.11}_{-0.14}$	2400	$8.2^{+0.3}_{-0.6}$
GW190517_055101	$61.9^{+10.0}_{-9.6}$	$26.0^{+4.2}_{-4.0}$	$36.4^{+11.8}_{-7.8}$	$24.8^{+6.9}_{-7.1}$	$0.53^{+0.20}_{-0.19}$	$2.11^{+1.79}_{-1.00}$	$0.38^{+0.26}_{-0.16}$	$57.8^{+9.4}_{-9.1}$	$0.87^{+0.05}_{-0.07}$	460	$10.7^{+0.4}_{-0.6}$
GW190519_153544	$104.2^{+14.5}_{-14.9}$	$43.5^{+6.8}_{-6.8}$	$64.5^{+11.3}_{-13.2}$	$39.9^{+11.0}_{-10.6}$	$0.33^{+0.19}_{-0.22}$	$2.85^{+2.02}_{-1.14}$	$0.49^{+0.27}_{-0.17}$	$98.7^{+13.5}_{-14.2}$	$0.80^{+0.07}_{-0.12}$	770	$15.6^{+0.2}_{-0.3}$
GW190521	$157.9^{+37.4}_{-20.9}$	$66.9^{+15.5}_{-9.2}$	$91.4^{+29.3}_{-17.5}$	$66.8^{+20.7}_{-20.7}$	$0.06^{+0.31}_{-0.37}$	$4.53^{+2.30}_{-2.13}$	$0.72^{+0.29}_{-0.29}$	$150.3^{+35.8}_{-20.0}$	$0.73^{+0.11}_{-0.14}$	940	$14.2^{+0.3}_{-0.3}$

TABLE VI. Median and 90% symmetric credible intervals on selected source parameters

example of GW data analysis results

$$h_k = F_k^{(+)} h_+ + F_k^{(\times)} h_\times$$

$$h_+(t) = A_{\rm GW}(t)(1+\cos^2\iota)\cos\phi_{\rm GW}(t),$$
$$h_\times(t) = -2A_{\rm GW}(t)\cos\iota\sin\phi_{\rm GW}(t),$$

Properties of the Binary Black Hole Merger GW150914

B. P. Abbott *et al.**
(LIGO Scientific Collaboration and Virgo Collaboration)
(Received 18 February 2016; revised manuscript received 18 April 2016; published 14 June 2016)

PRL 116, 241102 (2016) PHYSICAL REVIEW LETTERS week ending 17 JUNE 2016

TABLE I. Summary of the parameters that characterize GW150914. For model parameters we report the median value as well as the range of the symmetric 90% credible interval [4]; where useful, we also quote 90% credible bounds. For the logarithm of the Bayes factor for a signal compared to Gaussian noise we report the mean and its 90% standard error from 4 parallel runs with a nested sampling algorithm [5]. The source redshift and source-frame masses assume standard cosmology [6]. The spin-aligned EOBNR and precessing IMRPhenom waveform models are described in the text. Results for the effective precession spin parameter χ_p used in the IMRPhenom model are not shown as we effectively recover the prior; we constrain $\chi_p < 0.71$ at 90% probability, see left panel of Fig. 5. The Overall results are computed by averaging the posteriors for the two models. For the Overall results we quote both the 90% credible interval or bound and an estimate for the 90% range of systematic error on this determined from the variance between waveform models. The sky location associated with GW150914 is presented in Fig. 4 and discussed in the text.

	EOBNR	IMRPhenom	Overall
Detector-frame total mass $M/M_\odot$	$70.3^{+5.3}_{-4.8}$	$70.9^{+4.0}_{-3.9}$	$70.6^{+4.6\pm0.5}_{-4.5\pm1.3}$
Detector-frame chirp mass $\mathcal{M}/M_\odot$	$30.2^{+2.5}_{-1.9}$	$30.6^{+1.8}_{-1.8}$	$30.4^{+2.1\pm0.2}_{-1.9\pm0.5}$
Detector-frame primary mass $m_1/M_\odot$	$39.4^{+5.5}_{-4.9}$	$38.5^{+5.6}_{-3.6}$	$38.9^{+5.6\pm0.6}_{-4.3\pm0.4}$
Detector-frame secondary mass $m_2/M_\odot$	$30.9^{+4.8}_{-4.4}$	$32.2^{+3.6}_{-4.8}$	$31.6^{+4.2\pm0.1}_{-4.7\pm0.9}$
Detector-frame final mass $M_{\rm f}/M_\odot$	$67.1^{+4.6}_{-4.4}$	$67.6^{+3.6}_{-3.5}$	$67.4^{+4.1\pm0.4}_{-4.0\pm1.2}$
Source-frame total mass $M^{\rm source}/M_\odot$	$65.0^{+5.0}_{-4.4}$	$65.0^{+4.0}_{-3.6}$	$65.0^{+4.5\pm0.8}_{-4.0\pm0.7}$
Source-frame chirp mass $\mathcal{M}^{\rm source}/M_\odot$	$27.9^{+2.3}_{-1.8}$	$28.1^{+1.7}_{-1.6}$	$28.0^{+2.0\pm0.3}_{-1.7\pm0.3}$
Source-frame primary mass $m_1^{\rm source}/M_\odot$	$36.3^{+5.3}_{-4.5}$	$35.3^{+5.2}_{-3.4}$	$35.8^{+5.3\pm0.9}_{-3.9\pm0.1}$
Source-frame secondary mass $m_2^{\rm source}/M_\odot$	$28.6^{+4.4}_{-4.2}$	$29.6^{+3.3}_{-4.3}$	$29.1^{+3.8\pm0.1}_{-4.3\pm0.7}$
Source-frame final mass $M_{\rm f}^{\rm source}/M_\odot$	$62.0^{+4.4}_{-4.0}$	$62.0^{+3.7}_{-3.3}$	$62.0^{+4.1\pm0.7}_{-3.7\pm0.6}$
Mass ratio q	$0.79^{+0.18}_{-0.19}$	$0.84^{+0.14}_{-0.20}$	$0.82^{+0.17\pm0.01}_{-0.20\pm0.03}$
Effective inspiral spin parameter $\chi_{\rm eff}$	$-0.09^{+0.19}_{-0.17}$	$-0.05^{+0.13}_{-0.15}$	$-0.07^{+0.16\pm0.01}_{-0.17\pm0.05}$
Dimensionless primary spin magnitude a_1	$0.32^{+0.45}_{-0.28}$	$0.32^{+0.53}_{-0.29}$	$0.32^{+0.49\pm0.06}_{-0.29\pm0.01}$
Dimensionless secondary spin magnitude a_2	$0.57^{+0.40}_{-0.51}$	$0.34^{+0.54}_{-0.31}$	$0.44^{+0.50\pm0.08}_{-0.40\pm0.02}$
Final spin $a_{\rm f}$	$0.67^{+0.06}_{-0.08}$	$0.66^{+0.04}_{-0.06}$	$0.67^{+0.05\pm0.01}_{-0.07\pm0.02}$
Luminosity distance D_L/Mpc	390^{+170}_{-180}	440^{+150}_{-180}	$410^{+160\pm20}_{-180\pm40}$
Source redshift z	$0.083^{+0.033}_{-0.036}$	$0.093^{+0.029}_{-0.036}$	$0.088^{+0.032\pm0.005}_{-0.037\pm0.008}$
Upper bound on primary spin magnitude a_1	0.65	0.74	0.69 ± 0.08
Upper bound on secondary spin magnitude a_2	0.93	0.78	0.89 ± 0.13
Lower bound on mass ratio q	0.64	0.68	0.66 ± 0.03
Log Bayes factor $\ln \mathcal{B}_{s/n}$	288.7 ± 0.2	290.3 ± 0.1	...

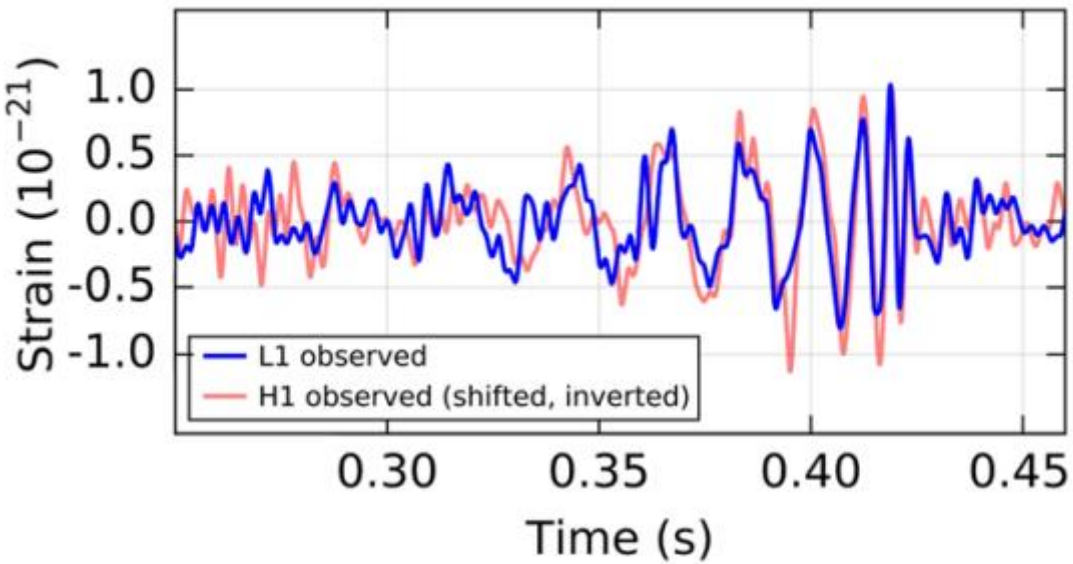

Figure 1 The instrumental strain data in the Livingston detector (blue) and Hanford detector (red), as shown in Figure 1 of [1]. Both have been bandpass- and notch-filtered. The Hanford strain has been shifted back in time by 6.9 ms and inverted. Times shown are relative to 09:50:45 Coordinated Universal Time (UTC) on September 14, 2015.

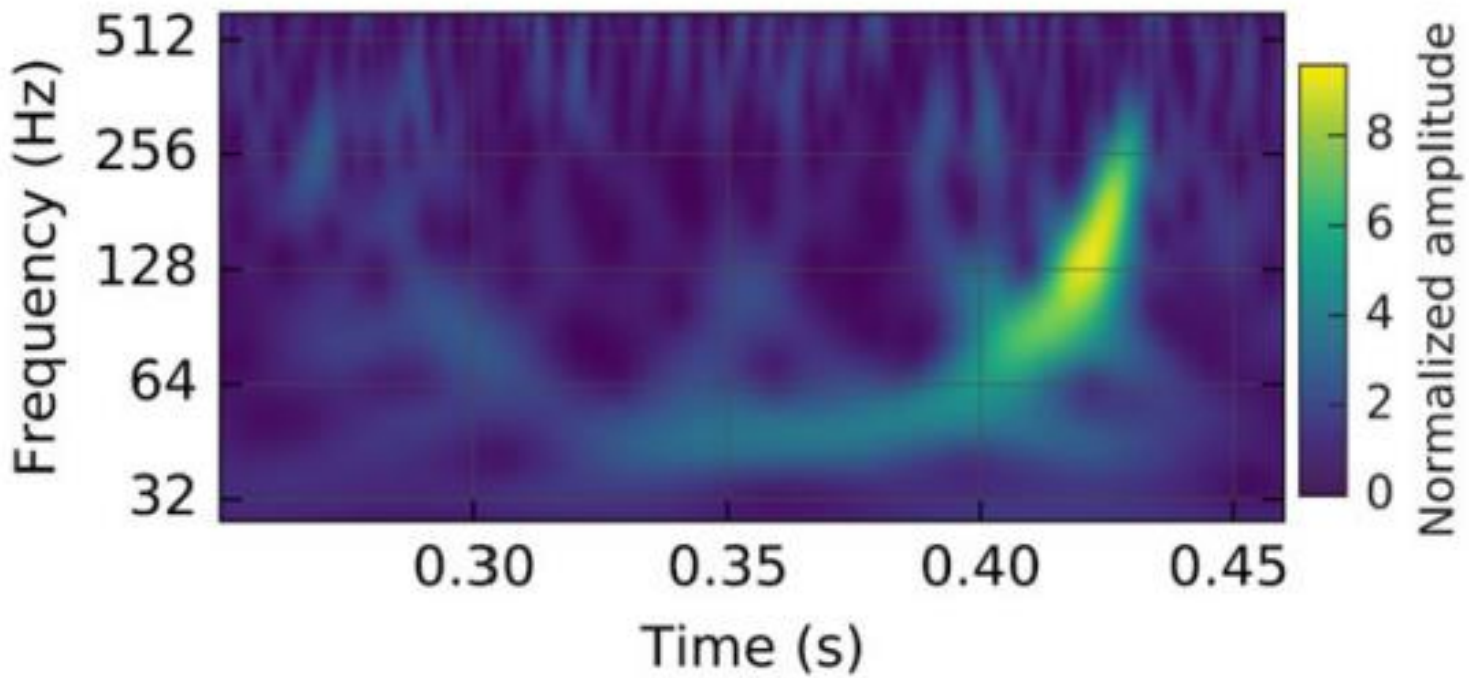

Figure 2 A representation of the strain-data as a time-frequency plot (taken from [1]), where the increase in signal frequency ("chirp") can be traced over time.

Around the time of peak amplitude the bodies therefore had an orbital separation R given by

$$R = \left(\frac{GM}{\omega^2_{\mathrm{Kep}}|_{\mathrm{max}}} \right)^{1/3} = 350\,\mathrm{km}. \tag{9}$$

$$r_{\mathrm{Schwarz}}(m) = \frac{2Gm}{c^2} = 2.95 \left(\frac{m}{\mathrm{M}_\odot} \right) \mathrm{km}$$

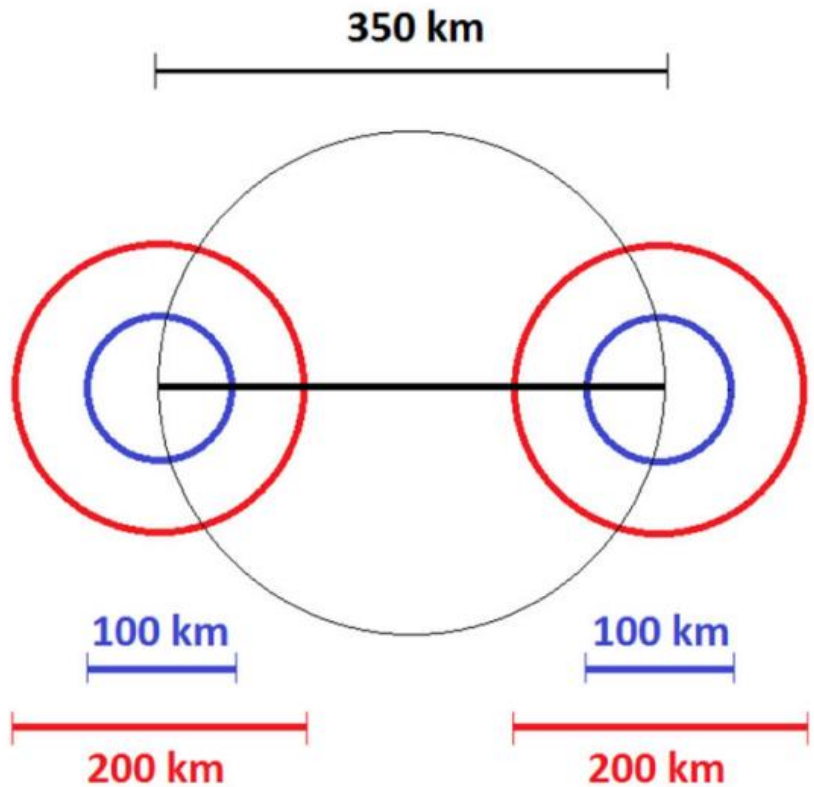

Figure 4 A demonstration of the scale of the orbit at minimal separation (black, 350 km) vs. the scale of the compact radii: Schwarzschild (red, diameter 200 km) and extremal Kerr (blue, diameter 100 km). Note the masses here are equal; as Sec. 4.2 explains, the system is even more compact for unequal masses.

MMA 성공 예: GW170817 “중력파 + 빛” 관측 성공

중력파 검출기(LIGO)와 감마선 위성 망원경(Fermi)등이 각각 GCN에 관측 포스팅
GW170817/GRB170817
➔ 동일한 위치에서 중력파 방출 관측 1.7 초 후에 감마선 폭발이 관측됨
➔ 시공간적 일치로부터 동일 근원 가능성을 염두에 두고 전 세계 80여개 관측 그룹에서 후속 빛 관측 + 중성미자 관측 시도

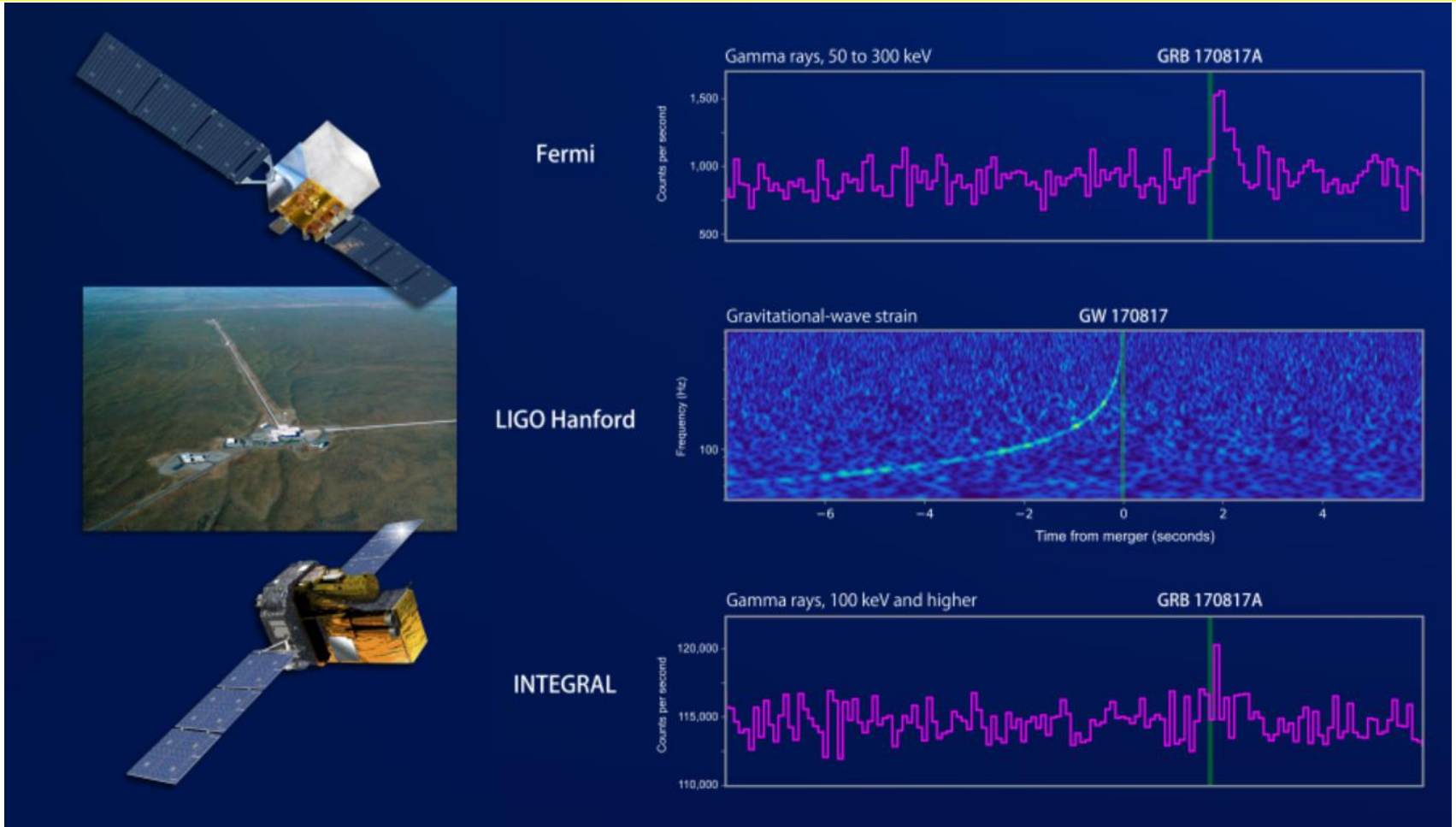

지구 중력파 검출기의 위치(위도, 경도)에 따라

중력파 신호의 도착 시각(GPS time), 편광 등이 달라짐

➔ **천구상의 위치,** 중력파원 신호의 성질(질량)등의 측정에 유리

➔ 중력파원의 정체 (블랙홀 vs 중성자별), 위치, 거리 정보 ➔ **빛 후속관측**

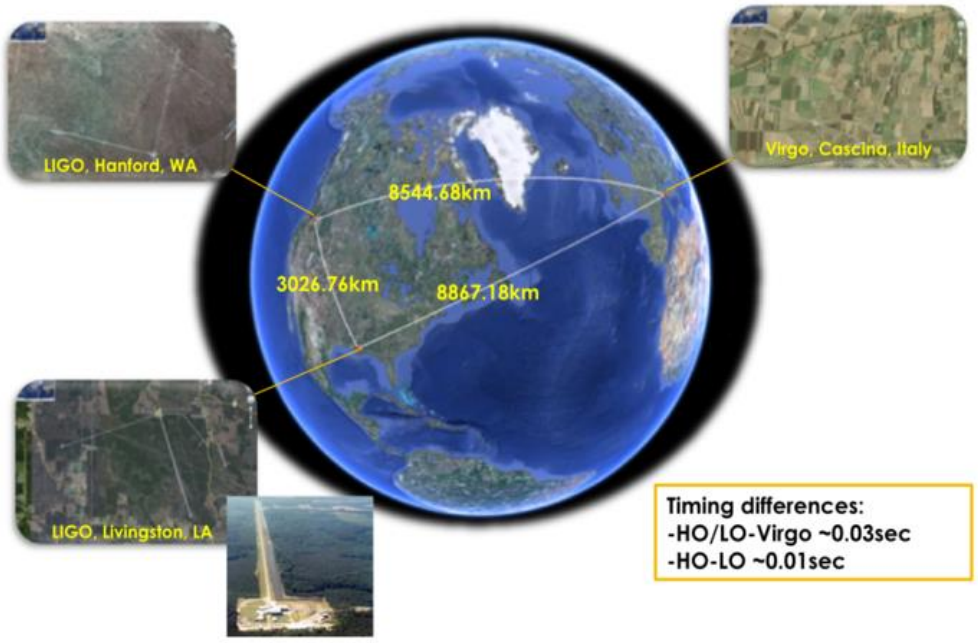

현재 존재하는 중력파 검출기는 모두 북반구

➔ 천구상의 위치 오차가 “길쭉하다”

sky location of GW150914

time delay : 6.9ms between Livinston and Hanford observatories

150 deg^2 (50% probability) – 610 deg^2 (90% probability)

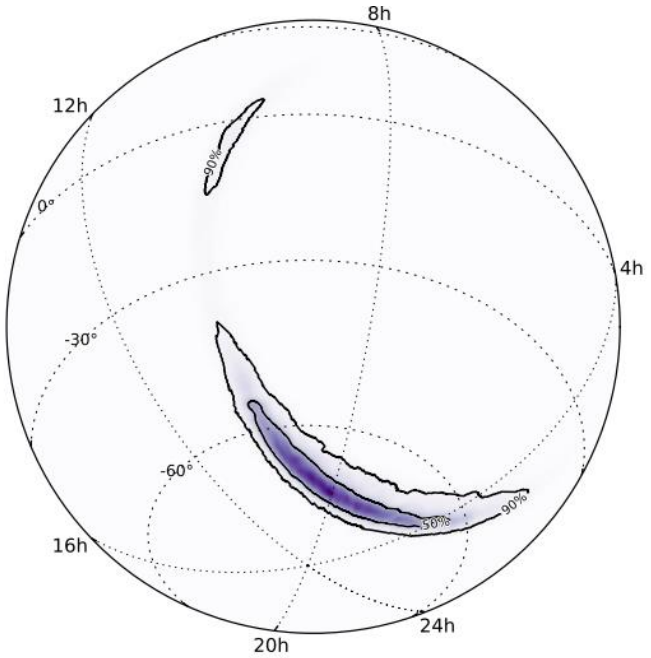

about 31 arcmin = 0.5 deg

The angle covered by the diameter of the full moon is about 31 arcmin or 1/2°, so astronomers would say the Moon's angular diameter is 31 arcmin, or the Moon subtends an angle of 31 arcmin.

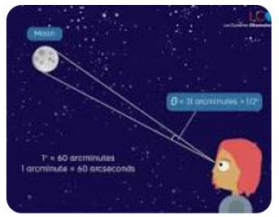

1 deg = 60 armic = 3600 arcsec

short gamma-ray bursts (sGRB

2초 이하의 짧은 시간 동안 감마선이
폭발적으로 방출되는 현상

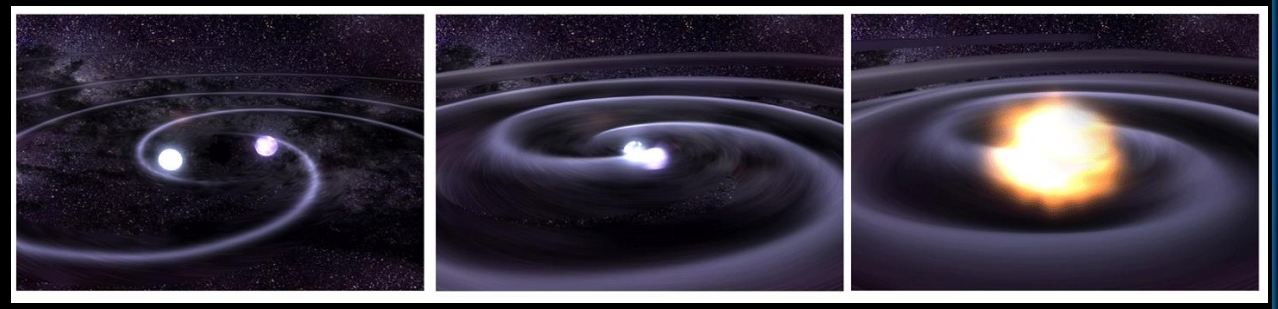

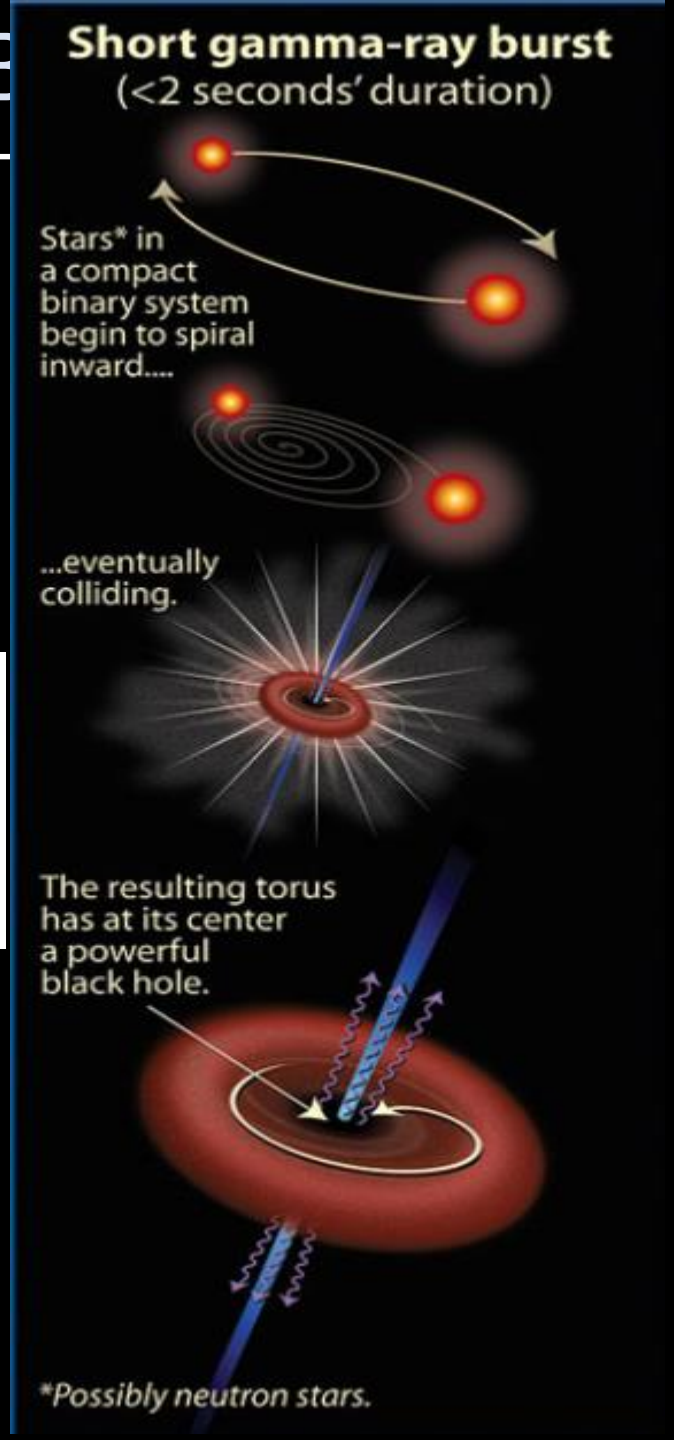

후속 빛관측으로 모은하 찾아냄 (NGC 4993, d~40 Mpc)
감마선폭발 후 킬로노바(kilonova) 생성 확인

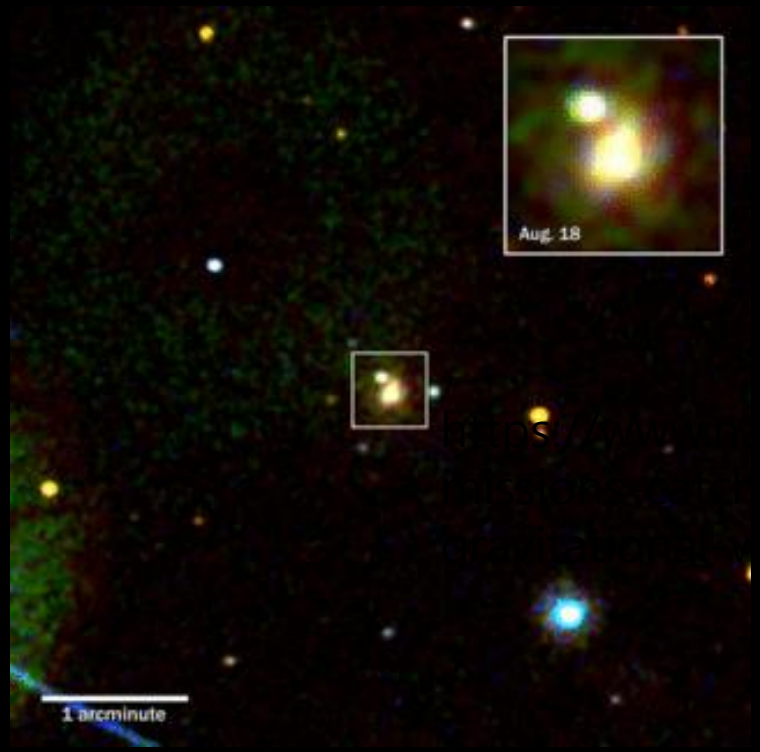

Swift's UV/Optical image

~5 hours after GW170817/GRB170817

HST image

within 12 hrs
up to 6 days afterwads

Inset: Magnified views of NGC4993 ***Credits: NASA/Swift***

GW170817 두 중성자별의 병합(coalescence)의 과정과 결과

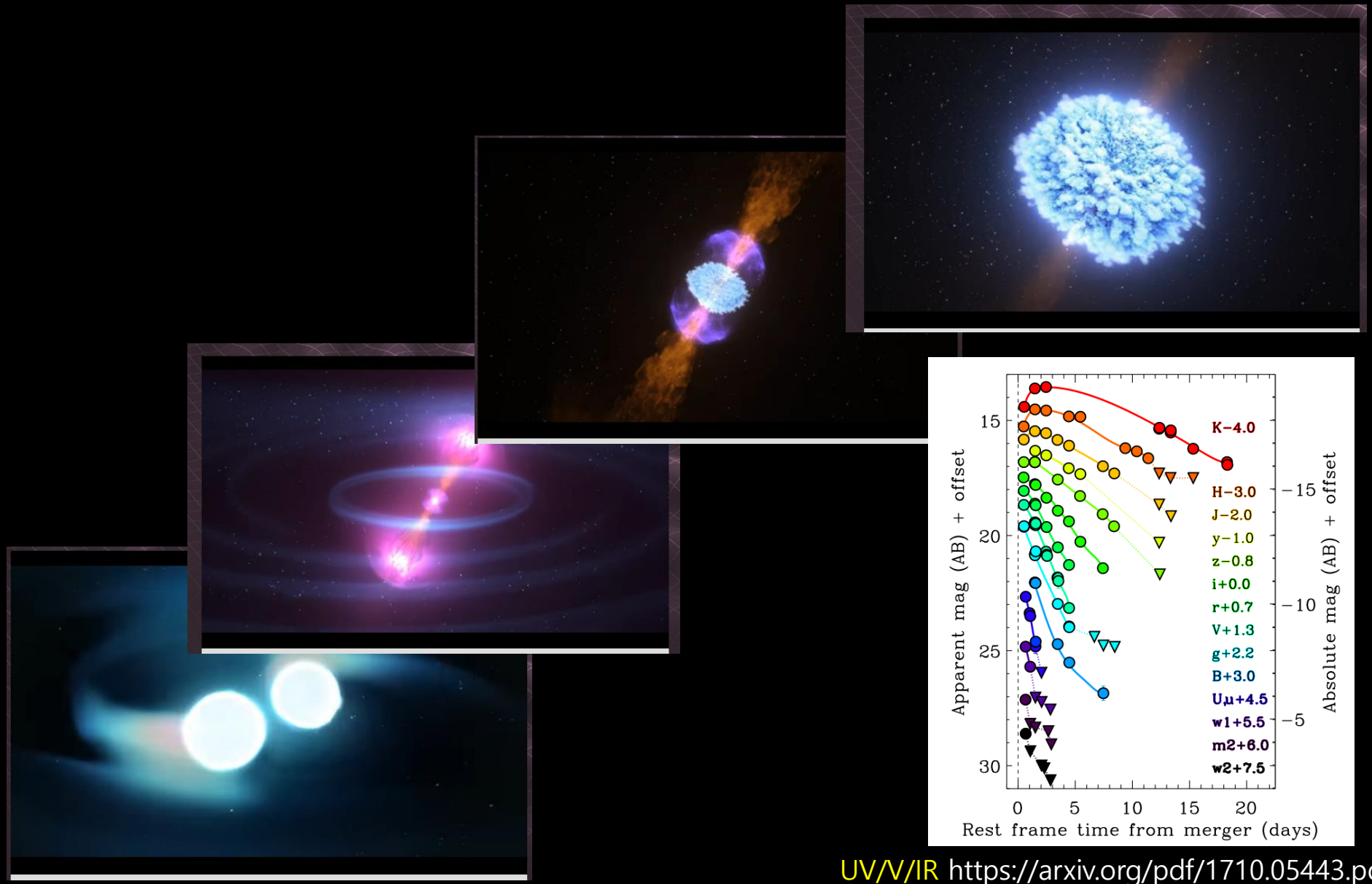

UV/V/IR https://arxiv.org/pdf/1710.05443.pdf

킬로노바 kilonova

중성자가 많은 환경 조성, 빠른 중성자포획 핵반응 (r-process) ➔ 가시광선 등 빛 방출

➔ "금"등 무거운 동위원소 기원

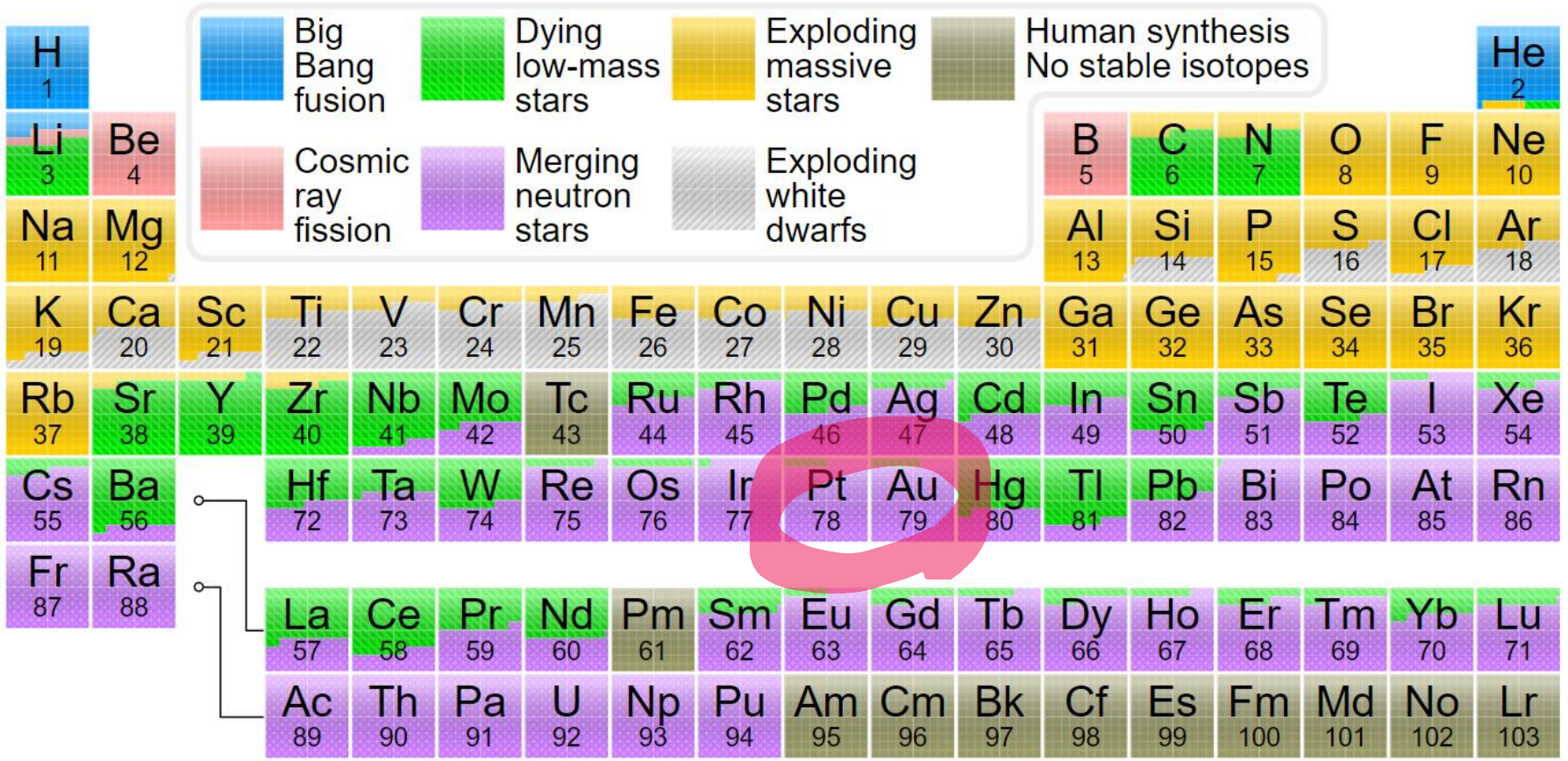

Applications of multi-messenger astronomy

Nature **551**, 85–88 (02 November 2017)

Hubble constant

Cosmology | High-energy astrophysics

recession velocity = Hubble constant H_0 x distance to a celestial body (Hubble flow)

EM observation (host galaxies)

GW observation (BH-BH or NS-NS)

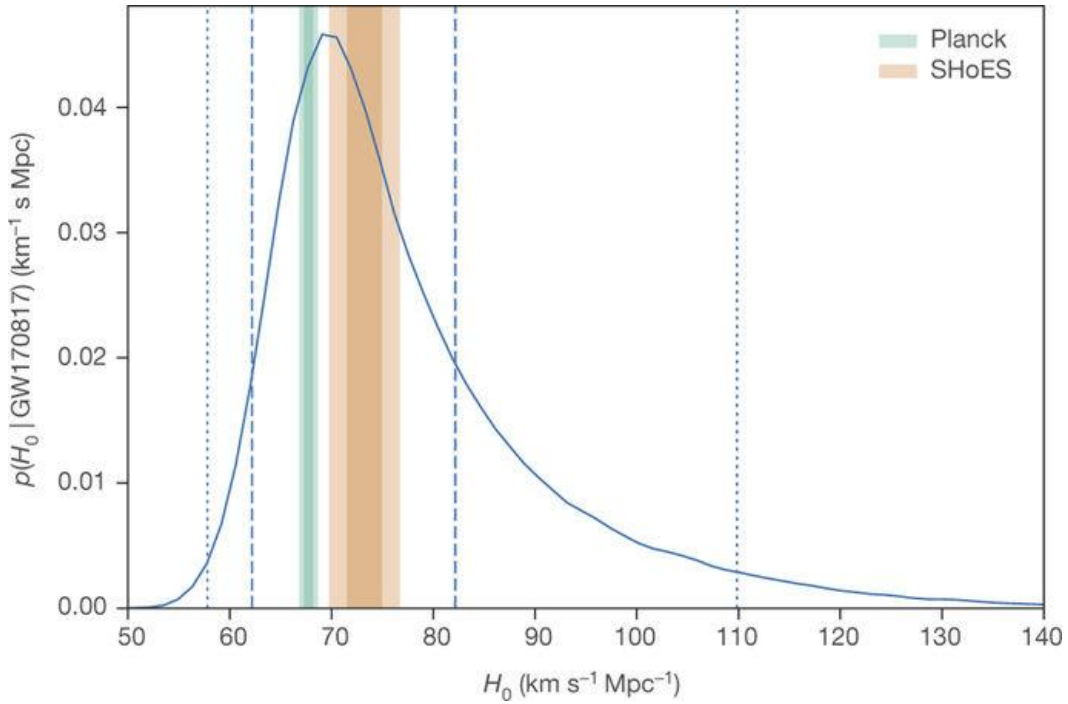

$$d = 43.8^{+2.9}_{-6.9}\ \mathrm{Mpc}$$

$$H_0 = 70.0^{+12.0}_{-8.0}\ \mathrm{km\ s^{-1}Mpc^{-1}}$$

How to improve the precision of D_L & sky localization ? ➔ important for MMA

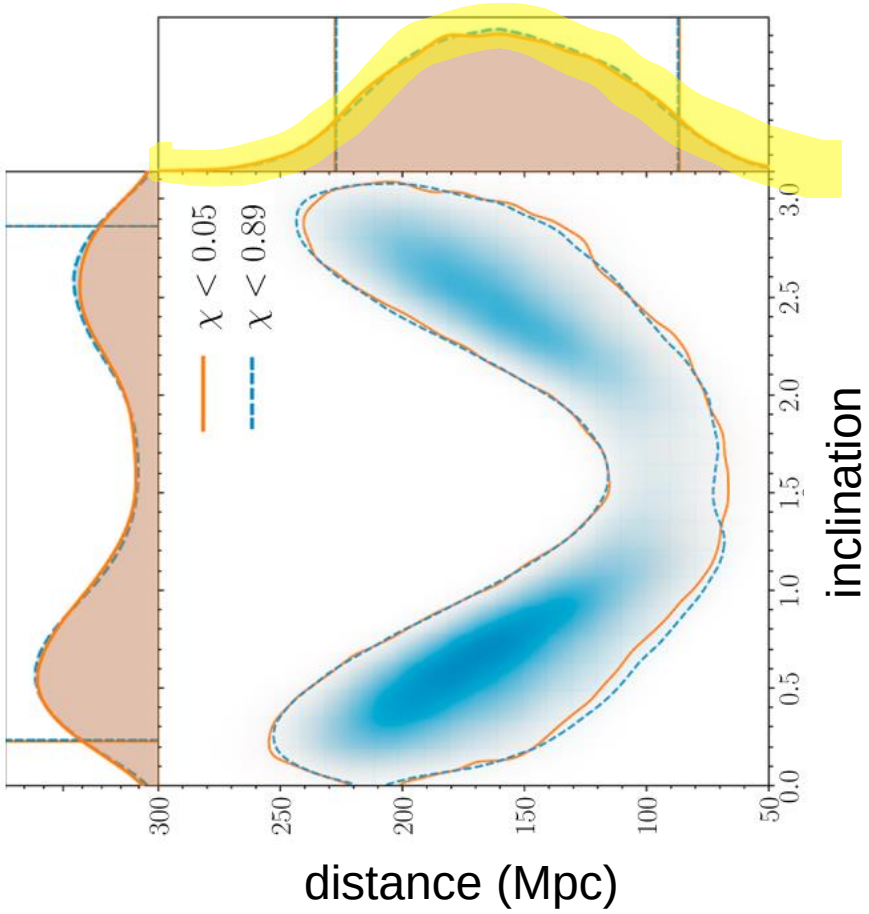

distance – inclination correlation

graph from GW190425 discovery paper

THE ASTROPHYSICAL JOURNAL LETTERS

중성자별 충돌 ➔ 감마선 폭발 + 킬로노바 Kilonova

중력파 방출 ➔ 감마선 ~ 전파 까지의 모든 빛 방출

관측으로 확인!

KNTNet 외계행성 탐색 시스템(한국천문연구원)

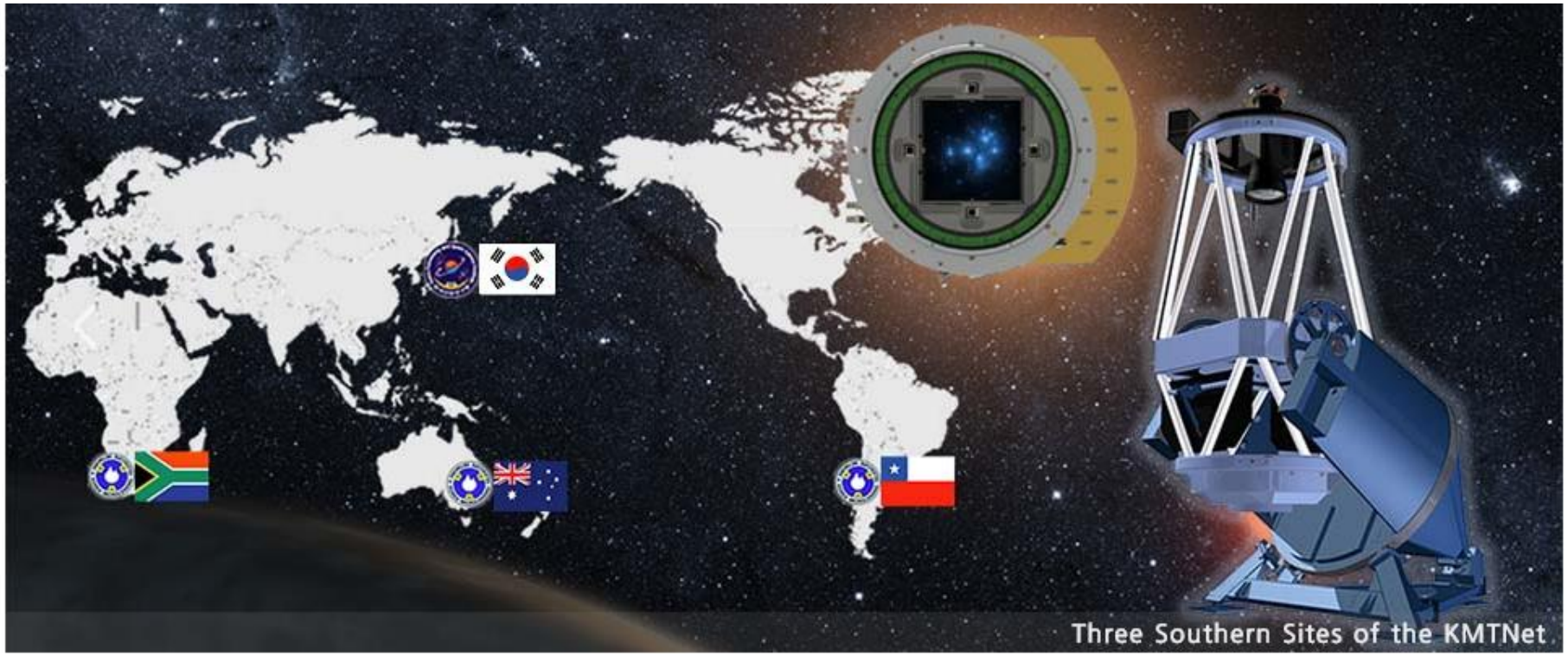

다중신호 천문학 + 중력파 천체물리학 연구에 유용한 개념들

다중신호 천문학 연구 예

10 Lookback time

The *lookback time* $t_{\rm L}$ to an object is the difference between the age $t_{\rm o}$ of the Universe now (at observation) and the age $t_{\rm e}$ of the Universe at the time the photons were emitted (according to the object). It is used to predict properties of high-redshift objects with evolutionary models, such as passive stellar evolution for galaxies. Recall that $E(z)$ is the time derivative of the logarithm of the scale factor $a(t)$; the scale factor is proportional to $(1 + z)$, so the product $(1+z)\,E(z)$ is proportional to the derivative of z with respect to the lookback time, or

$$t_{\rm L} = t_{\rm H} \int_0^z \frac{dz'}{(1+z')\,E(z')} \tag{30}$$

(Peebles, 1993, pp 313–315; Kolb & Turner 1990, pp 52–56, give some analytic solutions to this equation, but they are concerned with the age $t(z)$, so they integrate from z to ∞). The lookback time and age are plotted in Figure 6

https://arxiv.org/abs/astro-ph/9905116

3 Redshift

우주 전체를 다룰 때
시간 ← → 거리 개념이
등가적으로 활용된다

lookback time, redshift

The *redshift* z of an object is the fractional doppler shift of its emitted light resulting from radial motion

$$z \equiv \frac{\nu_e}{\nu_o} - 1 = \frac{\lambda_o}{\lambda_e} - 1 \tag{8}$$

where ν_o and λ_o are the observed frequency and wavelength, and ν_e and λ_e are the emitted. In special relativity, redshift is related to radial velocity v by

$$1 + z = \sqrt{\frac{1 + v/c}{1 - v/c}} \tag{9}$$

where c is the speed of light.

In terms of cosmography, the cosmological redshift is directly related to the scale factor $a(t)$, or the "size" of the Universe. For an object at redshift z

$$1 + z = \frac{a(t_o)}{a(t_e)} \tag{12}$$

where $a(t_o)$ is the size of the Universe at the time the light from the object is observed, and $a(t_e)$ is the size at the time it was emitted.

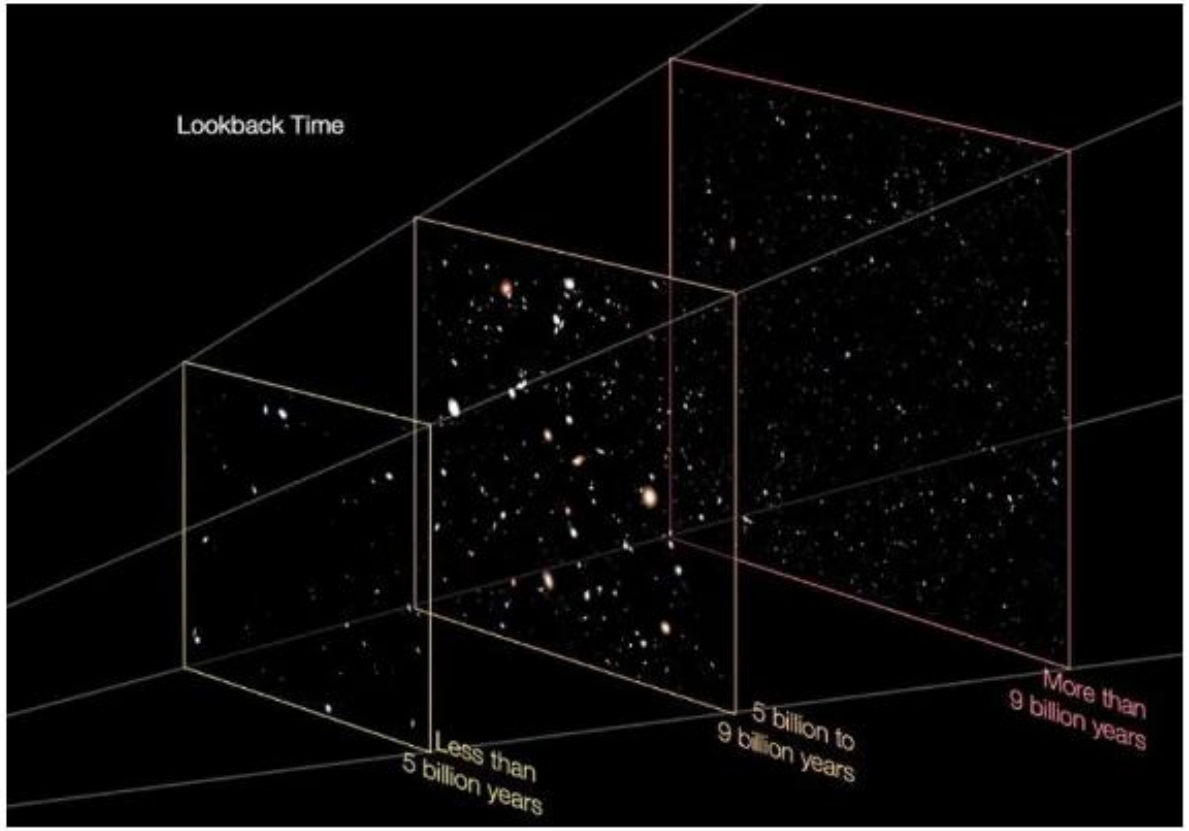

Fewer galaxies are seen nearby and at great distances than at intermediate ones, but that's due to a combination of galaxy mergers and evolution and also being unable to see the ultra-distant, ultra-faint galaxies themselves. Many different effects are at play when it comes to understanding how the light from the distant Universe gets redshifted. [-] NASA / ESA

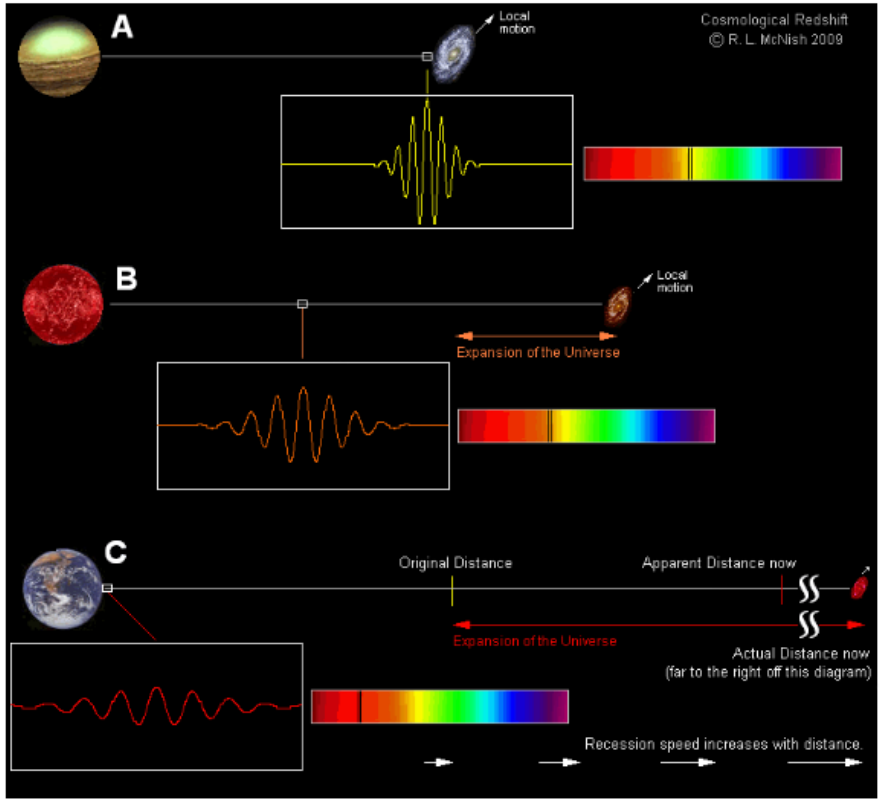

The farther a galaxy is, the faster it expands away from us and the more its light appears redshifted. A galaxy moving with the expanding Universe will be even a greater number of light years away, today, than the number of years (multiplied by the speed of light) that it took the light emitted from it to reach us. But we can only understand redshifts and blueshifts if we attribute them to a combination of motion (special relativistic) and the expanding fabric of space (general relativistic) contributions both. [-] LARRY MCNISH OF RASC CALGARY CENTER

https://www.forbes.com/sites/startswithabang/2020/03/07/ask-ethan-what-causes-light-to-redshift/

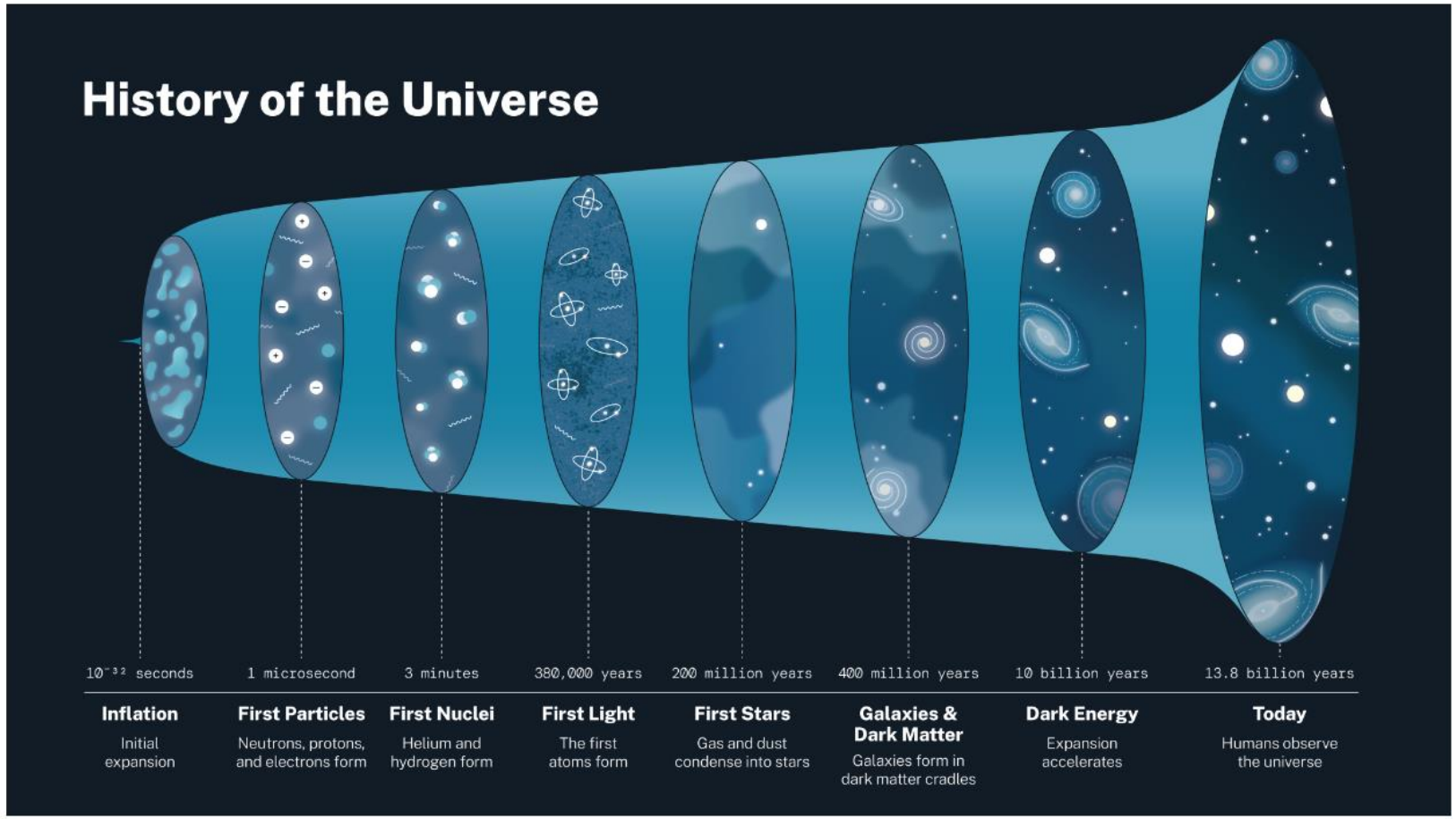

The history of the universe is outlined in this infographic.

NASA

멀리 떨어진 천문현상을 다룰 때는
comoving distance, proper distance,
luminosity distance를 모두 구분할 필요가 있다.

Distance measures in cosmology

David W. Hogg

Institute for Advanced Study, 1 Einstein Drive, Princeton NJ 08540
hogg@ias.edu

2000 December

2 Cosmographic parameters

The *Hubble constant* H_0 is the constant of proportionality between recession speed v and distance d in the expanding Universe;

$$v = H_0\, d \tag{1}$$

The subscripted "0" refers to the present epoch because in general H changes with time. The dimensions of H_0 are inverse time, but it is usually written

$$H_0 = 100\, h\ \mathrm{km\,s^{-1}\,Mpc^{-1}} \tag{2}$$

where h is a dimensionless number parameterizing our ignorance. (Word on the street is that $0.6 < h < 0.9$.) The inverse of the Hubble constant is the *Hubble time* t_H

$$t_\mathrm{H} \equiv \frac{1}{H_0} = 9.78 \times 10^9\, h^{-1}\ \mathrm{yr} = 3.09 \times 10^{17}\, h^{-1}\ \mathrm{s} \tag{3}$$

and the speed of light c times the Hubble time is the *Hubble distance* D_H

$$D_\mathrm{H} \equiv \frac{c}{H_0} = 3000\, h^{-1}\ \mathrm{Mpc} = 9.26 \times 10^{25}\, h^{-1}\ \mathrm{m} \tag{4}$$

https://arxiv.org/abs/astro-ph/9905116

These quantities set the scale of the Universe, and often cosmologists work in geometric units with $c = t_{\rm H} = D_{\rm H} = 1$.

The mass density ρ of the Universe and the value of the cosmological constant Λ are dynamical properties of the Universe, affecting the time evolution of the metric, but in these notes we will treat them as purely kinematic parameters. They can be made into dimensionless density parameters $\Omega_{\rm M}$ and Ω_Λ by

$$\Omega_{\rm M} \equiv \frac{8\pi\, G\, \rho_0}{3\, H_0^2} \tag{5}$$

$$\Omega_\Lambda \equiv \frac{\Lambda\, c^2}{3\, H_0^2} \tag{6}$$

(Peebles, 1993, pp 310–313), where the subscripted "0"s indicate that the quantities (which in general evolve with time) are to be evaluated at the present epoch. A third density parameter Ω_k measures the "curvature of space" and can be defined by the relation

$$\Omega_{\rm M} + \Omega_\Lambda + \Omega_k = 1 \tag{7}$$

3 Redshift

The *redshift* z of an object is the fractional doppler shift of its emitted light resulting from radial motion

$$z \equiv \frac{\nu_{\rm e}}{\nu_{\rm o}} - 1 = \frac{\lambda_{\rm o}}{\lambda_{\rm e}} - 1 \tag{8}$$

7 Luminosity distance

The *luminosity distance* $D_{\rm L}$ is defined by the relationship between bolometric (ie, integrated over all frequencies) flux S and bolometric luminosity L:

$$D_{\rm L} \equiv \sqrt{\frac{L}{4\pi\, S}} \tag{20}$$

It turns out that this is related to the transverse comoving distance and angular diameter distance by

$$D_{\rm L} = (1+z)\, D_{\rm M} = (1+z)^2\, D_{\rm A} \tag{21}$$

(Weinberg, 1972, pp 420–424; Weedman, 1986, pp 60–62). The latter relation follows from

THE ASTROPHYSICAL JOURNAL LETTERS, 826:L13, 2016 JULY 20
Preprint typeset using LaTeX style AASTeX6 v. 1.0

LOCALIZATION AND BROADBAND FOLLOW-UP OF THE GRAVITATIONAL-WAVE TRANSIENT GW150914

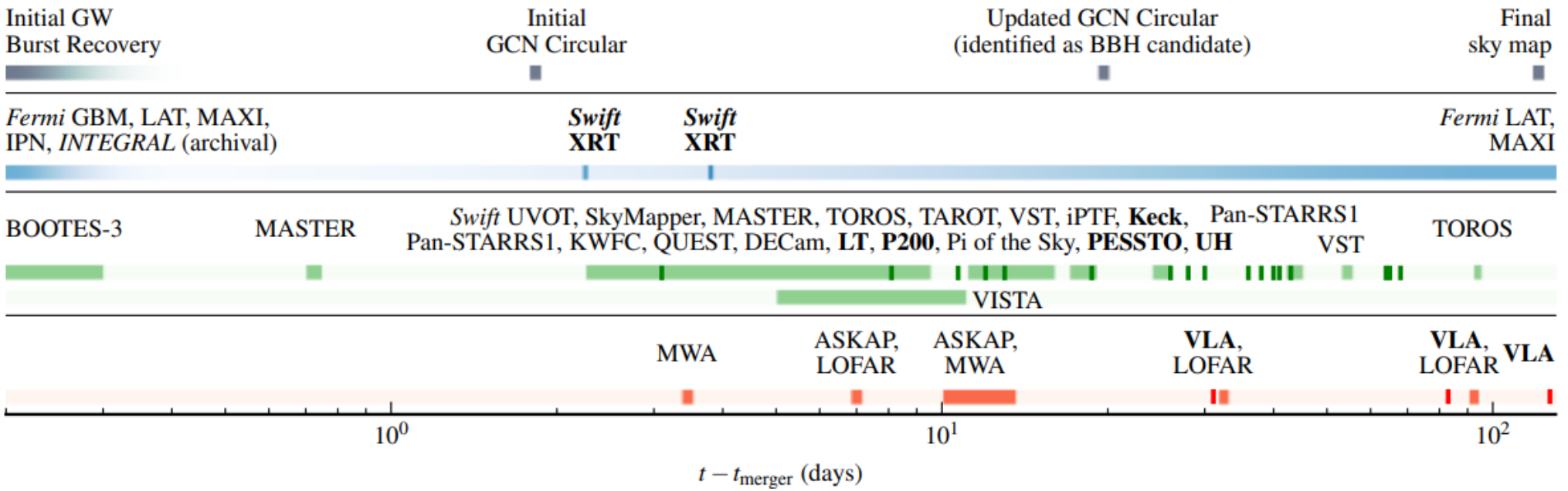

https://arxiv.org/pdf/1602.08492

Table 1. Summary of Tiled Observations

Facility/ Instrument	Band[a]	Depth[b]	Time[c]	Area (deg^2)	Contained Probability (%) cWB	LIB	BSTR[d]	LALInf	GCN
Gamma-ray									
Fermi LAT	20 MeV–300 GeV	1.7×10^{-9}	(every 3 hr)	—	100	100	100	100	18709
Fermi GBM	8 keV–40 MeV	$0.7–5 \times 10^{-7}$ (0.1–1 MeV)	(archival)	—	100	100	100	100	18339
INTEGRAL	75 keV–1 MeV	1.3×10^{-7}	(archival)	—	100	100	100	100	18354
IPN	15 keV–10 MeV	1×10^{-7}	(archival)	—	100	100	100	100	—
X-ray									
MAXI/GSC	2–20 keV	1×10^{-9}	(archival)	17900	95	89	92	84	19013
Swift XRT	0.3–10 keV	5×10^{-13} (gal.)	2.3, 1, 1	0.6	0.03	0.18	0.04	0.05	18331
		$2–4 \times 10^{-12}$ (LMC)	3.4, 1, 1	4.1	1.2	1.9	0.16	0.26	18346
Optical[e]									
DECam	i, z	$i < 22.5, z < 21.5$	3.9, 5, 22	100	38	14	14	11	18344, 18350
iPTF	R	$R < 20.4$	3.1, 3, 1	130	2.8	2.5	0.0	0.2	18337
KWFC	i	$i < 18.8$	3.4, 1, 1	24	0.0	1.2	0.0	0.1	18361
MASTER	C	< 19.9	-1.1, 7, 7	710	50	36	55	50	18333, 18390, 18903, 19021
Pan-STARRS1	i	$i < 19.2 - 20.8$	3.2, 21, 42	430	28	29	2.0	4.2	18335, 18343, 18362, 18394
La Silla–QUEST	g, r	$r < 21$	3.8, 5, 0.1	80	23	16	6.2	5.7	18347
SkyMapper	i, v	$i < 19.1, v < 17.1$	2.4, 2, 3	30	9.1	7.9	1.5	1.9	18349
Swift UVOT	u	$u < 19.8$ (gal.)	2.3, 1, 1	3	0.7	1.0	0.1	0.1	18331
	u	$u < 18.8$ (LMC)	3.4, 1, 1						18346
TAROT	C	$R < 18$	2.8, 5, 14	30	15	3.5	1.6	1.9	18332, 18348
TOROS	C	$r < 21$	2.5, 7, 90	0.6	0.03	0.0	0.0	0.0	18338
VST@ESO	r	$r < 22.4$	2.9, 6, 50	90	29	10	14	10	18336, 18397
Near Infrared									
VISTA@ESO	Y, J, K_S	$J < 20.7$	4.8, 1, 7	70	15	6.4	10	8.0	18353
Radio									
ASKAP	863.5 MHz	5–15 mJy	7.5, 2, 6	270	82	28	44	27	18363, 18655
LOFAR	145 MHz	12.5 mJy	6.8, 3, 90	100	27	1.3	0.0	0.1	18364, 18424, 18690
MWA	118 MHz	200 mJy	3.5, 2, 8	2800	97	72	86	86	18345

[a]Band: photon energy, optical or near-infrared filter (or C for clear unfiltered light), wavelength range, or central frequency.

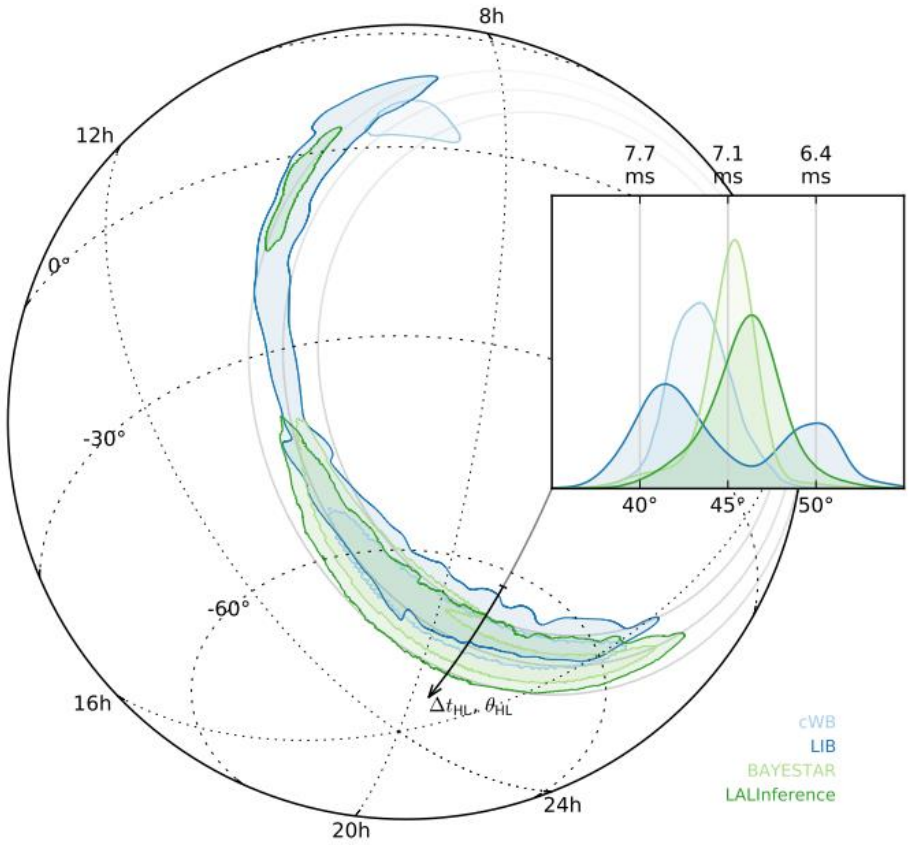

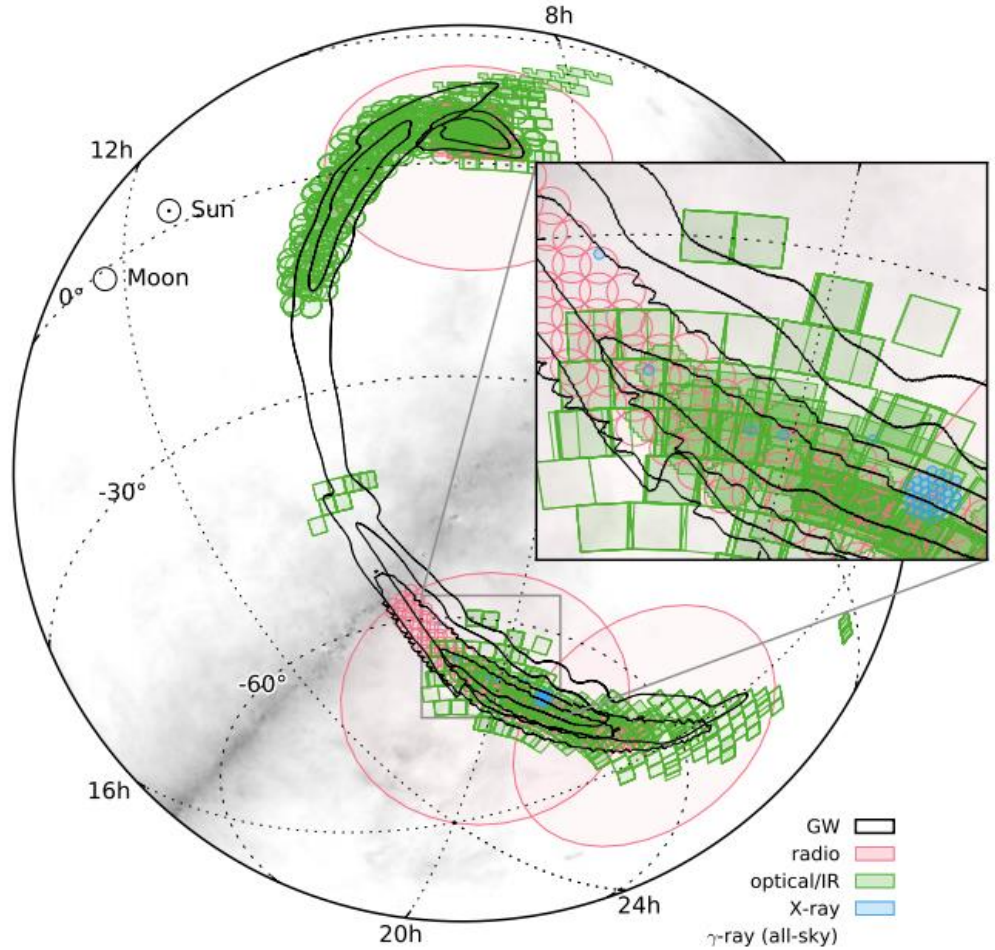

Figure 2. Comparison of different GW sky maps, showing the 90% credible level contours for each algorithm. This is an orthographic projection centered on the centroid of the LIB localization. The inset shows the distribution of the polar angle $\theta_{\rm HL}$ (equivalently, the arrival time difference $\Delta t_{\rm HL}$).

Astrophysics > Cosmology and Nongalactic Astrophysics

[Submitted on 6 Jan 2019 (v1), last revised 22 Mar 2019 (this version, v2)]

First measurement of the Hubble constant from a dark standard siren using the Dark Energy Survey galaxies and the LIGO/Virgo binary-black-hole merger GW170814

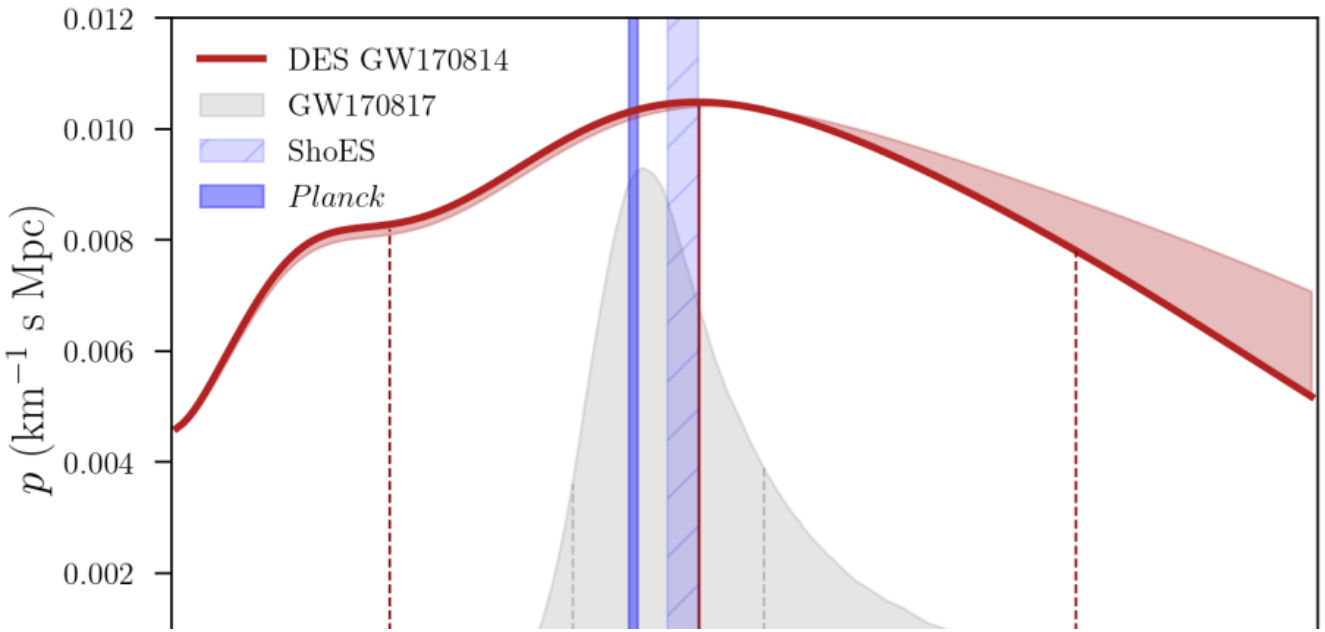

Figure 2. Hubble constant posterior distribution obtained by marginalizing over $\sim 77,000$ possible host galaxies (red line), showing the maximum value (solid vertical line). The maximum a posteriori and its 68% confidence level is $H_0 = 75^{+40}_{-32}$ km s^{-1} Mpc^{-1} for a flat prior in the range [20,140] km s^{-1} Mpc^{-1}. The shaded region represents the change in the posterior when different fractions of the localization volume

$$p(H_0|d_{\rm GW}, d_{\rm EM}) \propto p(d_{\rm GW}, d_{\rm EM}|H_0)p(H_0)$$

We assume that all cosmological parameters except for H_0 are fixed (Flat ΛCDM cosmology with $\Omega_m = 0.3$ and $\Omega_\Lambda = 0.7$). We treat the joint GW and EM likelihood $p(d_{\rm GW}, d_{\rm EM}|H_0)$ as the product of two individual likelihoods (since the processes involved in producing the data from the two experiments are independent) marginalized over all variables except for the true luminosity distance d_L and solid angle $\hat{\Omega}_{\rm GW}$ of the GW source, and for the true host galaxy redshift z_i and solid angle $\hat{\Omega}_i$. Note that the solid angles $\hat{\Omega}$ are vectors with the angular position of the source/galaxy as direction, and they all subtend the same area ($\sim 3 \times 10^{-3}$ deg^2) as the sky is pixelized with HEALPIX maps in this work. If

We also need to marginalize over the galaxies' redshifts and sky positions, with a reasonable choice of prior $p(z_i, \Omega_i)$. If one assumes that the galaxies are uniformly distributed in comoving volume V, and volume–limited within $V_{\rm max}$:

$$p(z_i, \hat{\Omega}_i)\, {\rm d}z_i\, {\rm d}\hat{\Omega}_i \propto \frac{1}{V_{\rm max}} \frac{{\rm d}^2 V}{{\rm d}z_i {\rm d}\hat{\Omega}_i} {\rm d}z_i\, {\rm d}\hat{\Omega}_i \propto \frac{1}{V_{\rm max}} \frac{r^2(z_i)}{H(z_i)} {\rm d}z_i\, {\rm d}\hat{\Omega}_i\,, \quad (3)$$

Example: Marginalization

If ϕ(a, b, c) is the potential on the left, then the marginalization of ϕ(a, b, c) onto {a, b} is the marginal of ϕ(a, b) on the right.

a	b	c	ϕ(a, b, c)
0	0	0	0.1
0	0	1	0.2
1	0	0	0.1
1	1	0	0.1
1	1	1	0.1

a	b	ϕ(a, b)
0	0	0.3
1	0	0.1
1	1	0.2

$$P(X) = \sum_y P(X, Y = y) = \sum_y P(X|Y = y) \times P(Y = y)$$

$$P(X) = \int_y P(X, Y = y) {\rm d}y$$

$$P(A, B|C) = P(A|B, C) \times P(B|C)$$

joint probability conditional probability x marginal probability

$$P(\mathbf{\Theta}|data) = \frac{P(data|\mathbf{\Theta}) \times P(\mathbf{\Theta})}{P(data)}$$

$$P(data) = \int_{\mathbf{\Theta}} P(data|\mathbf{\Theta}) \times P(\mathbf{\Theta}) \, \mathrm{d}\mathbf{\Theta}$$

https://towardsdatascience.com/probability-concepts-explained-marginalisation-2296846344fc

GW170817: Measurements of Neutron Star Radii and Equation of State

The LIGO Scientific Collaboration and The Virgo Collaboration

On 17 August 2017, the LIGO and Virgo observatories made the first direct detection of gravitational waves from the coalescence of a neutron star binary system. The detection of this gravitational-wave signal, GW170817, offers a novel opportunity to directly probe the properties of matter at the extreme conditions found in the interior of these stars. The initial, minimal-assumption analysis of the LIGO and Virgo data placed constraints on the tidal effects of the coalescing bodies, which were then translated to constraints on neutron star radii. Here, we expand upon previous analyses by working under the hypothesis that both bodies were neutron stars that are described by the same equation of state and have spins within the range observed in Galactic binary neutron stars. Our analysis employs two methods: the use of equation-of-state-insensitive relations between various macroscopic properties of the neutron stars and the use of an efficient parametrization of the defining function $p(\rho)$ of the equation of state itself. From the LIGO and Virgo data alone and the first method, we measure the two neutron star radii as $R_1 = 10.8^{+2.0}_{-1.7}$ km for the heavier star and $R_2 = 10.7^{+2.1}_{-1.5}$ km for the lighter star at the 90% credible level. If we additionally require that the equation of state supports neutron stars with masses larger than $1.97\,\mathrm{M}_\odot$ as required from electromagnetic observations and employ the equation-of-state parametrization, we further constrain $R_1 = 11.9^{+1.4}_{-1.4}$ km and $R_2 = 11.9^{+1.4}_{-1.4}$ km at the 90% credible level. Finally, we obtain constraints on $p(\rho)$ at supranuclear densities, with pressure at twice nuclear saturation density measured at $3.5^{+2.7}_{-1.7} \times 10^{34}\,\mathrm{dyn\,cm^{-2}}$ at the 90% level.

https://ui.adsabs.harvard.edu/abs/2018PhRvL.121p1101A/abstract

중성자별-중성자별 쌍성에서 방출되는 중력파 신호를 정밀하게 분석하면
쌍성의 거리, 질량외에도 **중성자별의 구성성분 (상태방정식)**도 알아낼 수 있다

➔ **고주파수 대역 감도 개선** 필요한 이유

From: Interpreting binary neutron star mergers: describing the binary neutron star dynamics, modelling gravitational waveforms, and analyzing detections

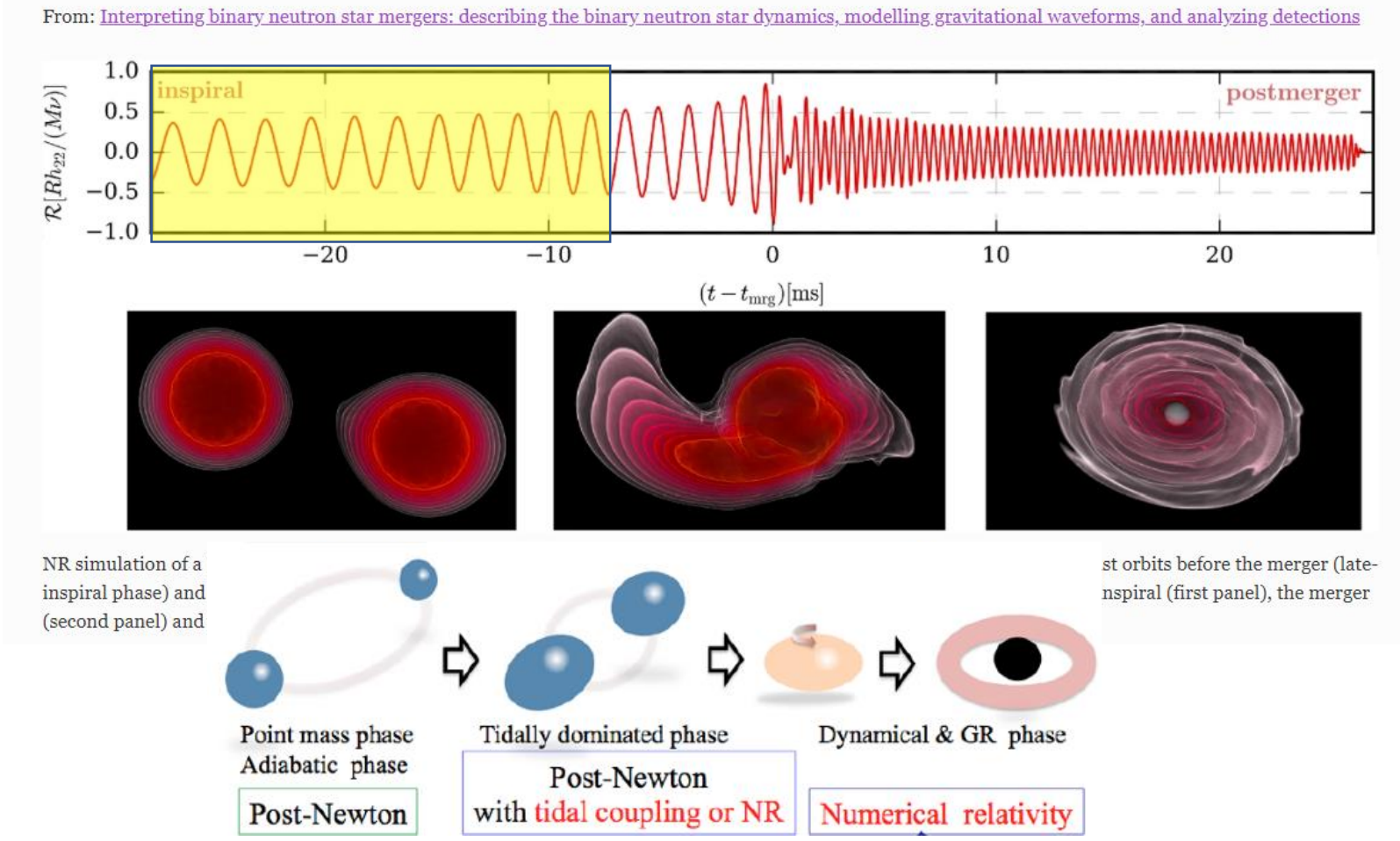

https://link.springer.com/article/10.1007/s10714-020-02751-6/figures/1

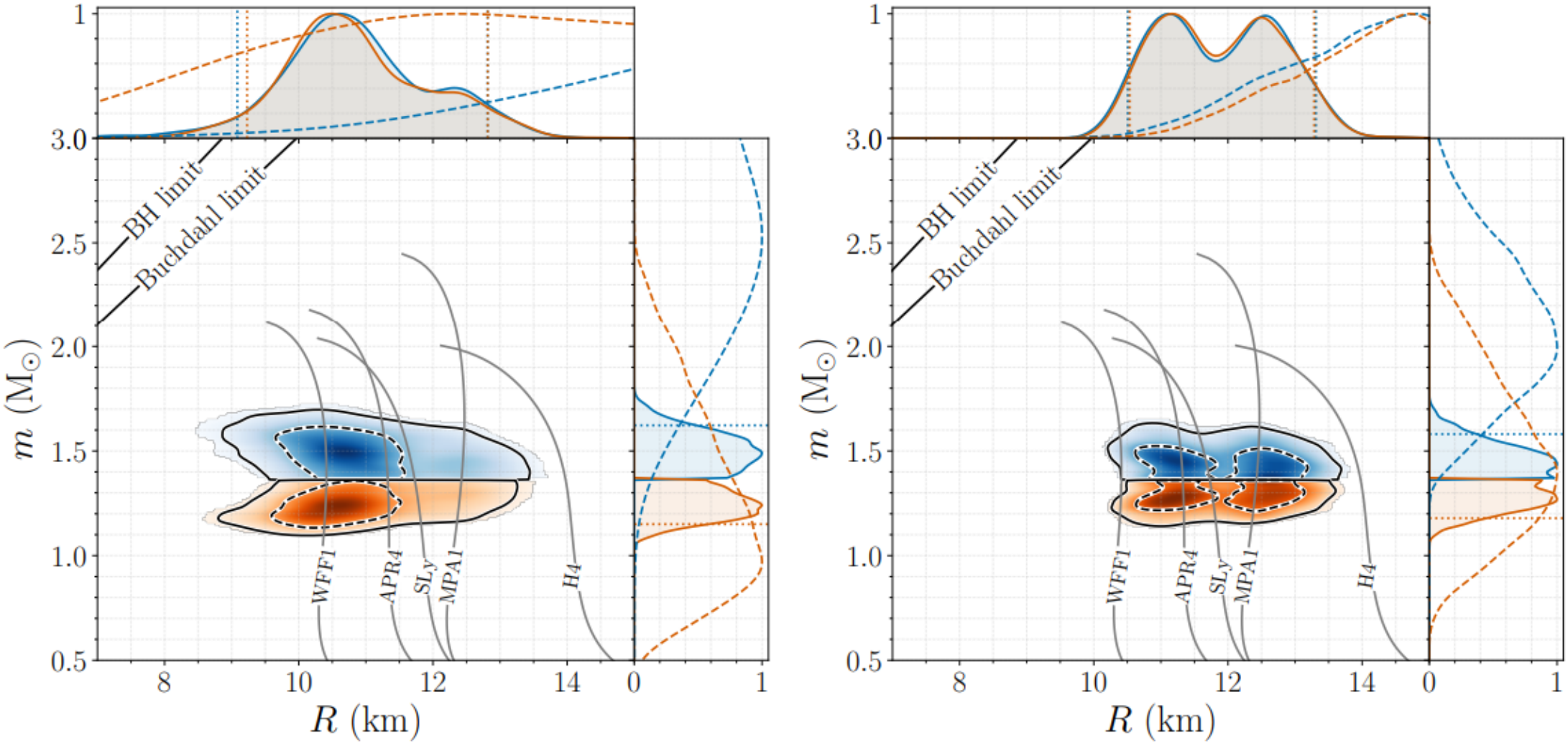

FIG. 3. Marginalized posterior for the mass m and areal radius R of each binary component using EOS-insensitive relations (left panel) and a parametrized EOS where we impose a lower limit on the maximum mass of $1.97\,\mathrm{M}_\odot$ (right panel). The top blue (bottom orange) posterior corresponds to the heavier (lighter) NS. Example mass-radius curves for selected EOSs are overplotted in gray. The lines in the top left denote the Schwarzschild BH ($R = 2m$) and Buchdahl ($R = 9m/4$) limits. In the one-dimensional plots, solid lines are used for the posteriors, while dashed lines are used for the corresponding parameter priors. Dotted vertical lines are used for the bounds of the 90% credible intervals.

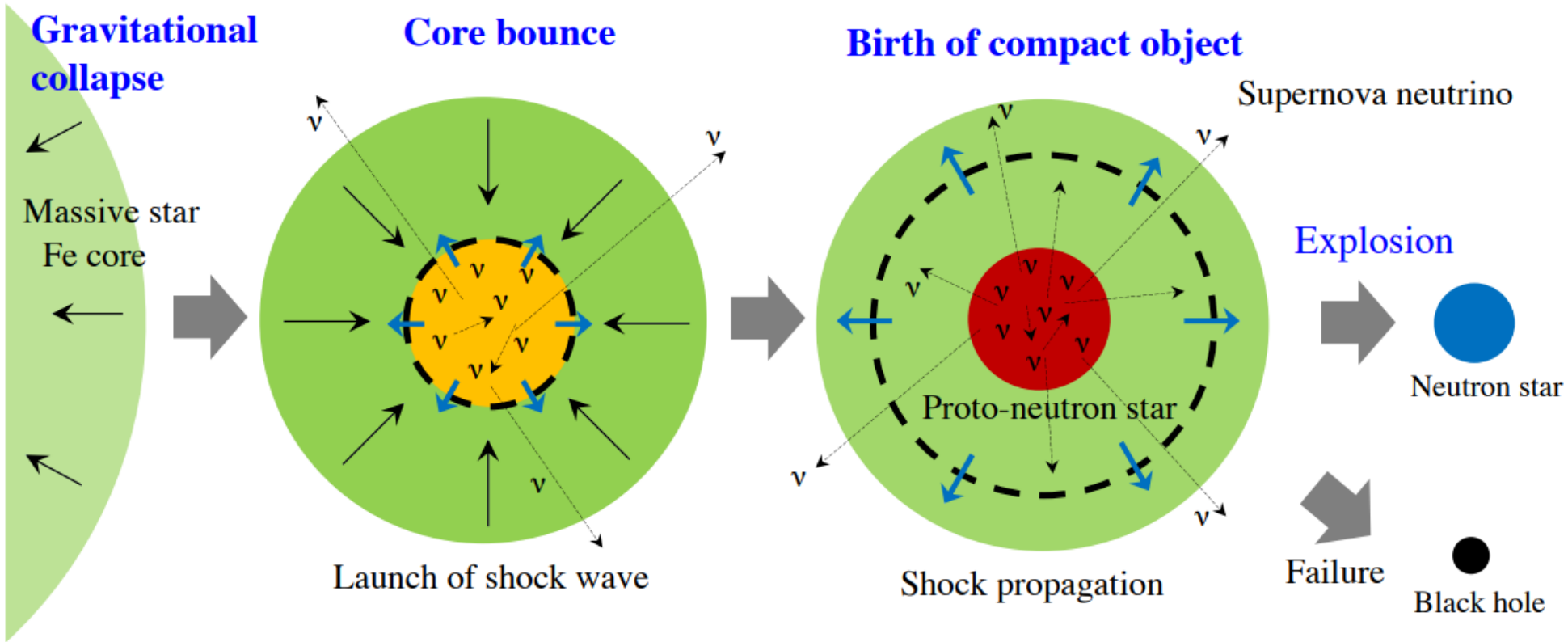

Fig. 2 Schematic diagrams of the evolution of supernova cores from massive stars to compact objects. Starting with the gravitational collapse of the Fe core, the central core is compressed and neutrinos are trapped inside due to interactions with hot and density matter. The central core bounces back by a matter around the nuclear saturation density and the shock wave is launched.

Equation of state in neutron stars and supernovae

Kohsuke Sumiyoshi *, Toru Kojo, and Shun Furusawa

핵자 = 양성자 + 중성자
갯수/질량밀도가 중요

양성자비율

핵자의 페르미운동량 $p_F \sim 300$ MeV

$$Y_p = n_p/n, \text{ is } \sim 0.1 \text{ at } n \sim n_0$$

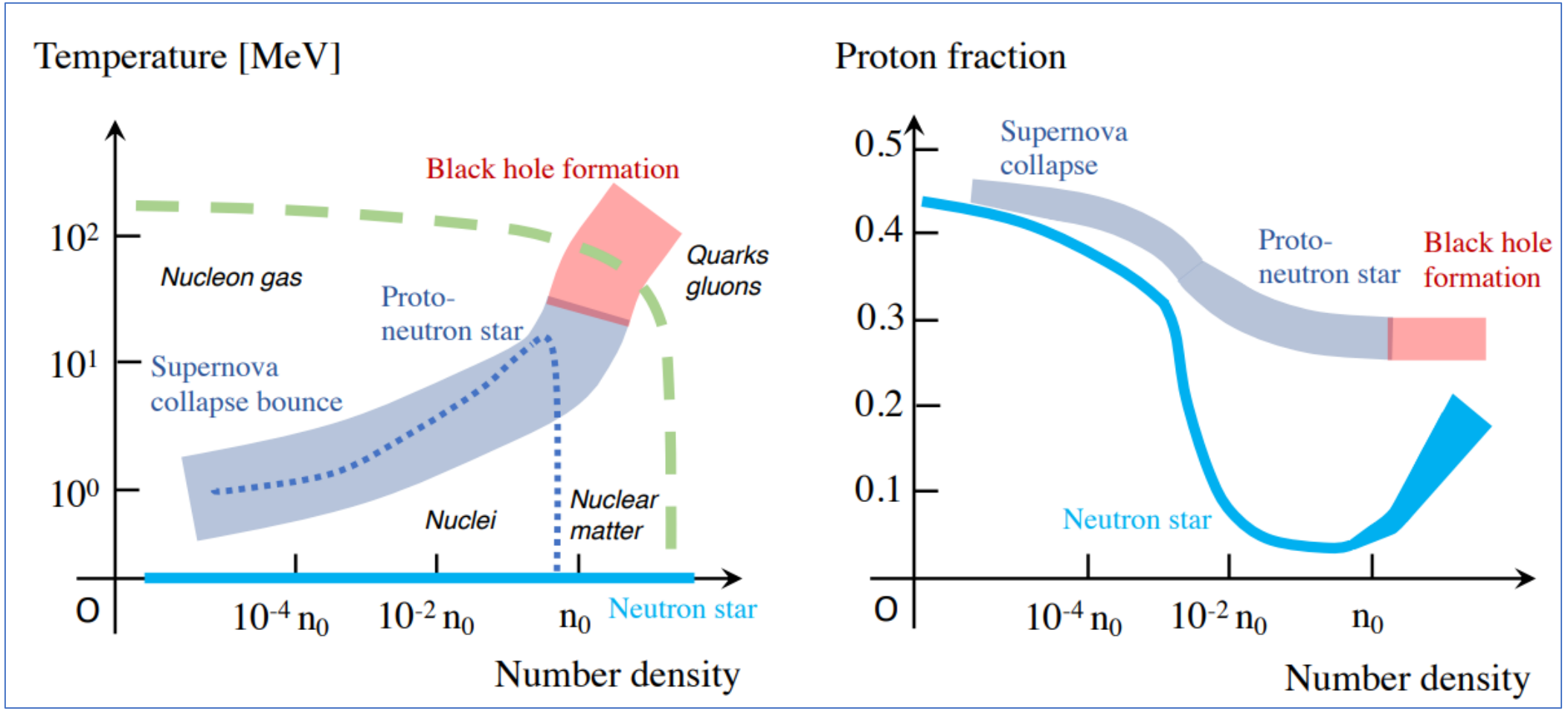

https://arxiv.org/pdf/2207.00033

$$\frac{dM(r)}{dr} = 4\pi r^2 \rho(r)$$

$$\frac{dP(r)}{dr} = -\frac{GM(r)\rho(r)}{r^2}\left(1+\frac{P}{\rho}\right)\left(1+\frac{4\pi r^3 P}{M(r)}\right)\left(1-\frac{2GM}{r}\right)^{-1}$$

"Tolman-Oppenheimer-Volkoff (TOV) equation, a general relativistic version of the Newton equation for gravity" quoted from the reference

For a gas in the relativistic limit, the energy density scales as $\rho \propto p_F^4 \propto n^{4/3}$. Using the relation $\mu = \partial\rho/\partial n$ (μ: chemical potential) and the thermodynamic relation $P = \mu n - \rho$, one can write

$$\rho_{\rm rela}(n) = cn^{4/3} \quad \rightarrow \quad P_{\rm rela} = \rho_{\rm rela}/3\,. \tag{3}$$

This regime is relevant for electrons in Fe cores or neutron stars. Meanwhile, if fermions with the masses m are non-relativistic ($m \gg p_F$), the energy density behaves as $\rho \sim c_1 mn + c_2 n^{5/3}/m$ with c_1, c_2 being some constants. In this case

$$\rho_{\rm NR}(n) = c_1 mn + c_2\frac{n^{5/3}}{m} \quad \rightarrow \quad P_{\rm NR} = \frac{2}{3}c_2\frac{n^{5/3}}{m} \propto \rho_{\rm NR}^{5/3} m^{-8/3}\,. \tag{4}$$

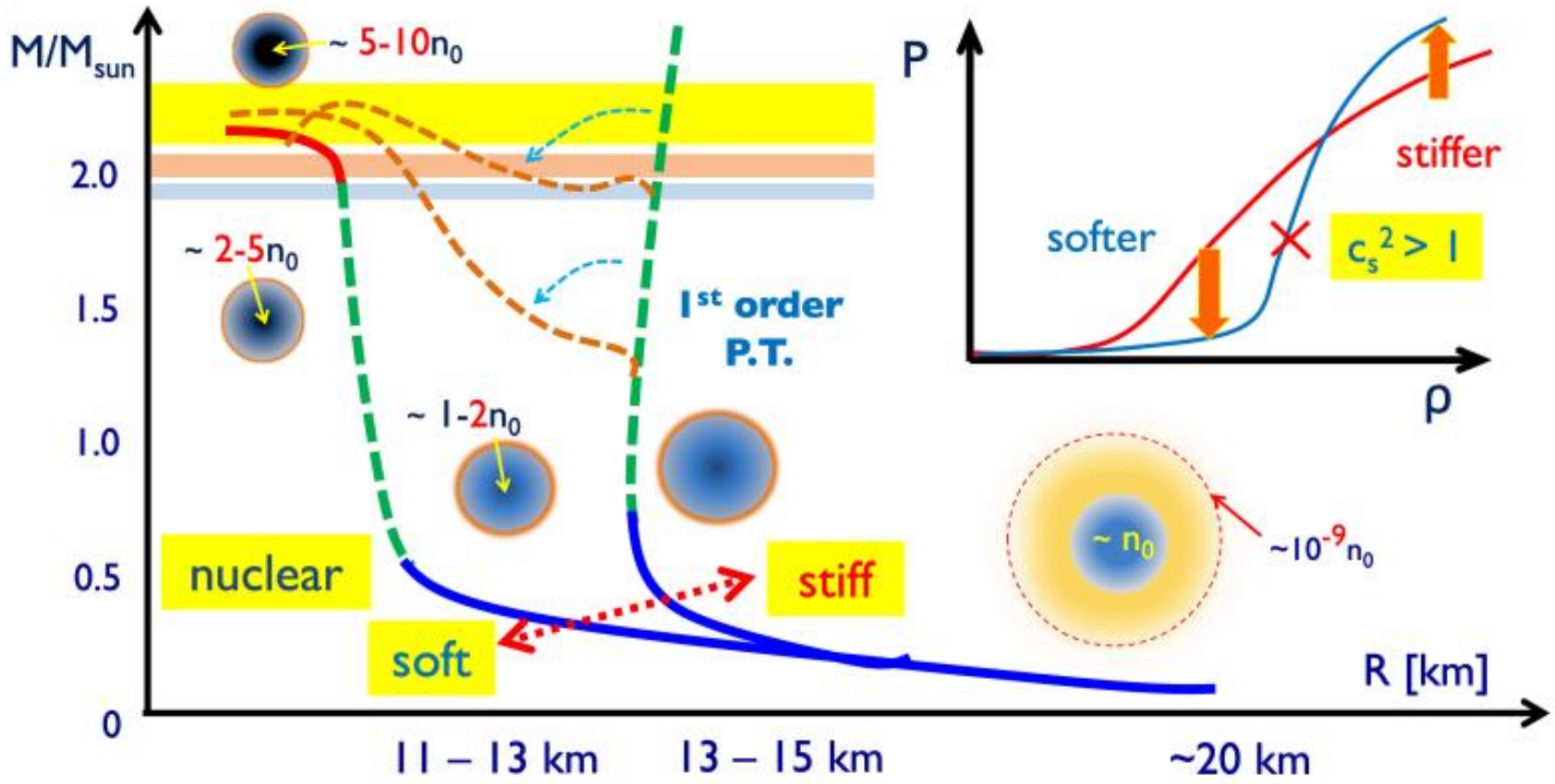

Fig. 3 *M-R* curves as functions of the central density n_c. For a small M neutron stars have large radii due to loosely bound crust. When the central density reaches $n_c = 1 \sim 2n_0$, the dilute matter is highly compressed and the size of a neutron star is characterized by a matter beyond the saturation point. The curves go up with small variation in the radii. The exception is equations of state with the first order transitions which lead to kinks in the *M-R* curves. The top right figure illustrates how

21세기는 중력파와 다중신호 천문학의 시대

거대과학, 국제협력, 융합연구

초정밀고도화된 장비(센서)

➔ 정밀 우주론 (precision cosmology)

정밀 천문학 (precision astronomy) 가능

➔ 시뮬레이션, 머신러닝 활용/역할 증대

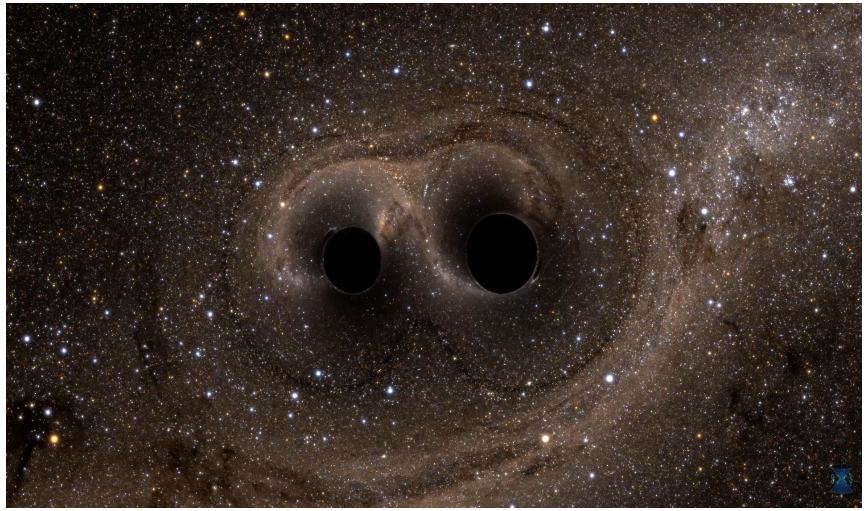

국제협력연구에 필요한 소양

수학, 자연과학, 공학 +

분석력, 사고력 +

고도의 사회성(듣기) +

언어사교능력 (말하기) +

글쓰기 +

빅데이터 저장/분류/시각화 (infographic)

➔ Public outreach가 점점 더 중요해짐

https://www.iau.org/public/